MARTIN MARIETTA ENERGY SYSTEMS LIBRARIES
3 4456 0364501 8

ORNL-3257
UC-34 – Physics
TID-4500 (17th ed., Rev.)

ELECTRONUCLEAR DIVISION
ANNUAL PROGRESS REPORT
FOR PERIOD ENDING DECEMBER 31, 1961

CENTRAL RESEARCH LIBRARY
DOCUMENT COLLECTION
LIBRARY LOAN COPY
DO NOT TRANSFER TO ANOTHER PERSON
If you wish someone else to see this document, send in name with document and the library will arrange a loan.

OAK RIDGE NATIONAL LABORATORY
operated by
UNION CARBIDE CORPORATION
for the
U.S. ATOMIC ENERGY COMMISSION

Printed in USA. Price $2.00. Available from the

Office of Technical Services
U. S. Department of Commerce
Washington 25, D. C.

LEGAL NOTICE

This report was prepared as an account of Government sponsored work. Neither the United States, nor the Commission, nor any person acting on behalf of the Commission:

A. Makes any warranty or representation, express or implied, with respect to the accuracy, completeness, or usefulness of the information contained in this report, or that the use of any information, apparatus, method, or process disclosed in this report may not infringe privately owned rights; or

B. Assumes any liabilities with respect to the use of, or for damages resulting from the use of any information, apparatus, method, or process disclosed in this report.

As used in the above, "person acting on behalf of the Commission" includes any employee or contractor of the Commission to the extent that such employee or contractor prepares, handles or distributes, or provides access to, any information pursuant to his employment or contract with the Commission.

ORNL-3257
UC-34 – Physics
TID-4500 (17th ed., Rev.)

Contract No. W-7405-eng-26

ELECTRONUCLEAR DIVISION

ANNUAL PROGRESS REPORT

For Period Ending December 31, 1961

Robert S. Livingston, Director
Alexander Zucker, Associate Director

DATE ISSUED

AUG 17 1962

OAK RIDGE NATIONAL LABORATORY
Oak Ridge, Tennessee
operated by
UNION CARBIDE CORPORATION
for the
U. S. ATOMIC ENERGY COMMISSION

MARTIN MARIETTA ENERGY SYSTEMS LIBRARIES
3 4456 0364501 8

Summary

With 27.5-Mev N^{3+} ions accelerated in the 63-Inch Cyclotron, new results were obtained on the angular and energy distributions of transfer reactions, transfer reaction systematics, the effect of angular momentum on the statistical model of the nucleus, and on angular distribution of alpha particles which result from a direct reaction of N^{14} with Li^6 and Li^7. In continuation of the 22-Mev proton program at the 86-Inch Cyclotron, the structure of nuclei is being studied with pickup reactions and inelastic scattering of protons, and the details of energy levels in neutron-deficient isotopes are being analyzed in the rare-earth region. An optical model search program is being used in theoretical studies related to these experimental programs. The 86-Inch Cyclotron continues to be the chief source for neutron-deficient isotopes, now being produced for commercial processors.

Fixed-frequency acceleration of electrons to kinetic energies comparable to their mass equivalent was achieved in Electron Analogue II. The successful operation of this 8-sector electron cyclotron fully confirms the orbit studies and construction techniques. This demonstrates the feasibility of an 800 to 1000 Mev proton accelerator for which conceptual designs are being prepared.

The high-field 2-in. ID solenoid was completed and now operates with steady magnetic fields in excess of 100 kilogauss. It is being used in studies of the properties of superconductors, such as the niobium-zirconium alloys. At 4°K a model magnet with 5000-turns of Nb-Zr produced a self field of 32 kilogauss before the superconductor returns to the resistive state.

Fabrication and installation of the Oak Ridge Isochronous Cyclotron (ORIC) is approaching completion. This versatile three-sector AVF machine is being readied for a period of test operation at a reduced power level before being operated at design level, 1 ma of 75-Mev protons or 100-Mev nitrogen ions.

Note added in proof: ORIC was first test operated on March 18, 1962; with a temporary rf power supply an 8-Mev proton beam was obtained at full radius. The low voltage required on the dee, 13 kv, indicates that the protons remain in phase and in focus for at least 300 orbits. Very little adjustment of the magnet currents from the calculated values was required. A program of test operation at limited energy will be undertaken to test the cyclotron component systems, to determine the performance characteristics, and to obtain data needed for completion of the deflector and ion optics system.

Contents

SUMMARY iii

1. HEAVY-PARTICLE PHYSICS 1

Transfer Reactions 1
- $B^{10}(N^{14},O^{15})Be^{9}$ Ground States 2
- $B^{10}(N^{14},C^{13})C^{11}$ Ground States 3
- $B^{11}(N^{14},C^{13})C^{12}$ Ground States 3
- $Mg^{24}(N^{14},N^{13})Mg^{25}$ 3
- $B^{10}(N^{14},N^{13})B^{11}$ 5
- $B^{10}(N^{14},C^{13})C^{11}$ 5
- Nucleon Transfers from Cl^{35} 5

Angular-Momentum Effects in Nitrogen-Induced Reactions 6

Differential Cross Sections of the $Li^{6}(N^{14},\alpha)O^{16}$ and $Li^{7}(N^{14},\alpha)O^{17}$ Reactions 10

The Capture Reaction $N^{14} + P^{31} \rightarrow Ti^{45} + \gamma$ 11

2. PHYSICS RESEARCH WITH 22-Mev PROTONS 12

Nuclear-Reaction Experiments 12

Nuclear Levels in Er^{165} 15

Instrumentation and Data Handling 20

3. NUCLEAR REACTION THEORY 22

Optical-Model Search Program 22
- Direct Nuclear Reactions 22
- Alpha-Particle Reaction Cross Sections 23
- Deuteron Elastic Scattering 23
- Heavy-Ion Scattering 25

4. APPLIED PHYSICS PROGRAM 27

5. CYCLOTRON OPERATION 30

Operation of the 63-Inch Cyclotron 30

Operation of the 86-Inch Cyclotron 31

6. ACCELERATOR DEVELOPMENT 32

Cyclotron Analogue II 32
- First Operation 33
- Energy Measurements 35
- Future Work 35

The Mc^2 Isochronous Cyclotron 36
Research Program for Mc^2 Cyclotron 36
Experiment Areas 38
Magnetic Field Study 38
Radio-Frequency Cavities 39
Magnet 40
Vacuum System 42
Cyclotron Building 42

7. MAGNET STUDIES 44

High-Field Solenoid 44

Cryogenic Electromagnets 46
Superconducting Materials 46
Model Superconducting Magnets 48
Magnet Design 49

Bubble-Chamber Study 49

8. THE OAK RIDGE ISOCHRONOUS CYCLOTRON 52

The ORIC Magnetic Field 52
Magnet Installation 52
AVF Coils 53
Field Measuring Program 54
Data Processing and Orbit Studies 57

The ORIC Resonator and Radio-Frequency System 59
The Resonator 60
The Oscillator and RF Drive 61

ORIC Control System 63
Cyclotron Control System 64
Personnel Radiation Protection 64
Equipment Protection 65
Patch Panels for Experimenters 65

PAPERS PRESENTED AT SCIENTIFIC AND TECHNICAL MEETINGS 66

PUBLICATIONS 68

ADVISORY COMMITTEE 69

RESEARCH CONSULTANTS 69

MISCELLANEOUS ACTIVITIES OF THE ELECTRONUCLEAR DIVISION 70

DIVISION RESEARCH SEMINARS 72

1. Heavy-Particle Physics

M. L. Halbert E. Newman K. S. Toth
A. Zucker J. W. Wachter[1] Bruno Linder[2]

During the past year new results were obtained on the angular and energy distributions of transfer reactions, transfer reaction systematics, the effect of angular momentum on the statistical model of the nucleus, and the angular distribution of alpha particles which result from a direct-reaction mechanism of N^{14} with Li^6 and Li^7. The total cross section of the reaction $N^{14} + P^{31} \rightarrow Ti^{45} + \gamma$ was measured.

The ORNL 63-Inch Cyclotron, which was the accelerator used by the heavy-particle physics group for the past nine years, was shut down permanently on October 31, 1961. While waiting for the Isochronous Cyclotron to become operational, the group will use heavy ions produced by the new tandem accelerator.

TRANSFER REACTIONS

The study of single-nucleon transfer reactions, both neutron and proton, has continued. Essentially, two methods were used to measure the differential cross sections.

To study the angular distribution of proton-transfer reactions the basic two-detector coincidence system of Halbert and Zucker[3] was modified to include one additional criterion on the scattered particle. This addition was necessary because of the small positive Q values and the large elastic-scattering counting rates from target impurities; combined, these could produce confusion in certain angular ranges. In a proton-transfer reaction the outgoing particle is of different nuclear charge than the elastically scattered N^{14}. A measurement of the specific ionization dE/dx, together with the kinematic criteria, makes it possible to eliminate virtually all the counts due to elastic scattering. To incorporate the added selectivity into the existing system, the defining counter was replaced by a proportional counter and surface-barrier detector combination.[4] The output of the proportional counter was then used to provide information on the charge of the scattered particle. Figure 1.1 illustrates the separation of various elements in a typical dE/dx vs E oscilloscope picture.

[1]On leave from Y-12 Plant, Union Carbide Nuclear Co., Oak Ridge, Tenn.

[2]Summer Employee, Florida State University, Tallahassee.

[3]M. L. Halbert and A. Zucker, *Phys. Rev.* 115, 1635 (1959).

[4]*Electronuclear Research Div. Ann. Progr. Rept. Jan. 16, 1961*, ORNL-3083, p 11.

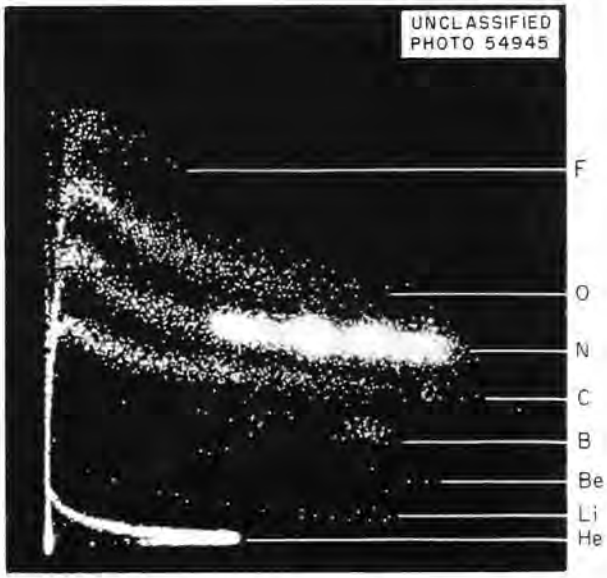

Fig. 1.1. A Typical Picture of dE/dx vs E from the Defining Counter at a Laboratory Angle of 30°.

$B^{10}(N^{14},O^{15})Be^9$ *Ground States*

The effect of the various coincidence gates on the reaction $B^{10}(N^{14},O^{15})Be^9$ *ground states* at a laboratory angle of 12° is shown in Fig. 1.2. At the top is the spectrum from the ungated defining counter. The pulse height of the elastically scattered N^{14} is peaked in channel 120, and the O^{15} spectrum is expected to be centered in channel 99. The center spectrum illustrates the effect of gating with the recoil counter only; the recoil counter was positioned so as to detect the recoiling Be^9. The elastic peak is reduced substantially (a factor of ~40), and the transfer peak may be seen at the left. The lowest spectrum in the figure illustrates the effect of the charge state combined with kinematical criteria. The elastic background is reduced to almost zero, and the peak corresponding to the ground-state transfer stands clearly defined.

In order to check the operation of the system, the differential cross section for the reaction $B^{10}(N^{14},O^{15})Be^9$ *ground states* was remeasured.[5] The upper curve of Fig. 1.3 shows the results. The points designated by circles were taken by recoil coincidence technique only, the squares by recoil-plus-charge identification. The agreement is excellent. The integrated cross section for the ground-state transfer is 1.34 ± 0.30 mb. The transfer cross section to all states for this reaction may be estimated from the "universal" curve[6] to be about 5 mb.

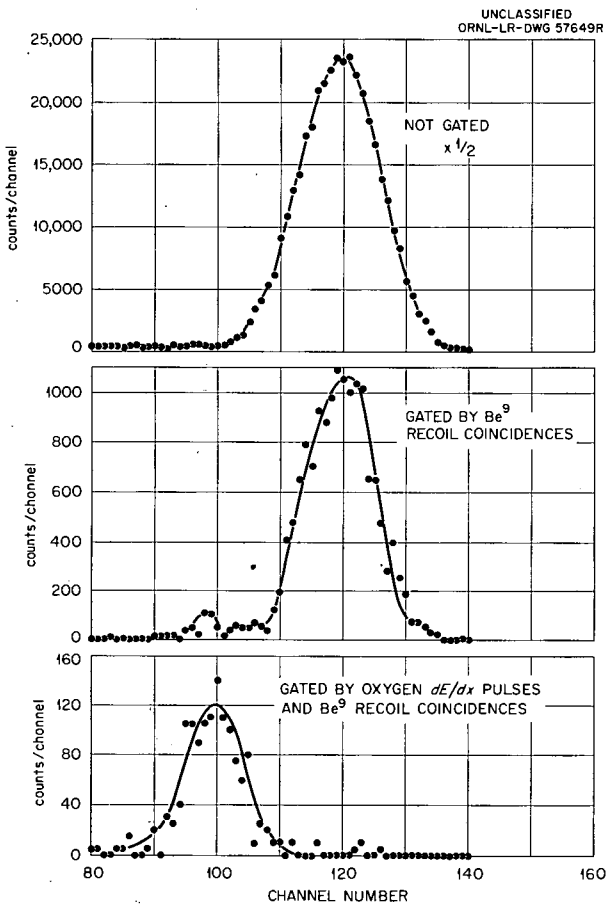

Fig. 1.2. Coincidence-Gated Spectra of the Defining Surface-Barrier Counter at a Laboratory Angle of 12°. Reading from top to bottom, the spectra represent an ungated run, gated by Be^9 recoils only, and gated by recoil-plus-charge selection. The O^{15} peak from the ground-state transfer $B^{10}(N^{14}, O^{15})Be^9$ is seen to the left of the N^{14} elastic peak in the gated spectra.

---

[5] *Electronuclear Research Div. Ann. Progr. Rept. Jan. 16, 1961*, ORNL-3083, p 4.

[6] M. L. Halbert *et al.*, *Phys Rev.* **106**, 251 (1957).

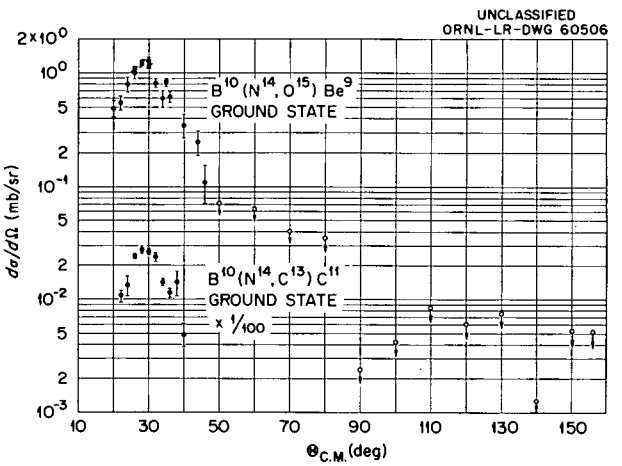

Fig. 1.3. Upper Curve Is the Differential Cross Section for the Proton-Transfer Reaction $B^{10}(N^{14}, O^{15})Be^9$ *Ground States.* Points designated by circles were taken by the recoil coincidence method only, squares with recoil-plus-charge identification. Open points are upper limits of the cross section. Lower curve is the differential cross section for the proton transfer $B^{10}(N^{14}, C^{13})C^{11}$ *ground states.* All data were taken with the recoil-plus-charge identification technique.

$B^{10}(N^{14},C^{13})C^{11}$ *Ground States*

In the reaction $B^{10}(N^{14},C^{13})C^{11}$ *ground states* the incident N^{14} ion loses a proton to the B^{10} nucleus. The Q value is +1.142 Mev.[7] The lower portion of Fig. 1.3 is a plot of the differential cross section as a function of the center-of-mass angle Θ. The cross section reaches a peak of 2.78 mb/steradian at an angle of about 28°. The integrated ground-state cross section for this reaction is 2.19 ± 0.49 mb. The cross section for all states has been measured to be about 4.5 mb at an incident ion energy[8] of 27 Mev. As in the case of the proton transferring to the incident N^{14}, it is seen that excited-state transfers must contribute appreciably to the total transfer cross section.

$B^{11}(N^{14},C^{13})C^{12}$ *Ground States*

To determine the effect of the Q value on ground-state cross sections and on angular distributions, the reaction $B^{11}(N^{14},C^{13})C^{12}$ *ground states* was studied. The Q value for this reaction is very large, namely, +8.407 Mev.[7] Because of this high Q a large portion of the angular range could be investigated without coincidence requirements. No counts with the correct pulse height were detected which could be unambiguously assigned to this reaction in the angular region from 4 to 60° (c.m.). An upper limit for the cross section is placed at 25 μb/steradian. Integrating this value from 0 to 180° gives a total ground-state cross section of <300 μb.

When the angular distributions are replotted as $d\sigma/dR_{min}$ vs R_{min} (ref 5), both observed reactions peak at a value of $r_0 = 2.15 \pm 0.1$ fermis, where

$$R_{min} = r_0(A_1^{1/3} + A_2^{1/3}) \ .$$

This value is the same as the $r_0 \approx 2.2$ fermis obtained by Toth[9] for ground-state neutron transfers.

Although the tunneling theory of Breit[10] does not include any possible effect of the Coulomb field on a transferring proton, the experimental data were compared with the predictions of the theory. The fit is indeed good, much more closely reproducing the initial slope of these angular distributions than for neutron transfers.

The second method of detection consists in stopping one of the reaction products, which is radioactive, in an array of catchers arranged so that the angular increment encompassed by each catcher is known. The catchers are then counted in shielded, calibrated Geiger counters, and the reaction product is identified by its characteristic half-life. The reaction products are also range-analyzed by varying the amount of absorber placed between the catchers and the target.

$Mg^{24}(N^{14},N^{13})Mg^{25}$

The angular distribution and ranges of N^{13} (10-min half-life) nuclei resulting from the reaction $Mg^{24}(N^{14},N^{13})Mg^{25}$ ($Q = -3.22$ Mev) were determined at a bombarding energy of 27.5 Mev. The data were then compared with those obtained[11] for the reaction $Mg^{25}(N^{14},N^{13})Mg^{26}$ ($Q = 0.57$ Mev) at the same bombarding energy to see the effect of Q value on angular distributions and on the population of final states in the residual nuclei. The N^{13} angular distributions were similar in appearance, though the Mg^{24} target data peaked at a center-of-mass angle approximately 10° less than for the reaction involving Mg^{25} as the target. The N^{13} integral range curves were replotted as a function of Q value (Fig. 1.4); it can be seen that the bulk of N^{13} particles have ranges corresponding to similar values of Q for both reactions. In fact, states up to 7 Mev in excitation in Mg^{26} contribute significantly to the transfer cross section, while in Mg^{25} states, only those up to about 4 Mev seem to participate in the transfer process. The explanation of this result may be related simply to the density of excited states, there being more low-lying excited states in an odd nucleus than in an even one.

The final-state populations for the two magnesium reactions indicate that ground-state transfers are unimportant and that excited-state transfers predominate, in contrast to data[12,13] obtained at

---

[7] F. Everling *et al.*, *Nuclear Phys.* 18, 529 (1960).

[8] H. L. Reynolds, D. W. Scott, and A. Zucker, *Phys. Rev.* 102, 237 (1956).

[9] K. S. Toth, *Phys. Rev.* 121, 1190 (1961); *Phys. Rev.* 123, 582 (1961)

[10] G. Breit, pp 1–15 in *Reactions Between Complex Nuclei. Proceedings of the Second Conference on Reactions Between Complex Nuclei, May 2–4, 1960, Gatlinburg, Tennessee*, Wiley, New York, 1960.

[11] M. L. Halbert and A. Zucker, *Phys. Rev.* 108, 336 (1957).

[12] K. S. Toth, *Phys. Rev.* 123, 582 (1961).

[13] E. Newman, to be published in the *Physical Review*.

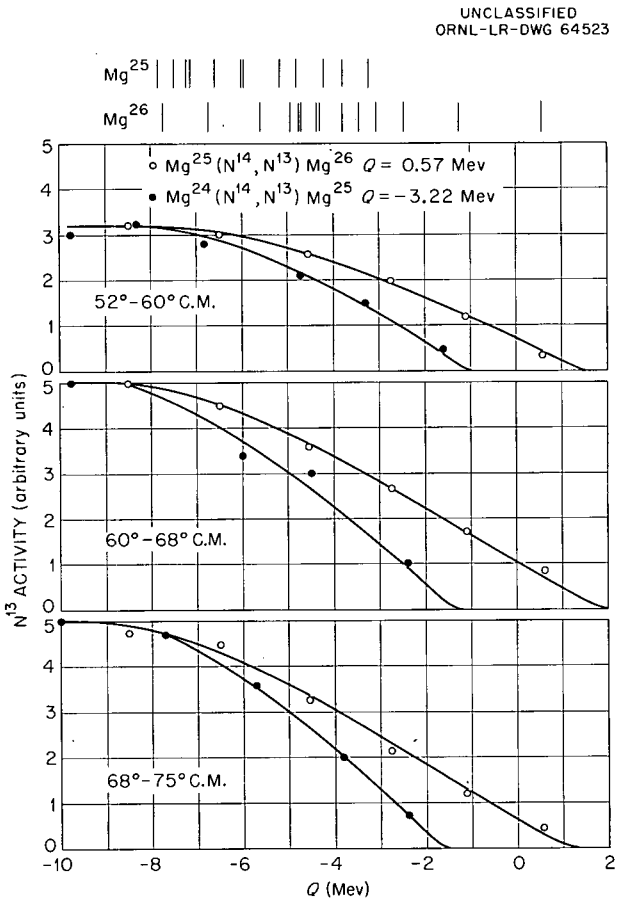

Fig. 1.4. Integral N^{13} Range Curves for Mg^{24} and Mg^{25} Targets at Three Angular Increments. The curves represent N^{13} activity plotted as a function of excitation in the residual nuclei Mg^{25} and Mg^{26}; this excitation is expressed as Q for the reactions. The two sets of data have been arbitrarily normalized to make the curves level off at the same N^{13} activity. The Mg^{25} and Mg^{26} level schemes are shown in terms of the Q values corresponding to neutron transfers to the various levels.

the same N^{14} incident energy but on targets of lower Z number, that is, N^{14} and B^{10}. The latter results show that at a bombarding energy of 27.5 Mev, approximately half the transfers leave both residual nuclei in their ground states. The difference in final-state population does not seem to be due to a Q-value effect because Q for $Mg^{25}(N^{14},N^{13})Mg^{26}$ is comparable to the Q's for the reactions involving N^{14} and B^{10} targets. These Q's range from 0.29 to 1.14 Mev. The explanation seems to be that as the bombarding energy is kept constant while the target Z number is increased, the term $(E_{c.m.} - E_{barrier})$ decreases, so that, effectively, the $E_{c.m.}$ is lowered either by decreasing the bombarding energy or by increasing $E_{barrier}$. Indeed, the effect noted here is the same as that noted in the study[9] of the reaction $N^{14}(N^{14},N^{13})N^{15}$; when the bombarding energy was lowered it was found that the ground-state transfer cross section decreased, while excited-state transfers increased in importance.

The angular distribution data for both magnesium reactions were replotted as $d\sigma/dR_{min}$ vs R_{min} (Fig. 1.5). The values of R_{min} can be related to the parameter r_0 by the formula

$$R_{min} = r_0(A_1^{1/3} + A_2^{1/3}) .$$

The values of r_0 are in this way found to be about 1.6 and about 1.55 fermis for Mg^{24} and Mg^{25} data respectively. The lines, drawn normalized to the experimental points, have slopes calculated from the tunneling theory of Breit.[10] It is seen that the experimental points lie on a line with less slope than the calculated one.

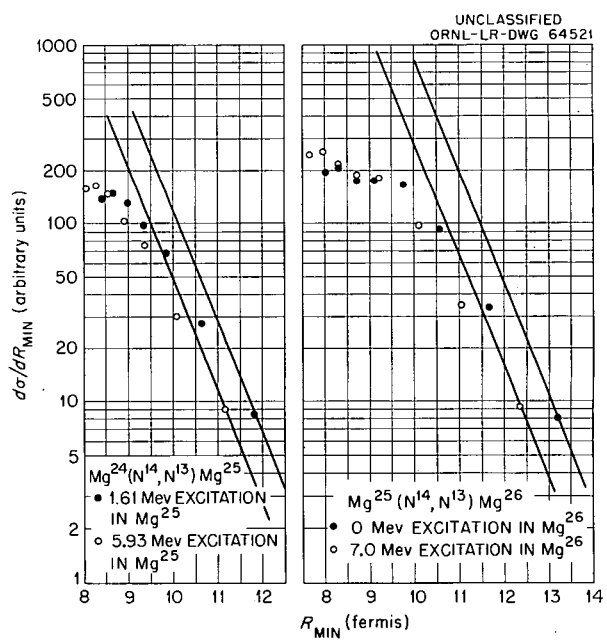

Fig. 1.5. Angular Distribution Data of Fig. 1.2 Plotted as $d\sigma/dR_{min}$ vs R_{min}. The lines, normalized to the experimental points, are drawn with slopes calculated from the tunneling theory of Breit.

$B^{10}(N^{14},N^{13})B^{11}$

The N^{13} angular distribution and ranges were obtained for the reaction $B^{10}(N^{14},N^{13})B^{11}$ at two bombarding energies, 27.5 and 19.5 Mev. The experimental data corroborated all the main points deduced from the results[9] for the reaction $N^{14}(N^{14},N^{13})N^{15}$. First, at 27.5 Mev the ground-state transfers accounted for about half the total transfer cross section; when the bombarding energy was lowered, the ground-state transfer cross section decreased, while the excited-state transfers became predominant. Second, excited-state transfers were detected at angles larger than those at which ground-state transfers were observed. Third, the r_0 determined for ground-state transfers was >2.0 fermis, in good agreement with r_0's of 2.2 fermis determined for other reactions where both residual nuclei were left in their ground states.

$B^{10}(N^{14},C^{13})C^{11}$

In the reaction $B^{10}(N^{14},C^{13})C^{11}$ the C^{11} nucleus, which has a 20-min half-life, is the recoil particle. The angular distribution and ranges of the C^{11} particles were investigated at bombarding energies of 27.5, 19.5, and 14.0 Mev for laboratory angles <55°. The angular range is limited by the fact that at angles >55° the C^{11} kinetic energy is small and the particle is stopped in the target. When the bombarding energy was lowered, the peak of the C^{11} angular distributions shifted to smaller angles, as expected for the recoil particle. The C^{13} distribution peak shifts, of course, to larger angles. Also, at a bombarding energy of 27.5 Mev no C^{11} nuclei resulting from transfers leaving both the C^{11} and C^{13} in their ground states were detected at the angles measured. This result agrees with the data (presented above) obtained for the same reaction with silicon-barrier detectors.

Nucleon Transfers from Cl^{35}

As is well known for neutron transfers where the nucleon is transferred from the incident N^{14} nucleus to the target nucleus, the cross sections when plotted against E^* fall on a "universal" curve.[14] The quantity E^* is given by

$$E^* = E_{c.m.} - E_{barrier} + Q$$

[14] M. L. Halbert *et al.*, *Phys. Rev.* **106**, 251 (1957).

A program was undertaken to measure thick-target transfer excitation functions in which the nucleon was transferred from the target nucleus to the projectile. A primary objective of this investigation was to see whether the cross sections for these reactions fell on the universal curve.

After a thick target was bombarded, the material was placed on an NaI(Tl) scintillation spectrometer. In the case of the proton-transfer reactions the positions emitted by O^{15} (2.1 min) were detected by means of their annihilation radiation. For neutron transfers, since N^{15} is stable, only those reactions could be studied in which the target nucleus was transformed into a radioactive species. The decay of a characteristic gamma ray of this species was then followed. The bombarding energy was varied by the interposition of nickel absorbers.

Figure 1.6 presents the cross section plotted against E^*. The open and closed circles represent the neutron and proton transfers respectively. The cross-hatched area indicates the general shape of the universal curve of ref 14. As may be observed, the universal curve drops much too rapidly at low

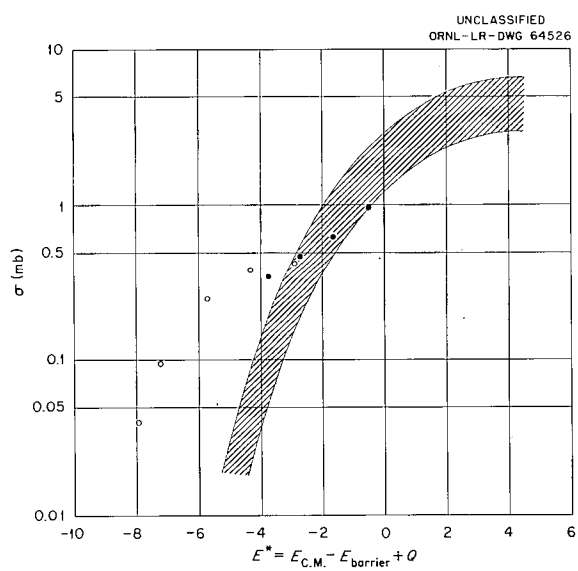

Fig. 1.6. Cross Section vs E^* for Two Transfer Reactions. The open and filled circles represent the neutron and proton transfers respectively. The cross-hatched area indicates the general shape of the universal curve of ref 14.

energies to reproduce the present data. Since this effect is present for both the neutron and proton transfers, it cannot be explained as being due to Coulomb effects.

One possible explanation is as follows: Toth[9] has found that for neutron transfers in the N^{14} + N^{14} system as the bombarding energy is lowered, the reaction proceeds preferentially to excited states. The universal curve was arrived at by studying neutron transfers in which N^{13} was the detected particle. Almost all the N^{13} detected was formed in its ground state, since excited states are unstable with respect to charged-particle decay. This could lead to an apparent decrease in cross section at lower bombarding energies when N^{13} is the detected particle, as opposed to when O^{15} or the residual target nucleus is detected.

ANGULAR-MOMENTUM EFFECTS IN NITROGEN-INDUCED REACTIONS

Ericson and Strutinski[15] showed that the statistical decay of compound nuclei of high angular momentum leads to forward and backward peaking of the evaporated particles; symmetry about 90° is retained. The anisotropy is related to the spin cutoff factor exp $[-j(j+1)/(2\sigma^2)]$ in the level density of the residual nucleus. With a view toward determining σ and other level-density parameters, measurements were made of energy and angular distributions of alpha particles from reactions induced by 28-Mev N^{14} ions. The targets studied included C^{12}, O^{16}, Na^{23}, and Al^{27}.

[15] T. Ericson and V. Strutinski, *Nuclear Phys.* 8, 284 (1958); 9, 689 (1959).

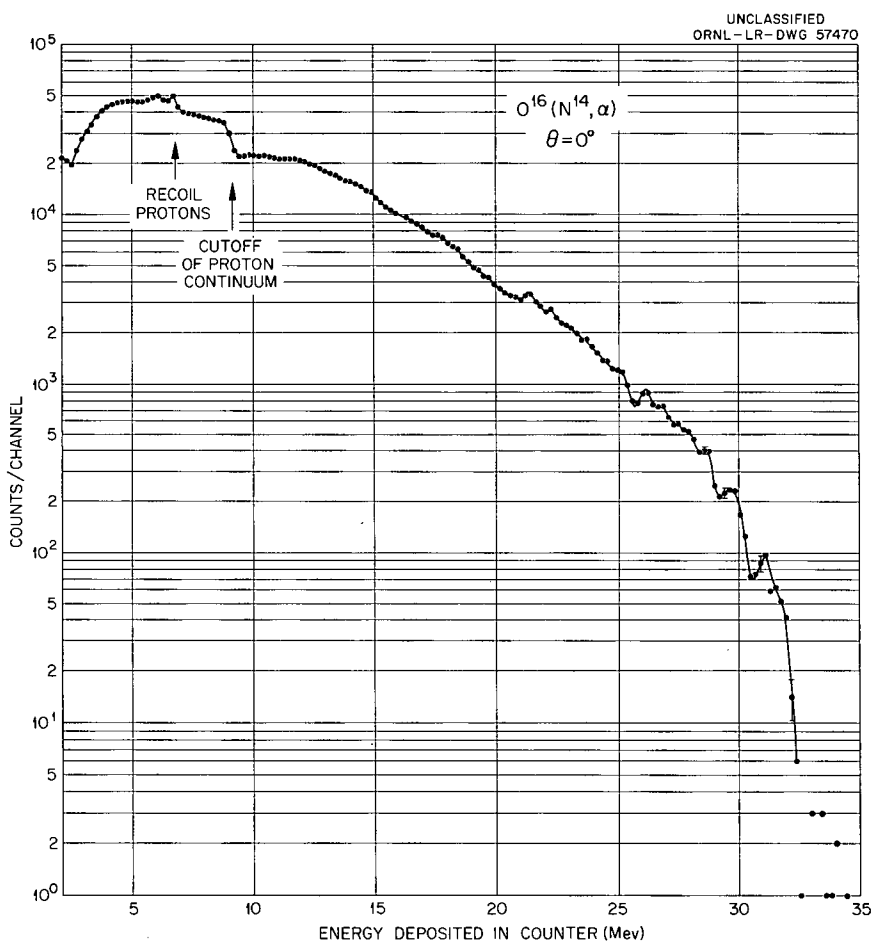

Fig. 1.7. Spectrum of Alpha Particles from Bombardment of Oxygen by 28-Mev N^{14}. The barrier thickness was equal to the range of 9-Mev protons; the proton cutoff is clearly evident.

The alpha particles were detected with a silicon surface-barrier counter of high resistivity (2500 ohm-cm) operated at a bias as high as 600 v, when it was necessary to stop 40-Mev alpha particles. In this thickness of silicon a proton cannot give up more than 10 Mev, so that the portion of the spectra above 10 Mev was free of proton pulses. For many runs the maximum alpha-particle energy was smaller, and the bias was adjusted so that the barrier was just slightly thicker than the range of the highest-energy alpha particles; thus the protons never obscured the upper portion of the alpha-particle spectrum.

Figure 1.7 shows a 0° spectrum for an oxygen target. The marked decrease in the number of alpha particles toward higher energy reflects the rapid change in level density of the residual Al^{26} nucleus as a function of its excitation energy. The bumps are probably due simply to random groupings of Al^{26} levels rather than to a direct interaction. In spectra taken at different angles and bombarding energies, the bumps appear at the same places if the data are plotted as a function of excitation energy.

A spectrum of alpha particles from carbon is shown in Fig. 1.8. Here the structure is very pronounced, each peak corresponding to several close-lying states in the residual Na^{22}. The spectra of alpha particles from sodium and aluminum are smooth and show a very rapid decrease in counting rate as the alpha-particle energy increases. Transitions to the ground state and the first few Mev of excitation in the residual nucleus are so rare that they were not observed.

For each target, similar spectra were obtained at 10 to 15 angles between 0 and 165°. The data were converted by the IBM 7090 to differential cross sections as a function of channel energy. Angular distributions for various channel energies were extracted from these results for the oxygen

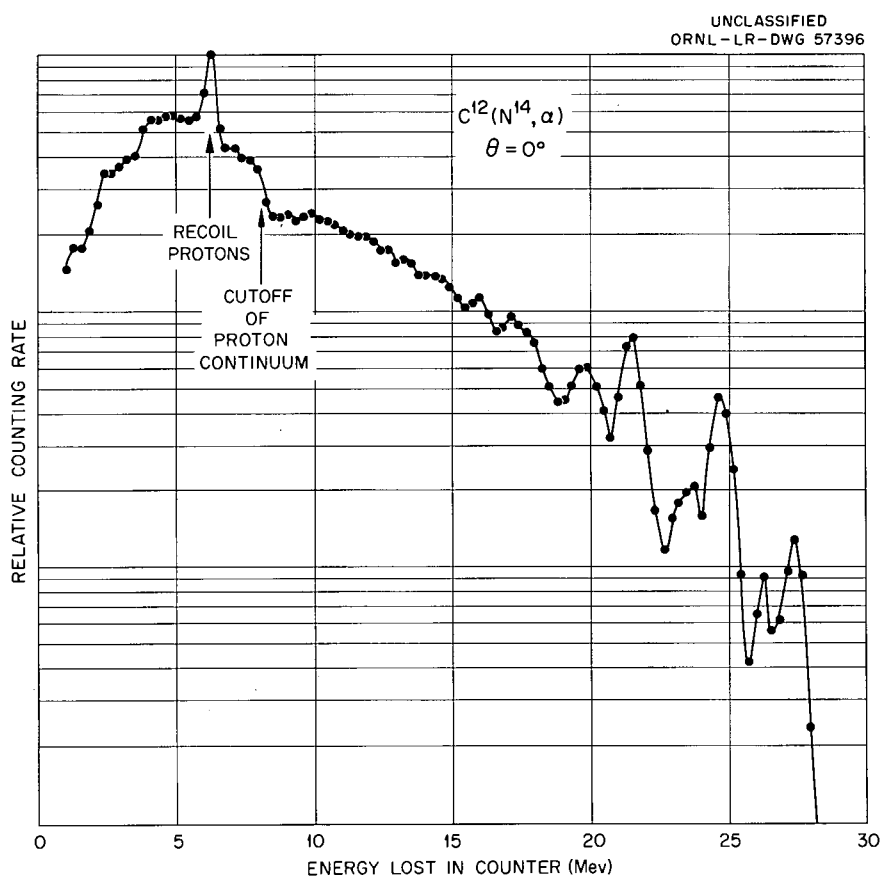

Fig. 1.8. Spectrum of Alpha Particles from Bombardment of Carbon by 28-Mev N^{14}. The bias and hence the proton cutoff are somewhat lower than for the spectrum of Fig. 1.7.

data, and least-squares fits were obtained with Legendre polynomials. This proved to be very laborious. For the remainder of the data a recently completed FORTRAN program will be used to do the arithmetic.

The hand-computed results for alpha particles from oxygen targets are shown in Fig. 1.9. The strong forward-backward peaking with 90° symmetry bears out the Ericson-Strutinski prediction. To obtain a value for the parameter σ, it is necessary to fit the data to this theory (or preferably its quantum counterpart, developed by Douglas and MacDonald[16]). The required computation is, however, very involved. A computer program is being written to calculate the theoretical coefficients of the Legendre polynomials as a function of σ. The best value of σ will then be determined by comparison with the coefficients obtained from the least-squares analysis of the experimental data. The curves in Fig. 1.9 represent least-squares fits to the functions

$$A_0 + A_2P_2\,(\cos\theta)\,,$$

$$B_0 + B_2P_2\,(\cos\theta) + B_4P_4\,(\cos\theta)\,.$$

The corresponding coefficients are given in Table 1.1.

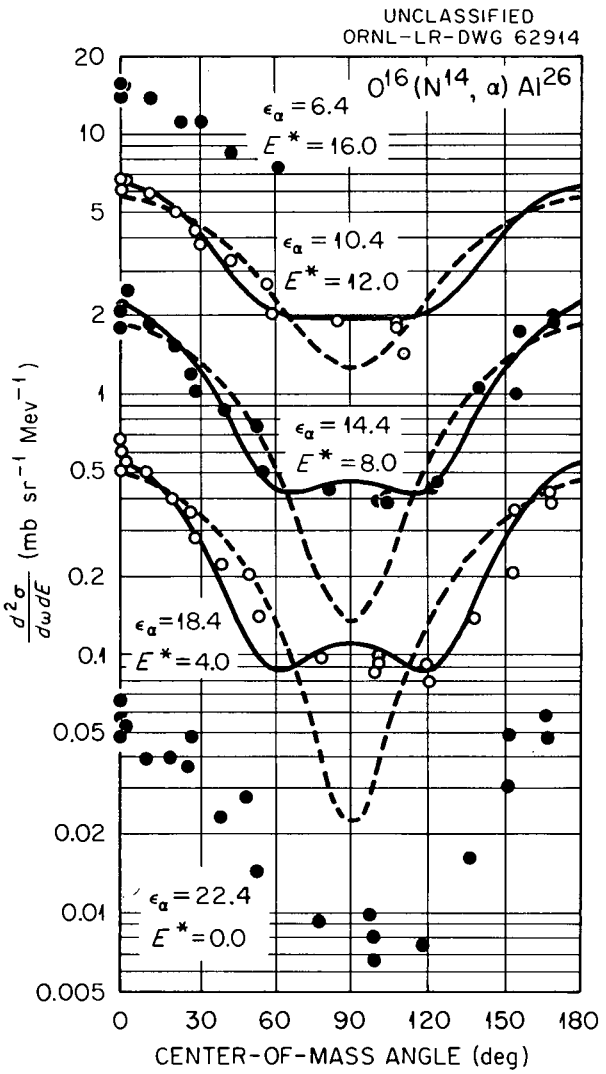

Fig. 1.9. Differential Cross Sections for Alpha Particles from the Bombardment of Oxygen by 28-Mev N^{14} as a Function of Channel Energy ϵ_α or Excitation E^* in the Residual Nucleus. Least-squares fits are shown for $A_0 + A_2P_2$ (cos θ) [dashed lines] and $B_0 + B_2P_2(\cos\theta) + B_4P_4$ (cos θ) [solid lines].

Table 1.1. Least-Squares Fits for Angular Distributions of Alpha Particles from 28-Mev N^{14} on O^{16} as a Function of Channel Energy ϵ_α

ϵ_α(Mev)	A_2/A_0	B_2/B_0	B_4/B_0
18.4	1.75	1.32	1.04
14.4	1.63	1.24	0.77
10.4	1.10	0.93	0.44

Preliminary results indicate that the symmetry about 90° with forward-backward peaking is characteristic of the angular distributions from the other targets as well. As an example, Fig. 1.10 shows the differential cross section for the carbon target summed over the first 3 Mev of excitation in the residual nucleus. The symmetry about 90° is evident out to the largest angle reached in this group of runs.

Effects of final-state angular momentum limitations also show up in the spectrum shape. In particular, the argument which leads to the well-known result[17] for the energy distribution $N(\epsilon)$,

$$N(\epsilon)\,d\epsilon = \text{const}\;\epsilon\sigma_c(\epsilon)\;\omega(E^*)\;d\epsilon$$

[16] A. C. Douglas and N. MacDonald, *Nuclear Phys.* 13, 382 (1959).

[17] J. M. Blatt and V. F. Weisskopf, *Theoretical Nuclear Physics*, p 367, Wiley, New York, 1952.

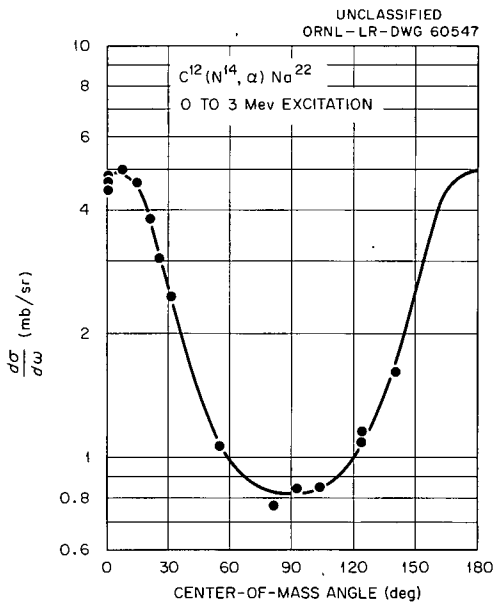

Fig. 1.10. Differential Cross Section for Alpha Particles from the Bombardment of Carbon by N^{14} Summed over the First 3 Mev of Excitation Energy of the Residual Nucleus.

(where ϵ is the channel energy, σ_c is the cross section for the inverse reaction, and $\omega(E^*)$ is the level density of residual nucleus at excitation E^*), fails when the angular momentum is limited. To explore this point, the oxygen data were treated as if the above expression were valid, and the apparent level density was determined at each angle. It was found that all the data would fit a level density of the form

$$\omega(E^*) = C \exp 2\sqrt{a(E^* + 1.0)} \ .$$

A constant-temperature level density was definitely ruled out. Examples of the fits are shown in Fig. 1.11; the parameter a in each case is unique within ± 0.1 Mev^{-1}. The best fits were sometimes difficult to establish because of uncertainty in how to treat the data above the threshold for second alphas, but it was nevertheless clear that a increased steadily from about 1.1 Mev^{-1} at 0° to about 1.6 Mev^{-1} at 90°, and decreased beyond 90°. This is, of course, not a real variation in level density but rather a demonstration of the breakdown of the simple expression

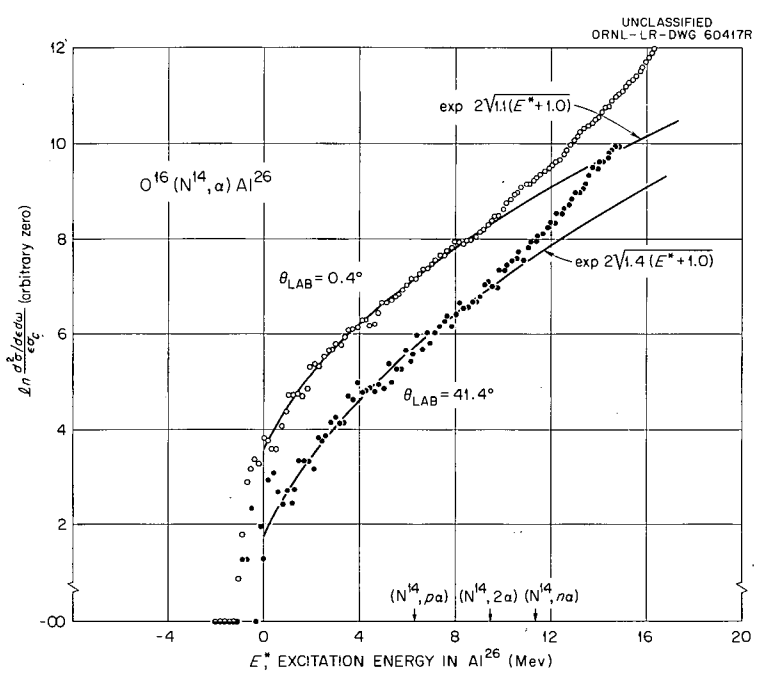

Fig. 1.11. Apparent Level Density of Alpha Particles from the Bombardment of Oxygen by N^{14}. The arrows indicate the thresholds for reactions in which the observed alpha particle may be the second particle emitted from the compound nucleus.

assumed for $N(\epsilon)$. The same result is evident from Fig. 1.9, in that the anisotropy decreases with excitation energy in Al^{26}.

DIFFERENTIAL CROSS SECTIONS OF THE $Li^6(N^{14},\alpha)O^{16}$ AND $Li^7(N^{14},\alpha)O^{17}$ REACTIONS

The angular distributions of alpha particles from the bombardment of Li^6 and Li^7 by 27.6-Mev nitrogen ions were measured with the 63-Inch Cyclotron. Isotopically enriched lithium targets were prepared by evaporating metallic lithium onto 0.000002-in.-thick nickel backings. To avoid chemical contamination, targets were prepared in an evaporation chamber mounted on the cyclotron scattering chamber and were moved remotely into the target position. For the same reason, remotely controlled foil changers were employed at the particle detectors to permit aluminum absorbers to be changed while under vacuum. The target thickness was estimated to be $\sim 200\ \mu g/cm^2$ from the energy loss of the nitrogen beam; it was monitored by elastic-scattering measurements. Both alpha and recoil particles were detected by silicon surface-barrier diodes and were counted in coincidence by a technique described previously.[18] For Li^6, the measurements included only reactions in which the O^{16} was left in the ground state; for Li^7, only those leading to the ground state or 870-kev excited state of O^{17} were included.

The differential cross sections for these reactions are shown in Figs. 1.12 and 1.13. Measurements in the backward direction, 90 to 135° (c.m.), were obtained by the coincidence technique; those in the forward direction were based on measurement of the alpha particles alone, since in this range the alpha-particle energies of 28 to 40 Mev exceed those of most competing reactions from target contaminants. In each case the measured yield was normalized to the yield at 75° c.m., and the limit strikes denote the probable error (LE = 0.50) of the resultant relative cross section.

The cross sections for both isotopes are qualitatively similar at the forward angles, except that a subsidiary peak at about 45° c.m. in Li^6 appears at $\sim 25°$ c.m. in the Li^7. In the backward direction the broad peak of 25 μb/steradian at 112.5° c.m.

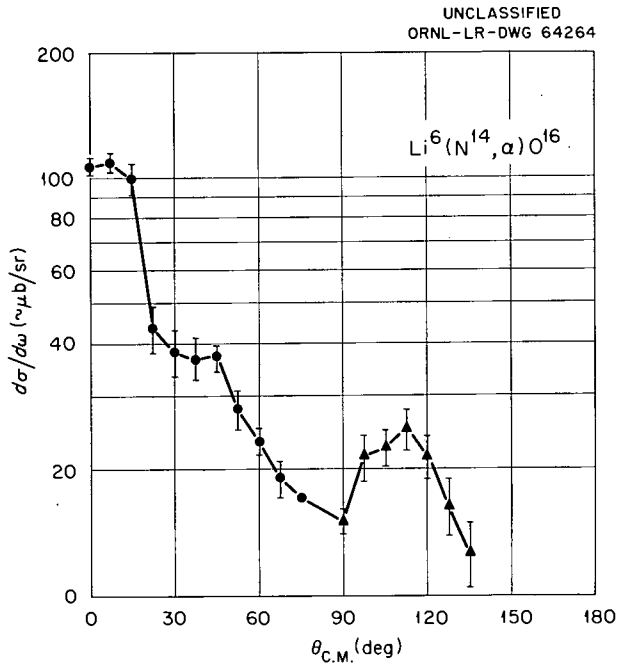

Fig. 1.12. Angular Distribution of Alpha Particles for the Reaction $Li^6(N^{14},\alpha)O^{16}$.

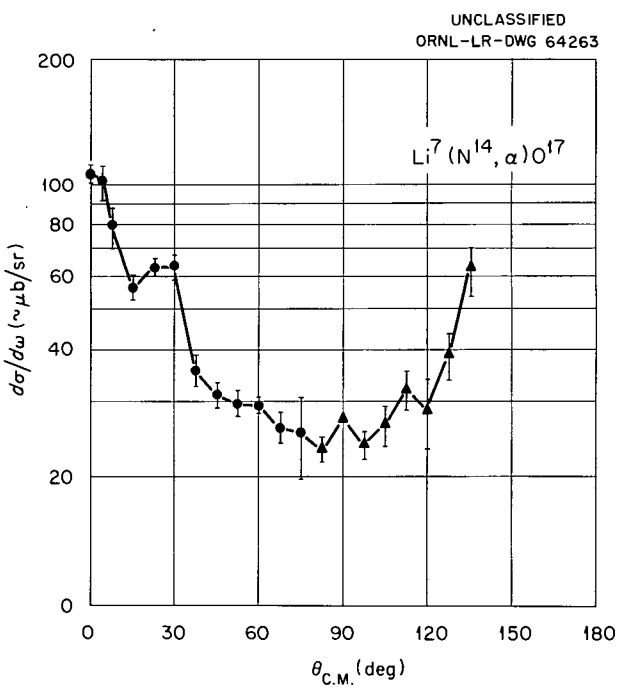

Fig. 1.13. Angular Distribution of Alpha Particles for the Reaction $Li^7(N^{14},\alpha)O^{17}$.

[18] M. L. Halbert and A. Zucker, *Phys. Rev.* 115, 1635 (1959).

for the Li^6 isotope suggests that a classical transfer process may take place. In the Li^7 measurements, which include two residual states of the O^{17} nucleus, the backward peak does not appear, nor is the Li^7 cross section symmetrical at about 90° c.m., as would be expected for an evaporation reaction.

Theoretical calculations of the $Li^6(N^{14},\alpha)O^{16}$ reaction are now in progress in which the "Sally" and "Julie" formulations of the distorted wave approximation are used. Present results suggest that these angular distributions are consistent with the assumption of a deuteron-transfer mechanism.

THE CAPTURE REACTION $N^{14} + P^{31} \rightarrow Ti^{45} + \gamma$

Recently some attempts were made to measure the total cross section for the capture of a complex nucleus by medium-weight nuclei. Upper limits for such reactions have been reported by Coleman *et al.*[19] The total capture cross section for $N^{14} + P^{31} \rightarrow Ti^{45} + \gamma$ at 27 Mev (laboratory) was measured by observing the yield of radioactive Ti^{45} from a thick target of phosphorus. Extensive chemical purification was employed to separate the Ti^{45} from other radioactive products, especially scandium. Auxiliary measurements of Ti^{45} production from the nitrogen bombardment of sulfur and chlorine were used to ascertain the contributions from these impurities.

After all corrections were applied, the total cross section is $\sigma_{capt} = 1.3 \pm 0.7\ \mu b$. The large uncertainty is due primarily to very low yields and difficulties in counting.

Lane and Lynn[20] recently published a paper on the gamma de-excitation in a compound nucleus. Their calculations were extended to include proton and alpha-particle evaporation as well as neutron emission. The results of this calculation give $\sigma_{capt} = 1.5\ \mu b$. The agreement with experiment is excellent, but this should be taken with considerable caution, since many approximations are made in the theory. At any rate, it appears that $E1$ emission is responsible for the gamma de-excitation mechanism, and the Γ_γ is about what would be expected from the bombardment of ground-state nuclei with photons.

---

[19] R. F. Coleman, D. N. Herbert, and J. L. Perkin, *Proc. Phys. Soc.* **77**, 526 (1961).

[20] A. M. Lane and J. E. Lynn, *Nuclear Phys.* **11**, 646 (1959).

2. Physics Research with 22-Mev Protons

C. D. Goodman C. B. Fulmer E. L. Olson
J. B. Ball B. Harmatz D. M. Smith[1]

The physics research program at the 86-Inch Cyclotron has continued along the lines followed in the previous year. The structure of nuclei is being studied with pickup reactions and with elastic and inelastic scattering of protons. The details of energy levels of neutron-deficient isotopes of the rare-earth region are being studied with internal-conversion spectrographs to investigate decay schemes.

NUCLEAR-REACTION EXPERIMENTS

The pickup-reaction experiments are designed to study in detail a sequence of isotopes so that the energy levels observed from the several targets can be interrelated and some interpretation in terms of nuclear models can be discerned. The particular choice of experiments is dictated principally by the availability of targets. For this reason, the projected study of the nuclei between $N = 20$ and $N = 40$ has slowed down after the completion of the experiments with available iron and cobalt isotopes; the study of the region near $N = 50$, which had previously been abandoned for lack of targets, was reactivated with the acquisition of Y^{89} and Nb^{93} targets and a complete set of enriched zirconium isotopes. These are rolled metallic foils, between 1.5 and 7 mg/cm^2 thick. The zirconium targets were obtained from the Isotopes Division and constitute a major advance in target-making technology. The yttrium and niobium foils were obtained from Argonne National Laboratory.

In a (p,d) pickup reaction, the final states of maximum parentage-overlap with the ground state of the target nucleus can easily be found by looking for the strong peaks in the deuteron spectra. For many targets these levels can be interpreted in terms of the j-j coupling shell model; these are the shell-model states of the target with one neutron missing.

In the iron region, significant departures from the j-j coupling model were noted; these were interpreted in terms of a closely related model, the spheroidal-potential shell model of Nilsson.[2]

In the zirconium region the spherical j-j coupling model seems to apply quite well, and the effect of residual interactions, that is, interactions not included in the shell-model potential well, is small but measurable.

The dominant feature of the zirconium isotopes is the filling of the $d_{5/2}$ shell. This is observed in the (p,d) reactions as an increasing cross section for the $d_{5/2}$ pickup group. In Zr^{90}, which has no $d_{5/2}$ neutrons, the group is absent entirely. From Zr^{91} to Zr^{96} the group grows in proportion to the number of $d_{5/2}$ neutrons expected on the basis of the j-j coupling shell model; that is, one $d_{5/2}$ neutron in Zr^{91}, two in Zr^{92}, and so on to six in Zr^{96}. The deuteron spectra for these targets are shown in Fig. 2.1. The $d_{5/2}$ group is the highest-energy group, since the pickup of a $d_{5/2}$ neutron leads to the ground state of the final nucleus in each of these cases.

The differential cross section for the $d_{5/2}$ group in $Zr^{92}(p,d)$ is shown in Fig. 2.2. The solid curve is the cross section for pickup of

[1]Present address: Texas Instrument Company, Dallas, Texas.

[2]S. G. Nilsson, *Kgl. Danske Videnskab. Selskab, Mat.-fys. Medd.* **29**, No. 16 (1955).

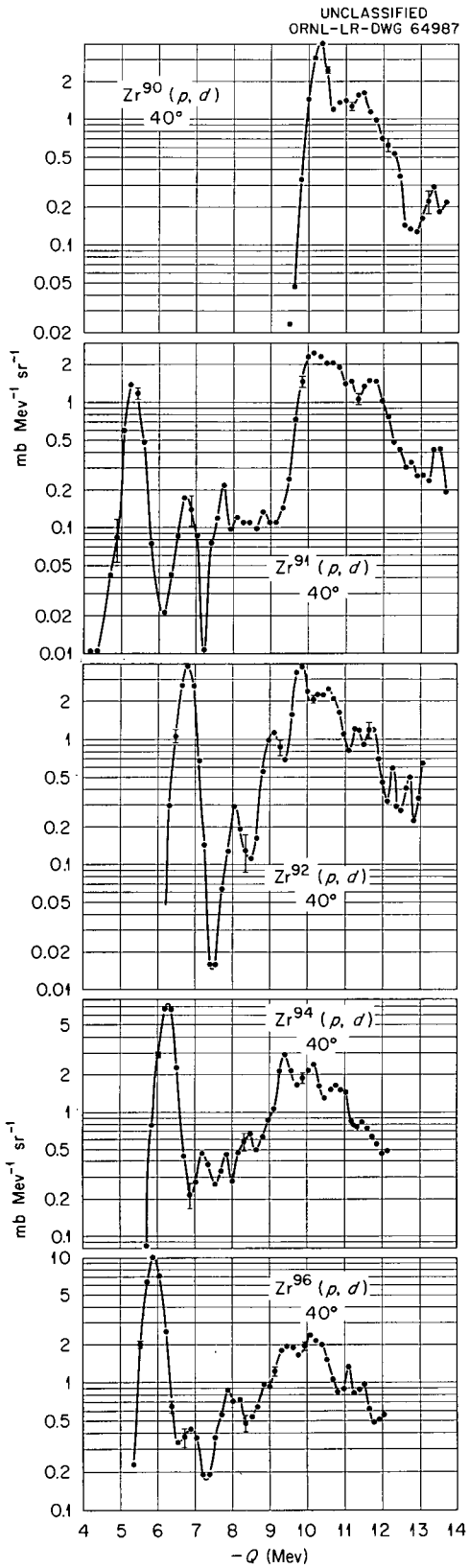

Fig. 2.1. The (p,d) Spectra for Zirconium Isotopes.

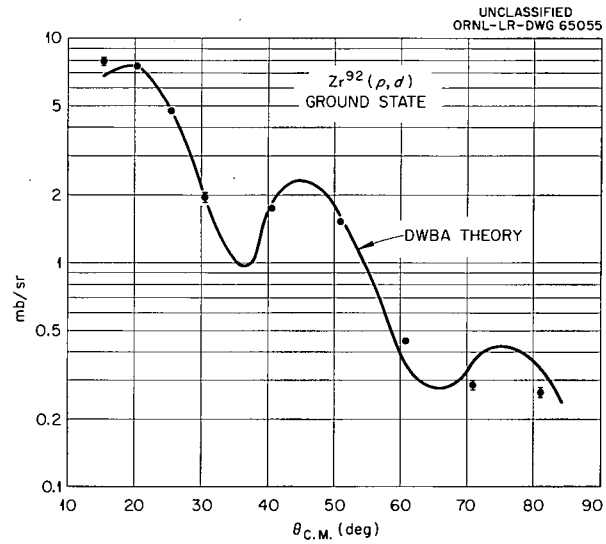

Fig. 2.2. Angular Distribution for $d_{5/2}$ Pickup from $Zr^{92}(p,d)Zr^{91}$.

one $d_{5/2}$ neutron, as calculated from the distorted-wave Born approximation theory. Table 2.1 shows the ratios of the observed cross sections for pickup of a single neutron.

Table 2.1. Relative Cross Sections Observed for $d_{5/2}$ Neutron Pickup from Zirconium Isotope Targets

The $Zr^{96}(p,d)$ cross section has been arbitrarily set equal to 6.0

Target	Relative Cross Section
Zr^{91}	1.6
Zr^{92}	2.1
Nb^{93}	1.9
Zr^{94}	4.0
Zr^{96}	6.0

Peaks in the (p,d) spectra (Fig. 2.1) due to pickup from other filled shells can also be seen. In $Zr^{90}(p,d)$, for example, the ground-state group corresponds to $g_{9/2}$ pickup and the next group to $p_{1/2}$ pickup. These groups are also observable in the other isotopes. The effects of residual interactions can be seen in these spectra. The

difference in Q value for the $d_{5/2}$ pickup in Zr^{91} and in Zr^{92} is the effect of the well-known pairing energy. A similar effect can be seen in the spectra from the odd-proton isotopes Y^{89} and Nb^{93}. In Nb^{93} the pickup of a $d_{5/2}$ neutron can lead to any of the angular momentum states which correspond to coupling of the $5/2$ neutron with the odd $g_{9/2}$ proton. That these states are spread over an energy interval of some 400 kev is evident from the spectrum in Fig. 2.3. In Y^{89} a similar effect is observed as a change in the Q value for the $p_{1/2}$ pickup; the odd proton is in the $p_{1/2}$ shell. Additional evidence for residual interactions is the appearance in the (p,d) spectra of peaks between the $d_{5/2}$ pickup and the $g_{9/2}$ pickup.

A simple picture of a (p,t) reaction is a pickup of a pair of neutrons from a shell-model bound state. On this basis one might expect that the

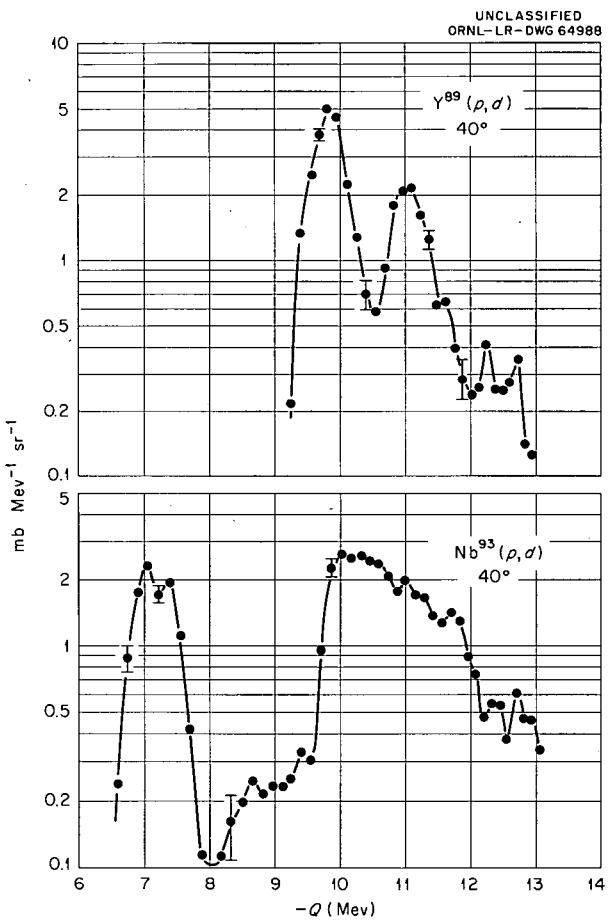

Fig. 2.3. The (p,d) Spectra for Y^{89} and Nb^{93} Targets.

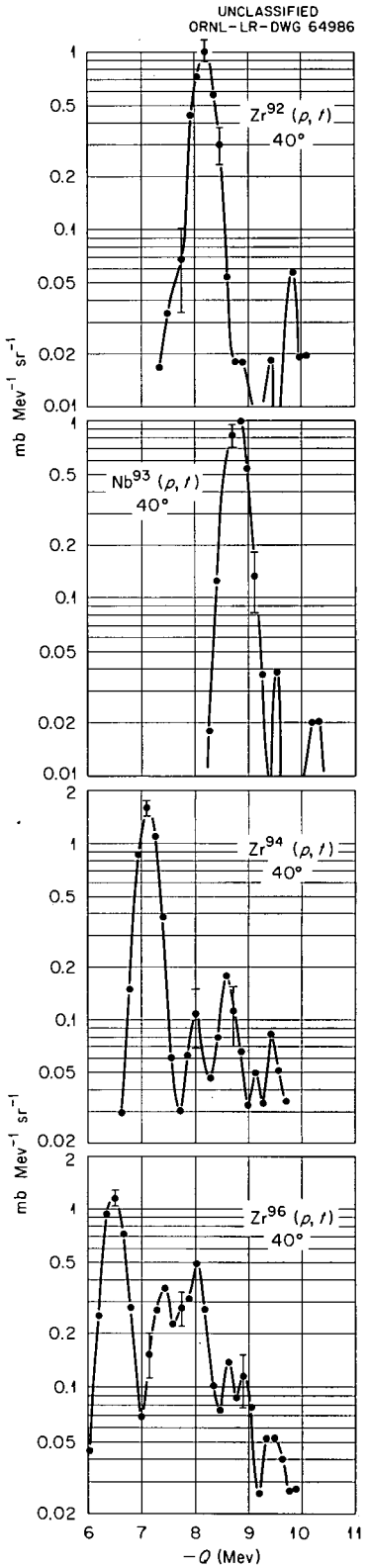

Fig. 2.4. The (p,t) Spectra for Zirconium Isotopes.

cross sections for the ground-state–to–ground-state reactions for Zr^{92}, Zr^{94}, and Zr^{96} would be in the ratios 1:2:3, since the number of pairs of $d_{5/2}$ neutrons should be in that ratio. This is not the case experimentally, as can be seen in Fig. 2.4. Apparently, pickup of two $d_{5/2}$ neutrons from Zr^{94} or from Zr^{96} does not necessarily leave the nucleus in the 0^+ ground state. In fact, in Zr^{96} the probability of exciting states of higher angular momentum is greater than that of leaving the ground state. That the other states are of higher angular momentum is known from the angular distributions of the triton energy groups.

The availability of silicon surface-barrier counters with good resolution for alpha particles has made it possible to examine the alpha-particle spectra from (p,α) reactions. A thin proportional counter was used as a dE/dx counter. Spectra from targets in the iron region and from targets in the zirconium region were examined. A few low-lying levels were resolved. Comparison of the (p,α) cross sections with (p,t) and (p,d) cross sections leading to the same final state indicates that the (p,α) cross section is roughly one-tenth that of the (p,t) reaction and one-hundredth that of the (p,d) reaction.

At excitation energies higher than the resolved energy levels, a forward-peaked continuum is apparent in the spectra. The overall appearance of the spectra suggests that pickup reactions and shell effects play a role similar to that in (p,d) and (p,t) reactions. In medium and light elements a contribution to the alpha-particle spectrum from compound-nucleus evaporation is also apparent.

NUCLEAR LEVELS IN Er^{165}

The electron-capture decay of Tm^{165} (29-hr) to levels in Er^{165} was studied with the internal-conversion electron spectrograph. The thulium activity was produced with 22-Mev protons in the ORNL 86-Inch Cyclotron. Table 2.2 presents the extensive data on transition energies, relative intensities, and multipolarities. The level structure of Er^{165} proposed in Fig. 2.5 incorporates all of the stronger radiation. The criteria employed in constructing the decay scheme include transition energy fits, multipolarities, relative intensities (measured or deduced), consistency of rotational parameters, and feeding and decay branching ratios. Mottelson and Nilsson[3] have made an analysis of intrinsic states for odd-A nuclei in the region of Er^{165} ($N = 97$). They have calculated the energies of the intrinsic states which are characterized by the asymptotic quantum numbers $K\pi[Nn_z\Lambda]$. The level structure of Er^{165} was studied[4] in connection with similar levels occurring in adjacent odd-N nuclei as well as with the predictions of Mottelson and Nilsson.

The parent, Tm^{165}, is most likely in the $\frac{1}{2}^+$ [411] state with a disintegration energy (Q_{ec}) of $\sim$2 Mev, as calculated from β^- decay systematics. In the decay scheme, a 77.2-kev ($E2$) transition is interpreted as a rotational excitation of the ground state ($\frac{5}{2}^-$ [523]). A 30-kev ($E1$) transition may proceed from the 77-kev ($\frac{7}{2}^-$) rotational state to a 47-kev ($\frac{5}{2}^+$) level; the observed branching is 3%. The designation of the 47-kev state as $\frac{5}{2}^+$ [642] is partly based on the intense $E1$ radiation proceeding to ground. The $E1$ multipole assignment is made on the basis of the observed L-subshell ratio. A study[4] of the levels of Yb^{167}, an isotope of Er^{165}, has established the intrinsic $\frac{5}{2}^+$ [642] state at 29.7 kev.

The decay scheme of Er^{165} shows a well-developed rotational band based at 297.2 kev ($\frac{1}{2}^-$ [521]) and preferentially feeding a close-lying band based at 242.7 kev ($\frac{3}{2}^-$ [521]). This is indicative of allowed transitions involving bands having the same asymptotic quantum numbers. Certain regularities appear[4] in the properties of the rotational spectra of $\frac{1}{2}^-$ [521] bands in the region of odd-N numbers 95 to 107. The $M1/E2$ mixing ratios for rotational transitions between $\frac{3}{2} \rightarrow \frac{1}{2}$ states are low (1.6 ± 0.5) except for the case of Er^{167}, where $M1/E2 = 7$. Seven experimental decoupling parameters a for the $K = \frac{1}{2}$ bands exhibit a smooth variation as a function of mass number, indicating a maximum of $+0.85$ for Yb^{171} and a value of $+0.56$ for Er^{165}. The empirical data on the values of B, the correction term for the simple rotational energy relationship, and for $3\hbar^2/\mathcal{J}$, the inertial parameter, are likewise

[3] B. R. Mottelson and S. G. Nilsson, *Kgl. Danske Videnskab. Selskab, Mat.-fys. Skrifter* 1, No. 8 (1959).

[4] B. Harmatz, T. H. Handley, and J. W. Mihelich, *Phys. Rev.* 114, 1082 (1959).

Table 2.2. Conversion-Electron Data for Decay of Tm^{165} (29-hr) → Er^{165}

Transition Energy (kev)	Intensity[a]						Remarks[b]
	K	L_I	L_{II}	L_{III}	M	N	
15.45					~80	20	$E2$
27.75		9	w		w		$M1 + E2$
30.05		3.3	2.3	3.3	w		$E1$
35.2		10	6	8	w		$E1$
47.15		260	< 175[d]	175	d	30	$E1$
53.2		140	50	d	d	14	$M1/E2 = 22$
54.45		~1500	d	d	460	115	$M1$
59.15		8	30	d			$M1/E2 = 1.4$
60.4		135	d	d	33	8	$M1$
70.55	>40	27	2.7	1.3		1.3	$M1/E2 = 140$
77.2	>80	15	190	200	110	22	$E2$
82.25	3.4	~0.7	1	1			$M1/E2 \approx 2$
86.9	w		2.4	<5[d]	1		$E2$
88.2	14	<5[d]			1		
113.6	400	60	6	1.8	14	3.3	$M1/E2 = 100$
141.4	2.5	w					
150.8	7.6	w					
156.0	1.1						
165.5	7.5	c	2[c]	1.9	c		$E2$
175.7	1.2						
181.55	1.2						
195.6	4.9						
197.25	1.0						
205.2	2.7						
209.9	5.0						
218.6	165	25	c	0.8	5.5	<2.9[d]	$M1$
221.5	~2						
223.9	1.2						
233.2	d						
234.6	3.1						
238.4	~3.3	<1.6[d]					
242.7	1270	185			45	12.5	$M1$
248.9	5						
249.7	4.5						

Table 2.2 (continued)

Transition Energy (kev)	Intensity[a]						Remarks[b]
	K	L_I	L_{II}	L_{III}	M	N	
264.4	*d*						
275.6	$< 2.9^d$						
279.1	7	*c*	1.7^c	0.56	1		$E2$
286.1	$< 1.6^d$						
292.3	13	2.2					
293.8	*w*						
295.9	83	*c*			*c*		
297.2	125	$\sim 16^c$	*c*	*d*	8		$E2$
306.9	2.8	*d*					
312.1	10	1.5			0.5		
330.5	2.9	0.4					
346.6	33	5			1.1		$M1$
356.3	22	3.6		~ 0.4	0.9		
365.3	6.2	1					
384.1	1.4	*w*					
389.2	4.5	0.6					
400.2	1.5	*d*					
420.7	1.4	*w*					
426.9	0.5						
429.9	0.4						
442.4	2.2	0.25					
448.1	1.8						
456.0	6.6	0.75					
459.9	11.7	2.1					
471.8	2.0	~ 0.3					
477.7	2.2						
487.0	5.2	0.8					
513.5	1.5						
526.5	2.0	*d*					
530.9	*w*						
542.2	4.8	*d*					
558.3	1.0	$< 0.37^d$					
563.7	8.7	1.3					
573.8	1.2	*d*					

Table 2.2 (continued)

Transition Energy (kev)	Intensity[a]						Remarks[b]
	K	L_I	L_{II}	L_{III}	M	N	
577.3	0.5						
589.4	3.0	0.45					
605.6	<0.37[d]						
608.1	~0.4[c]						
622.8	~0.5[c]						
664.6	1.0	*w*					
677.3	0.33						
680.5	~0.15[c]						
698.6	1.4	<0.4[d]					
747.4	<0.4[d]						
791.0	0.26						
806.8	14	2.1					
821.2	0.18						
826.9	~0.2[d]						
837.7	0.7	0.1					
892.8	0.8						
907.8	*w*						
932.4	0.11						
952.8	0.14						
1045.7	*w*						
1131.0	0.28	0.04					
1184.5	0.44	0.07					
1246.4	*w*						
1379.5	0.16						
1426.9	0.11						

[a]Intensity data are internally consistent; *w* indicates weak line.

[b]Multipole assignments are based on theoretical K/L and L-subshell ratios of M. E. Rose, *Internal Conversion Coefficients*, North-Holland Publishing Company, Amsterdam, 1958.

[c]Conversion line is partially resolved.

[d]Conversion line is a composite of two different lines.

consistent with the rotational interpretation for the postulated $\frac{1}{2}^-$ [521] bands. The presence of both the 242.7-kev ($M1$) and 165.5-kev ($E2$) transitions help to establish the spin and parity of the 242.7-kev level as $\frac{3}{2}^-$.

The next higher levels at 507.1 kev ($\frac{1}{2}^+$) and 589.4 kev ($\frac{3}{2}^+$) are connected by an 82.3-kev transition ($M1/E2 = 2$) of probable rotational character. This band is assigned as $\frac{1}{2}^+$ [651]. Branching ratios between the above states and

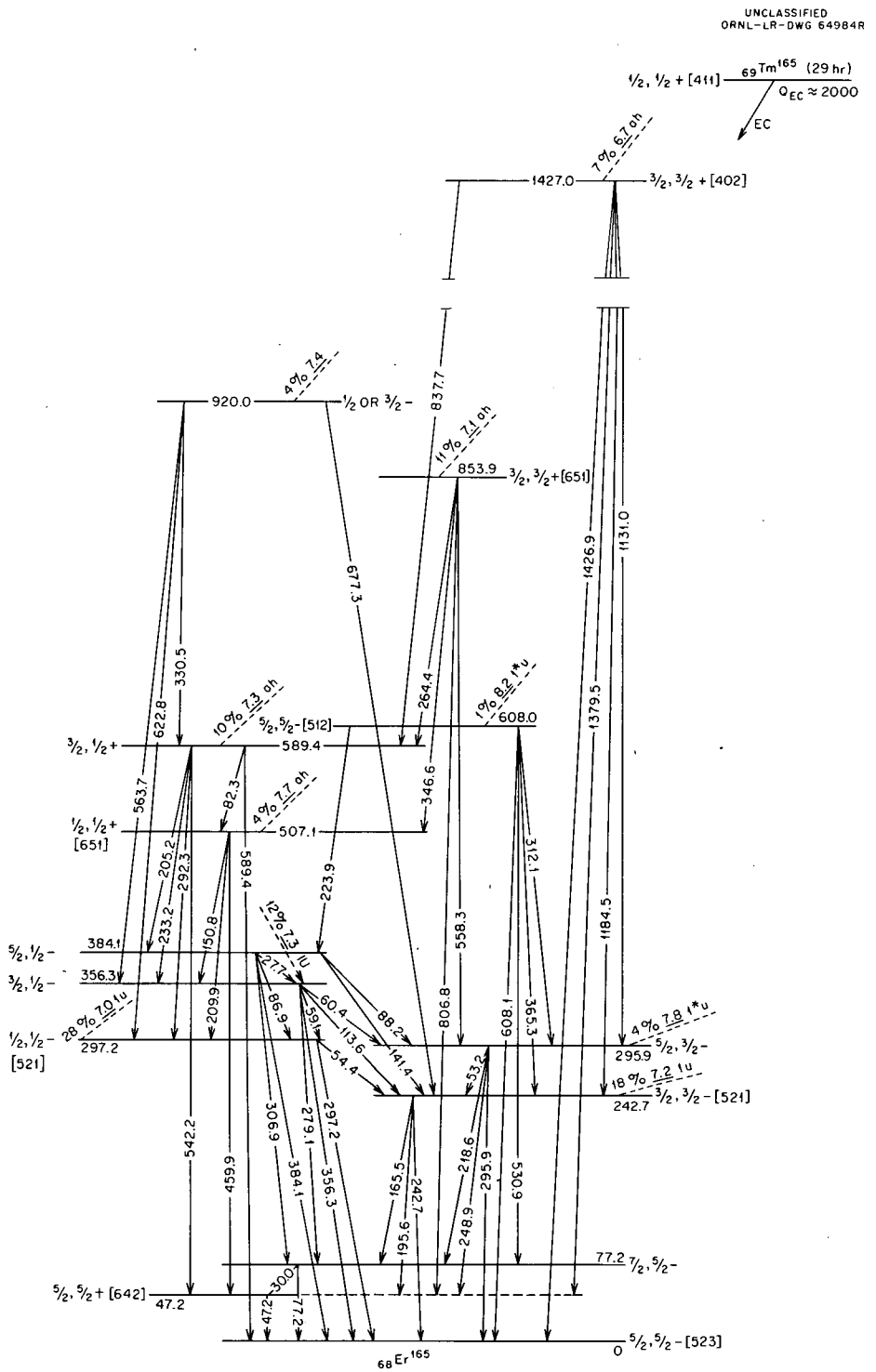

Fig. 2.5. Levels in Er^{165} Populated by Electron-Capture Decay of Tm^{165}. The symbolism used in the designation of intrinsic states is I, $K\pi\,[Nn_z\Lambda]$. Rotational sequences are aligned vertically. All energy values are given in kev. Electron-capture branches are shown by dashed lines, with relative intensities in percent and log ft values underlined. The classification of these branches according to selection rules follows the notation: allowed (a), first forbidden (one), first forbidden unique (one*), hindered (b), and unhindered (u).

the $\frac{1}{2}^-$ [521] band are in fair agreement with theory, where $K_i = K_f = \frac{1}{2}$ and pure dipole radiation is assumed.

A level at 608.0 kev is observed to populate five odd-parity levels of spins $\frac{3}{2}$, $\frac{5}{2}$, $\frac{7}{2}$ and is designated as an intrinsic $\frac{5}{2}^-$ [512] state. Intensity considerations and selection rules[5] indicate that a 1^*u electron-capture branch (log $ft = 8.2$) proceeds to it. For a level at 853.9 kev, an assignment of $\frac{3}{2}^+$ [651] is preferred, representing an intrinsic excitation associated with smaller eccentricity. Under this assumption, the electron-capture branch is ab, with log $ft = 7.1$. The postulation of the 920.0-kev state as $\frac{1}{2}^-$ or $\frac{3}{2}^-$ [510] is consistent with the observed feeding to states of $I \leq \frac{3}{2}$. Electron capture would proceed to it with a $1u$ (log $ft = 7.4$) transition.

The highest level observed is at 1427.0 kev and is assigned as $\frac{3}{2}^+$ [402] with an ab (log $ft = 6.7$) electron-capture feeding. The assignment is supported by the close agreement of experimental and theoretical reduced transition probabilities between the initial $\frac{3}{2}^+$ [402] state and the two members of the $\frac{3}{2}^-$ [521] band.

INSTRUMENTATION AND DATA HANDLING

A growing problem in nuclear-reaction experiments is to be able to handle the quantities of data involved. For example, the yttrium, zirconium, and niobium reaction studies, exclusive of checks and repeats, involved measuring three spectra at each of eight angles for seven targets, 168 spectra in all. Each spectrum contains 100 data points, so that there are 16,800 data points to be examined. Data-handling machinery was used to assist in the experiment; the system operates as follows: The data collected in a 400-channel analyzer are automatically punched on cards. The cards are transported to the IBM 7090 computer, where appropriate transformations are made on the raw data points to obtain true energy spectra. Punched cards containing the computer output are returned to the cyclotron laboratory, and point plots are made on a plotting machine attached to a card reader. The raw data and the computer output are also printed on pages suitable for filing in notebooks.

This system enables the experimenter to accumulate and process large quantities of data and to convert them to graphs without the drudgery of hand calculations and hand plotting. The system is not tied to any particular computer program nor to any particular format for the output cards.

As an additional aid to the experimenter, input and output subroutines were also written so that basic arithmetic programs which operate on the data can be written in a few minutes in FORTRAN. For example, a program to subtract spectrum A from spectrum B and take the logarithm of the difference involves only a few FORTRAN statements. One can run the experiment, write the program, have it compiled and executed, and soon have the results plotted from the output cards; the major delay is waiting for the messenger to transport the cards.

To assist in data reduction a new computer program called Kinematics II was written. This is similar in purpose to Kinematics I but calculates the angle transformation and cross-section transformations at specified laboratory angles instead of at specified center-of-mass angles. This program also calculates the momentum transfer, K, and scattering argument, KR.

Many of the experiments now being done involve the correlation of heights of coincident pairs of pulses from two counters. This is true for the $dE/dx-E$ counter system used in the (p,d), (p,t), and (p,α) work, as well as for correlation studies in which two particles are detected. Up to the present these correlated pulse heights have been recorded in a makeshift fashion with a multichannel analyzer on one of the counters and with from one to four single-channel analyzers on the other counter. An instrument is now under construction which will record the correlated pulse heights in a true two-parameter array.[6]

The total number of channels required is the product of the numbers required for adequate resolution for each counter. The instrument under construction has 20,000 channels, which form a

[5] G. Alaga, *Phys. Rev.* 100, 432 (1955); *Nuclear Phys.* 4, 625 (1957). S. A. Moszkowski, *Phys. Rev.* 82, 35(1951).

[6] This is one of three such instruments under construction by the Tullamore Electronics Division of the Victoreen Instrument Co. The specifications were arrived at in collaboration with G. D. O'Kelley, Chemistry Division, and D. A. Bromley, Yale University, representing the other groups to receive these analyzers.

basic array of 100 × 200 channels. This can be rearranged, by means of controls on the instrument, into several other arrays, such as 50 × 400 and 100 × 20 × 10.

To accommodate the high counting rates anticipated in the experiments, a fast-access memory must be provided. The dead-time specification of commercially available analyzers [about $(15 + N/2)$ μsec, where N is the channel number] was considered to be acceptable; this allows the use of existing technology.

Since this analyzer is capable of recording 20,000 data points in a single experiment, the data handling must be considered as an integral part of the system. Much of the design effort has gone into this aspect of the system. A display was devised which permits the experimenter to examine large quantities of data easily and rapidly, with particular emphasis on the correlations of two pulse heights. Two cathode-ray tubes are used to display simultaneously an X-Y map of the data, with intensity as an indication of counts on one tube and a single-slice spectrum on the other tube. An adjustable contour line is provided as an aid in reading the map, and the position of the slice is indicated on the map.

The display specifications and the high-counting-rate specification require that the fast memory be large enough to store all the data for a single experiment. A block diagram of the system concept is shown in Fig. 2.6. The equipment within the dashed line is the 20,000-channel analyzer, as being purchased.

The display permits examination of the data during an experiment. The link to the computer is by way of magnetic tape, which will be physically transported to the computer. Computer output can be examined on the display, which will permit examination of quantities of computer output regardless of its origin. A 20,000-point display can be generated in 1.5 sec.

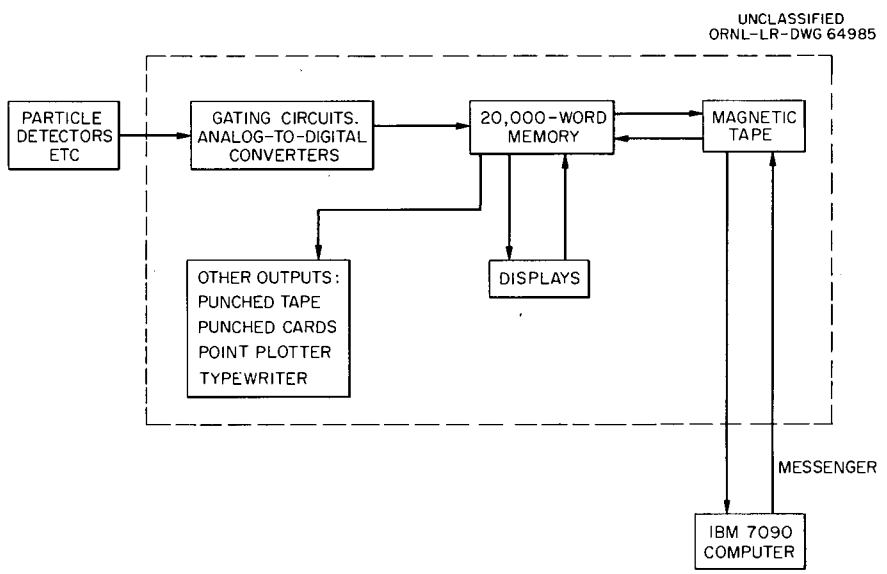

Fig. 2.6. Block Diagram of Data-Handling System for 20,000-Channel Analyzer. The portion within the dashed lines is the analyzer being fabricated by the Victoreen Instrument Company.

3. Nuclear Reaction Theory

R. H. Bassel R. M. Drisko Edith C. Halbert

OPTICAL-MODEL SEARCH PROGRAM

To aid in the studies of direct nuclear reactions and elastic scattering, an optical-model search program was written. The program minimizes the quantity

$$x^2(\lambda_1, \ldots, \lambda_i) = \sum_\theta \frac{[\sigma_{\text{theory}}(\theta, \lambda_1, \ldots, \lambda_i) - \sigma_{\text{exp}}(\theta)]^2}{[\Delta\sigma(\theta)]^2}$$

by means of a nonlinear least-squares technique, where the search parameters are the corrections to the first-guessed optical-model parameters. This program always assumes the Saxon form

$$V(r) = V_0\,[1 + e(r - R_r)/ar]^{-1}$$

for the real potential well. The spin-orbit potential, when used, is of the Thomas type and is always taken as proportional to the derivative of the real well.

Four models of imaginary-well shapes can be used in the program. The simplest is the Saxon well, which has the same geometrical parameters as the real well. The second is a Saxon well for which the radius and diffusivity are allowed to take different values from the real well. The third is a surface-peaking imaginary potential well, either as a Gaussian centered at radius R_g with width b, or as the derivative of the Saxon shape. In the fourth model the imaginary well is taken as the sum of the Saxon well and the surface-peaking derivative of the Saxon well.

The program will search on as many or as few parameters as desired and allows switching to a new mode of search, in which some other set of parameters is varied, with the previous calculation as a starting point.

Direct Nuclear Reactions

The matrix element in the distorted-wave Born approximation (DWBA) demands, in principle, wave functions which exactly explain the elastic scattering in the entrance and exit channels. The DWBA calculations assume, however, the wave functions generated by the optical model. It is of interest to determine whether these functions, which neglect compound effects, identity of particle, strong coupling, etc., and which are not realistically determined in the interior of the nucleus, can be consistently used in the evaluation of off-diagonal reaction processes. To check this point, the search program was used to generate optical-model parameters that fit experimental data when available. The corresponding wave functions are then used to perform DWBA calculations. Recently, Yntema, Zeidman, and Broek have measured[1] the elastic and inelastic scattering of alpha particles from Ni^{58}. Their data were used in the search program to generate three optical potentials which gave equally good fits to the elastic data. The parameters of these three potentials are listed in Table 3.1.

Calculations of the inelastic scattering were performed with these potentials. The results of the elastic- and inelastic-scattering analyses are shown in Fig. 3.1, along with the experimental data.[2] The inelastic angular distributions calculated by use of the wave functions given by the

[1] At Argonne National Laboratory.

[2] Details of the theory and the extensive numerical calculations will be published by Bassel, Drisko, Rost, and Satchler.

Table 3.1. Optical-Model Parameters for Alpha-Particle Scattering from Ni^{58}

Potential	V, Depth of Real Well (Mev)	W, Depth of Imaginary Well (Mev)	R_r, Radius of Real Well (fermis)	R_w, Radius of Imaginary Well (fermis)	a_r, Diffusivity of Real Well (fermis)	a_w, Diffusivity of Imaginary Well (fermis)
X	47.57	13.8	6.135	6.135	0.5494	0.5494
Y	45.58	18.85	6.178	5.346	0.5271	0.6619
Z	96.69	38.19	5.806	3.936	0.5168	0.8086

other potentials give identical results. However, preliminary calculations of (p,α) angular distributions show that potential Z gives results grossly different in magnitude and shape from those calculated from potentials X and Y.

In collaboration with G. R. Satchler[3] and E. Rost,[4] the distorted-wave code was extended to include spin-orbit coupling in the entrance and exit channels. This program will be used to investigate outgoing-particle polarizations in stripping reactions.

Alpha-Particle Reaction Cross Sections

P. H. Stelson[3] and F. K. McGowan[3] have measured (α,p), (α,n), and (α,γ) cross sections for alpha scattering from Ni^{58} over an alpha-particle energy range from 5 to 11 Mev. For potential Y (found by fitting to elastic-scattering data at 43 Mev) the total reaction cross sections predicted by the model were calculated over this energy range. This calculation gives agreement with the summed cross sections at 11 Mev but is too large by a factor of 10 at 5 Mev. By changing the depth of the imaginary well from 18.85 to 3 Mev, good agreement with the summed cross sections can be found over the entire energy range considered. The results are shown in Fig. 3.2. It is of interest to note that the calculated reaction cross section at 11 Mev is essentially independent of the depth of the imaginary well, varying from 326 to 335 mb as W is varied from 3 to 18.85 Mev. The predicted elastic angular distributions are, of course, quite different, having oscillatory structure at low W and passing to a smooth behavior at high W.

Deuteron Elastic Scattering

A systematic survey of the elastic scattering of deuterons has been started. Recently, careful measurements of 11.8-Mev deuteron scattering over an extensive range of elements (carbon through gold) have been made.[5] The optical-model searches have thus far yielded good fits to these data. The analyses seem to be showing a systematic trend in parameters as functions of target mass. In particular, the deuteron scattering from zirconium and cadmium can be well fitted with the simple model, in which real and imaginary wells have the same geometrical parameters and spin-orbit coupling is neglected. The parameters are:

	Zirconium	Cadmium
V, Mev	80	80
W, Mev	13.46	17.64
R, fermis	$1.344A^{1/3}$	$1.348A^{1/3}$
a, fermis	0.584	0.585

The results for the cadmium analysis are shown in Fig. 3.3.

In general, a wider range of A can be better fitted with the model in which the real and imaginery wells have Saxon shapes with different geometrical parameters. Although the best average

[3]Physics Division.

[4]Princeton University, Princeton, N.J.

[5]G. Igo, W. Lorenz, and U. Schmidt-Rohr, *Phys. Rev.* 124, 32 (1961) and references therein.

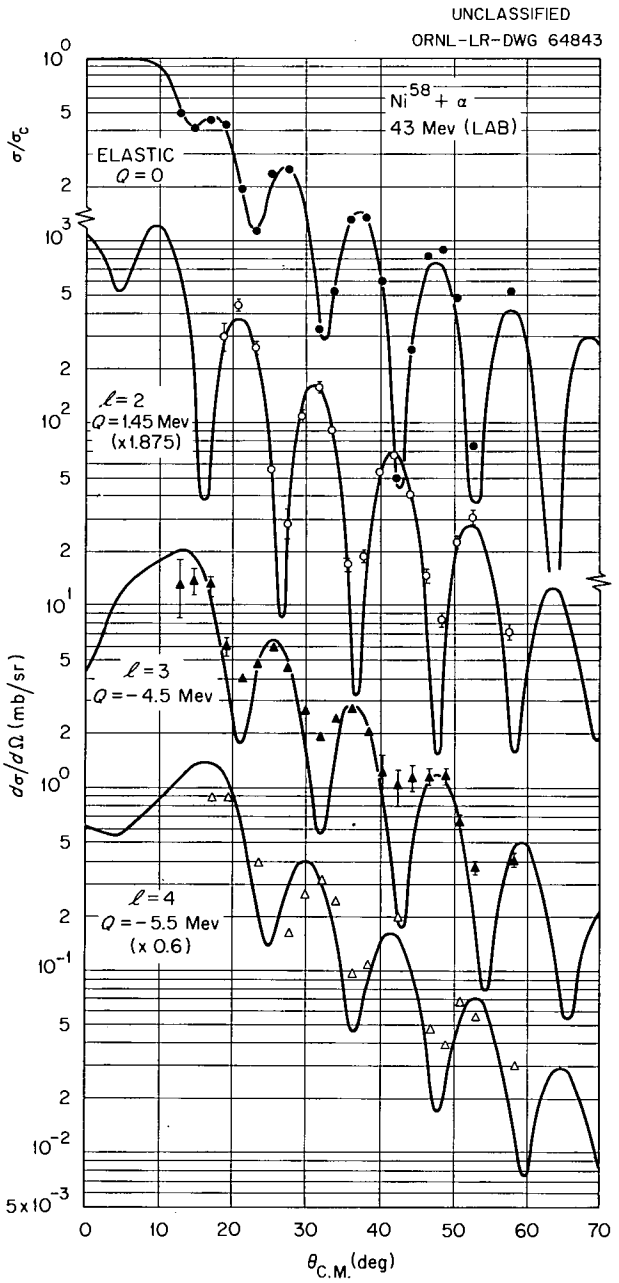

Fig. 3.1. Scattering of 43-Mev Alpha Particles by Ni^{58}. The distorted-wave curves were calculated with a Woods-Saxon distorting potential with $V = 47.6$, $W = 13.8$, $r_0 = 1.585$, $a = 0.55$. The elastic-scattering predictions are also shown (as the ratio to Rutherford). A Woods-Saxon potential with slightly different radii for real and imaginary parts gives a better fit to the elastic data around 50 and 60°, without changing the inelastic predictions.

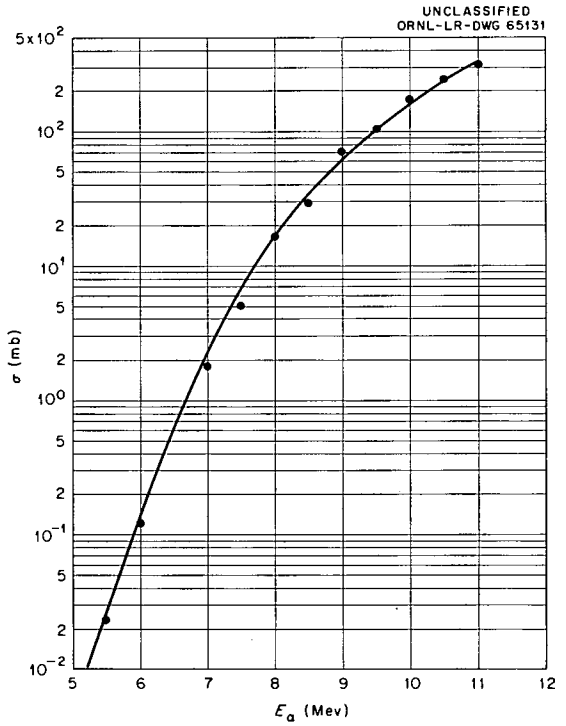

Fig. 3.2. The sum of (α,p), (α,n), and (α,γ) Cross Sections for Alpha-Particle Scattering from Ni^{58}. The crosses are experimental points; the curve is the optical-model prediction.

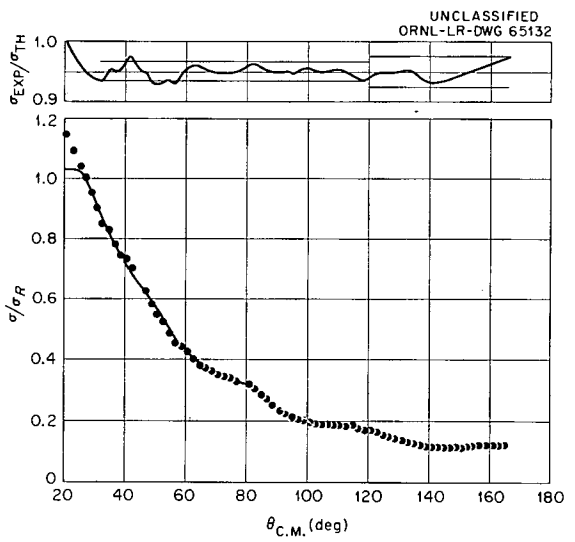

Fig. 3.3. Plot of σ/σ_R for 11.8-Mev Deuterons Scattering from Cadmium. The points are experimental, the curve theoretical. The upper curve is a plot of $\sigma_{exp}/\sigma_{theory}$; the bars are the experimental bounds to the cross section.

parameters have not yet been determined, some general similarities between parameters for different nuclei are:

$$60 < V < 65$$

$$5.8 < W < 6.5$$

$$1.12 < R_r/A_T^{1/3} < 1.22$$

$$1.7 < R_w/A_T^{1/3} < 1.9$$

$$0.63 < a_r < 0.75$$

$$0.6 < a_w < 0.72$$

The quality of the fits is quite good, similar to that shown for the cadmium analysis.

Heavy-Ion Scattering

The measurements of nitrogen scattering from aluminum and magnesium were analyzed with the optical model. The results, displayed in Figs. 3.4 and 3.5, show the Igo phenomenon.[6] That is, only contributions from the tail of the potential are important in the scattering. A calculation of the integrand of the *s*-wave amplitude, given in Fig. 3.6, for the scattering of nitrogen from aluminum shows that the contributions to this amplitude come from radii greater than 7 fermis. Over the range of important radii, the real potential depth is $\leqq 10$ Mev.

[6] G. Igo, *Phys. Rev.* 115, 1665 (1959).

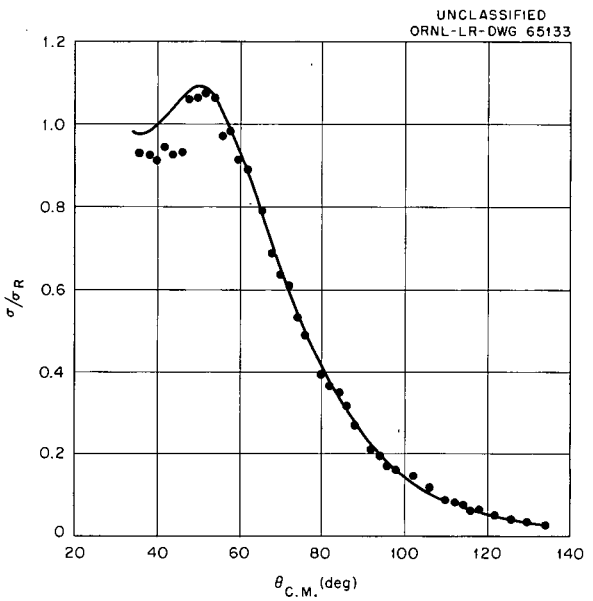

Fig. 3.4. Analysis of the Scattering of 27-Mev Nitrogen Ions from Aluminum. The points are experimental; the curve is calculated with a Saxon potential with $V = 39.6$, $W = 27.5$, $R = 6.36$, and $a = 0.626$.

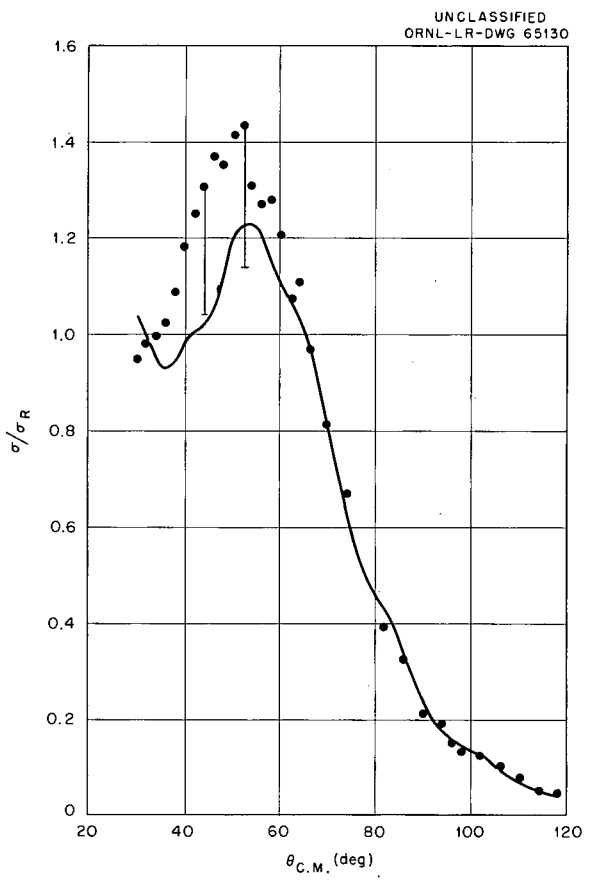

Fig. 3.5. Analysis of the Scattering of 28-Mev Nitrogen Ions from Magnesium. The points are experimental; the curve is calculated with a Saxon potential with $V = 53.4$, $W = 3.8$, $R = 5.24$, and $a = 0.691$.

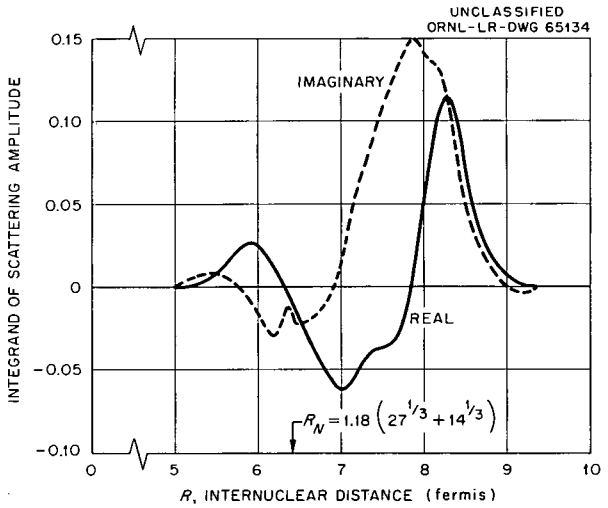

Fig. 3.6. Plot of the Integrand of the *s*-Wave Scattering Amplitude for Nitrogen Scattering from Aluminum. The major contribution to the *s*-wave scattering comes from internuclear distances greater than 7 fermis.

4. Applied Physics Program

J. J. Pinajian J. H. Cupp J. E. Beaver[1]

The use of the 86-Inch Cyclotron for irradiation services under AEC full-cost-recovery policy continued to increase during the past year (see Fig. 4.1). A total of 114 service irradiations with 22-Mev protons were made for the production of 38 radioisotopes and for studies of radiation damage and fission products. This represents a total of over 794 hr of beam time (see Table 4.1). Over

[1]Isotopes Division.

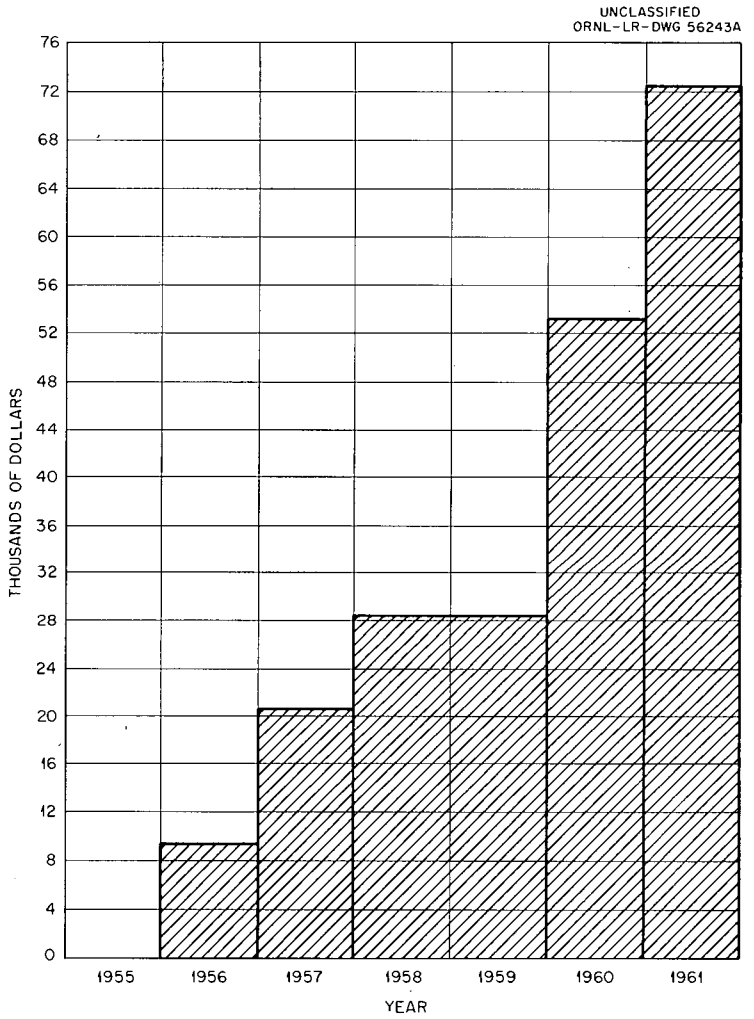

Fig. 4.1. Annual Charges for Irradiation Services, ORNL 86-Inch Cyclotron.

Table 4.1. Service Irradiations, ORNL 86-Inch Cyclotron

Isotope	Runs	Irradiation Time (hr)	Isotope	Runs	Irradiation Time (hr)
Be^{7}	6	33.5	Te^{123m}	1	5
Na^{22}	4	112	I^{124}	3	12
Al^{26m}	*a*	*a*	I^{125}	1	10
Ti^{44}	2	5	I^{130}	2	4
Sc^{44m}	11	40	Cs^{132}	2	6
V^{48}	3	3.75	Ce^{137}	1	10
Mn^{52}	1	1.0	Pm^{148}	1	5
Fe^{55}	1	3.0	Gd^{149}	1	2
Co^{56}	1	0.25	Eu^{149}	1	0.25
Co^{57}	14	184.5	Er^{150}	1	1.5
Co^{61}	4	19.3	Gd^{153}	1	10
Ge^{68}	2	10	Tm^{168}	2	5
Zn^{72}	1	1	Lu^{174}	1	1
Rb^{74}	1	4	W^{181}	1	10
As^{74}	14	139	Pt^{191}	1	0.25
Sr^{85}	4	40	Au^{195}	1	8
Y^{87}	1	6	Po^{209}	1	5
Y^{88}	3	13.5	Bi^{207}	4	27.25
$Te^{95,99}$	2	6	Radiation studies	3	18
Pd^{103}	3	8	Fission studies	4	21.85
Cd^{107}	2	1.75			

[a]Recovered from septum tubes.

4 curies of Co^{57} and 3 curies of As^{74} were produced. The individual yields continue to rise; the results for As^{74} production over the past several years are shown in Table 4.2.

Service irradiations were provided for 10 universities, 7 divisions of the Laboratory, and 4 commercial processors. The increase in the number of commercial processors using these cyclotron services means a much broader distribution of cyclotron-produced isotopes than is apparent in Table 4.3. The addition of the United Kingdom Atomic Energy Authority at Amersham, England, also provides for

Table 4.2. Production of As^{74} on the ORNL 86-Inch Cyclotron

Year	Runs	Average Rate (mc/hr)	Total (curies)
1958	14	16.0	1.99
1959	17	16.4	2.23
1960	16	18.5	3.13
1961	14	21.4	3.00

Table 4.3. Customer Distribution for Service Irradiations, ORNL 86-Inch Cyclotron

Universities
Carnegie Institute of Technology
Columbia University
Florida State University
Georgia Institute of Technology
Iowa State University
Princeton University
University of California
University of Chicago
University of Notre Dame
Western Reserve University
Hospitals
Argonne Cancer Hospital
Oak Ridge National Laboratory
Biology Division
Chemistry Division
Isotopes Division
Metallurgy Division
Physics Division
Reactor Chemistry Division
Thermonuclear Division
Commercial Processors
Abbott Laboratories
Nuclear Science and Engineering Corporation
Tracerlab, Inc.
Nuclear Corporation
U.S. Organizations
General Motors Company
Foreign Organizations
Hebrew University, Israeli
Saha Institute of Nuclear Physics, India
United Kingdom Atomic Energy Authority, England

a distribution of Be^7, Co^{57}, and Bi^{207} in both England and Europe. The 86-Inch Cyclotron continues to be the only source for most of the radioisotopes listed in Table 4.1.

The demand for high-specific-activity Co^{57} for use in Mössbauer studies has continued. In an effort to meet these demands, a technique for electroplating high-purity, low-cobalt nickel targets was developed. Ion-exchange-purified nickel salts are used in conjunction with an extremely high-purity, low-cobalt nickel anode. Nickel targets were produced with cobalt impurity reduced to 0.24 ppm. The problems that seem to have been associated with the chemistry involved in processing these targets for in-project users were eliminated by doing this work at the site of production. Electrostripping techniques were used for removing the cobalt and nickel from the face of the target. Sulfide precipitation removed the copper contamination, and ion exchange separation completed the isolation of the cobalt activity. Cobalt-57 solutions are routinely obtained with specific activity of >6.0 curies of Co^{57} per milligram of cobalt. The specific activity of carrier-free material would be 8.4 curies of Co^{57} per milligram of cobalt.

Lithium hydride–filled aluminum capsules were developed as substitute targets to replace the more expensive flat-plate targets used in producing small quantities of Be^7. The yield is 66% of that of flat-plate targets, but the cost is only one-third.

The problem of the oxidation of scandium during irradiation was resolved by placing a magnesium wire in contact with the scandium metal strips. This produces an electromotive cell; the magnesium wire is oxidized preferentially, and the resulting product Sc^{44m} remains as metal. Several irradiations performed in this fashion enabled the Princeton University group to evaporate Sc^{44m} metal in their apparatus.

Equipment was designed and successfully used for the irradiation of krypton gas with a proton beam at 15 μa. The $Rb^{83,84,86}$ activities were collected on cold traps during the bombardment and were subsequently collected in a dilute hydrochloric acid wash with 97% efficiency.

The thick-target yields at 22.4 Mev for the reactions $Se^{77}(p,\alpha)As^{74}$ and $As^{75}(p,n)Se^{75}$ were 1.9 and 9.3 mc/ma-hr respectively. The latter activity represents a specific activity of 13,700 curies per gram of selenium. This is a factor of over 1000 greater than that of the reactor-produced product; the higher specific activity is especially important for trace-element research in biological systems.

Note: As of December 1, 1961, responsibility for operation of the 86-Inch Cyclotron was transferred to the Isotopes Division. In the future the program for cyclotron production of isotopes will be reported by that division.

5. Cyclotron Operation

A. W. Riikola H. L. Dickerson C. L. Viar

The 63-Inch Cyclotron and the 86-Inch Cyclotron were operated routinely; they were available for experimental work 87 and 69%, respectively, of the scheduled operation time. As of October 31, 1961, the 63-Inch Cyclotron was put in standby. The responsibility for operating the 86-Inch Cyclotron was transferred to the Isotopes Division on December 1, 1961. These changes made the staff available for test operation of the components and the major system of the Isochronous Cyclotron.

OPERATION OF THE 63-INCH CYCLOTRON

The 63-Inch Cyclotron was available for experimental work about 87% of the scheduled operating time. The following breakdown of the operation of the machine is based on the average operating schedule of 66 hr/week:

	Percent
Normal operation conditions (87.5%)	
Bakeout and tuning machine	6.4
Beam improvement, getting beam up to acceptable bombardment intensities	1.5
Target-setup time, setting up, adjusting, and inspecting targets	24.8
Beam on target, actual bombardment time	52.4
Ion source changes	2.4
Operational interruptions (12.5%)	
Electrical troubles	1.7
Vacuum troubles	5.7
Miscellaneous, including routine maintenance	5.1
	100.0

As in the past, the major source of operational outage resulted from water leaks in the liner. The leaks were repaired, but, because of the anticipated shutdown of the machine, no effort was made to replace the liner. The machine was running very well during the last three months of operation; it was available to the experimenter about 92% of the scheduled operating time.

The duration of the 27-Mev N^{3+} bombardments varied from a few minutes to 40 or 50 hr. A total of 270 runs were made; the type and number are listed below:

Elastic and inelastic scattering	18
Light-particle spectra	4
Chemistry	12
Radiation damage	11
Heavy-particle stripping	18
Transfer reactions	165
Compound-nucleus reactions	36
Miscellaneous	6
	270

Operation of the 63-Inch Cyclotron was terminated on October 31, 1961. The termination had been planned to permit transfer of operation personnel to test operation of the Isochronous Cyclotron and to permit the physics staff to prepare to use this new machine. The termination was advanced somewhat, however, to make the old Beta magnet assembly in which the cyclotron is operated available for alterations by the Isotope Division.

Tentative plans are to keep the 63-Inch Cyclotron in standby condition for about a year. Utilities to the machine are being maintained by the Y-12

maintenance group, and periodic checks of the operational conditions will be made by the Electronuclear Division.

OPERATION OF THE 86-INCH CYCLOTRON

The schedule for the 86-Inch Cyclotron varied from week to week; the average operation time was about 110 hr/week. A breakdown of the scheduled operation time is shown below:

	Percent
Normal operation conditions (69.3%)	
Bakeout and tuning machine	9.7
Target-setup time	4.1
Beam on target	54.0
Routine ion-source changes and adjustments	1.5
Operational interruptions (30.7%)	
Electrical troubles	5.2
Vacuum troubles	7.6
Development, scheduled downtime for machine improvement	7.7
Miscellaneous	10.2
	100.0

Most of the major troubles, which necessitated removing the dees, were due to water leaks in the dees or liner. Electrical troubles were primarily due to failures of standoff insulators and to poor connections in the dee bias circuits and the channel-coil electrical leads. About 8% of the scheduled operation time was used for installation and testing of a dee-voltage regulator.

Some improvements were made in the machine in order to aid the operator in tuning and adjusting various components more readily for optimum beam conditions. To mention a few, controls for the quadrupole magnets and the 15° beam switching magnet were moved from the cyclotron vault to the control room. Quick disconnects were installed for the water lines in the cyclotron vault, for the T-position on the beam pipe, and for the water connections to the target carriage. Also, a remotely controlled air-operated ball-type valve was installed in the water supply line to the target to ensure more positive action in the event of rupture of internal targets during bombardment.

The types and number of bombardments made on the 86-Inch Cyclotron are outlined below:

Internal beam	
Service irradiations, isotope production	194
Physics, development, and research	40
Deflected beam	
Service irradiations	115
Others, mostly physics	179
Total	528

The responsibility for operating the 86-Inch Cyclotron was assumed by the Isotopes Division on December 1, 1961; operators had been in training during the year. The nuclear physics program utilizing 22-Mev protons will be continued, however, until the Isochronous Cyclotron is available.

6. Accelerator Development

J. A. Martin J. E. Mann R. S. Livingston

Fabrication and assembly of Cyclotron Analogue II was completed in August 1961, and satisfactory operation was readily obtained. Only very minor adjustments were required to obtain acceleration of electrons to the full design energy of 530 kev; for protons this would be equivalent to 970 Mev. This demonstration of the feasibility of accelerating particles in a fixed-frequency cyclotron to energies exceeding their equivalent rest mass is encouraging for the development of a high-intensity proton accelerator in the 800- to 1000-Mev energy range. Earlier preliminary studies for such a large isochronous cyclotron are being reviewed in more detail.

CYCLOTRON ANALOGUE II

Cyclotron Analogue II, an eight-sector, spiral-pole isochronous cyclotron, accelerates electrons to a kinetic energy of 530 kev. The cyclotron was designed to model the beam dynamics of a large fixed-frequency cyclotron for accelerating protons to the energy range from 800 to 900 Mev. The Analogue will be used to study the efficient extraction of a high-quality beam at the 8/4 radial resonance, which occurs at an electron kinetic energy of approximately 445 kev. The main features of the Analogue are given in Table 6.1; details of design and construction have been reported previously.[1-3]

Table 6.1. Cyclotron Analogue II, Design Specifications

Cyclotron unit (c/ω)	16.000 in.
Central field (B_0)	41.926 gauss
Orbit frequency	117.399 Mc
Axial focusing frequency (ν_z)	0.2
Energy for $\nu_r = 8/4$	445 kev
Energy for $\nu_z = 0$	530 kev

The air-cored magnet system of the Analogue (see Fig. 6.1) consists of three major parts: (1) a set of sector coils which provides the correct azimuthal variation in the magnetic field so that stable axial motion (focusing) is achieved at all energies; (2) a set of five main average field coils which provide the average field required for isochronous orbits to within about 1% accuracy; (3) 32 circular trimming coils which are used to adjust the magnetic field to the correct shape within a few parts in 10,000 to provide for isochronous operation. The magnetic field produced by the coil system is shown in Fig. 6.2.

The radial and the axial focusing, ν_r and ν_z, for electrons at various radii in this magnetic field, Fig. 6.3, are obtained by numerical integration of the equation of motion; a computer program developed for equilibrium orbit properties was used. For these calculations the magnetic field is defined by 32 points per sector azimuthally and 91 points radially. Axial focusing begins at a radius of 0.65 in., corresponding to an electron energy of 0.4 kev; axial focusing is finally lost at 13.76 in. at an energy of approximately 530 kev.

[1] J. A. Martin, *International Conference on High Energy Accelerators and Instrumentation, CERN 1959*, p 205.

[2] *Electronuclear Research Div. Ann. Progr. Rept. Mar. 1, 1960*, ORNL-3047, p 48.

[3] *Electronuclear Research Div. Ann. Progr. Rept. Jan. 16, 1960*, ORNL-3083, p 38.

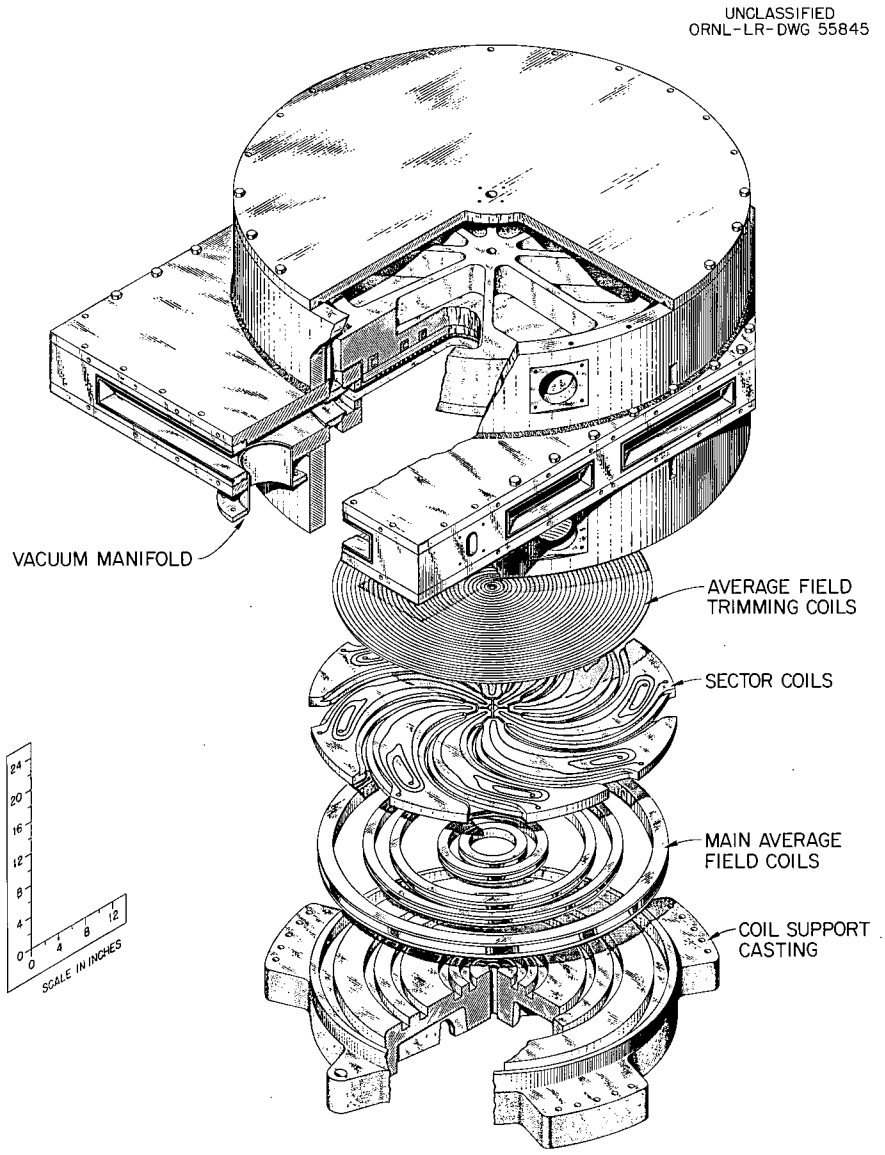

Fig. 6.1. Cyclotron Analogue II. In this view the lower half of the coil system has been dropped to reveal the design features of the trimming coils, the sector coils, and the main average field coils. Thirty regulated magnet power supplies are used.

First Operation

The first operation of the Analogue was achieved on August 4, 1961. With very minor adjustments of two of the average field coils, a beam was obtained out to the full design radius. Subsequent measurements indicated that full design energy was achieved. The only changes in coil currents necessary to obtain the beam at full radius were to increase the current in one of the central trimming coils, T_3, to produce a slight peak in the field at the center and to increase the current in M_5, the largest average coil, by approximately 0.2%.

At first the threshold energy gain per turn for acceleration to a radius of 13.7 in. (510 kev) was approximately 425 ev. At a radius of 12.25 in. (275 kev) a value of 140 ev was observed. The difference between these two thresholds indicates

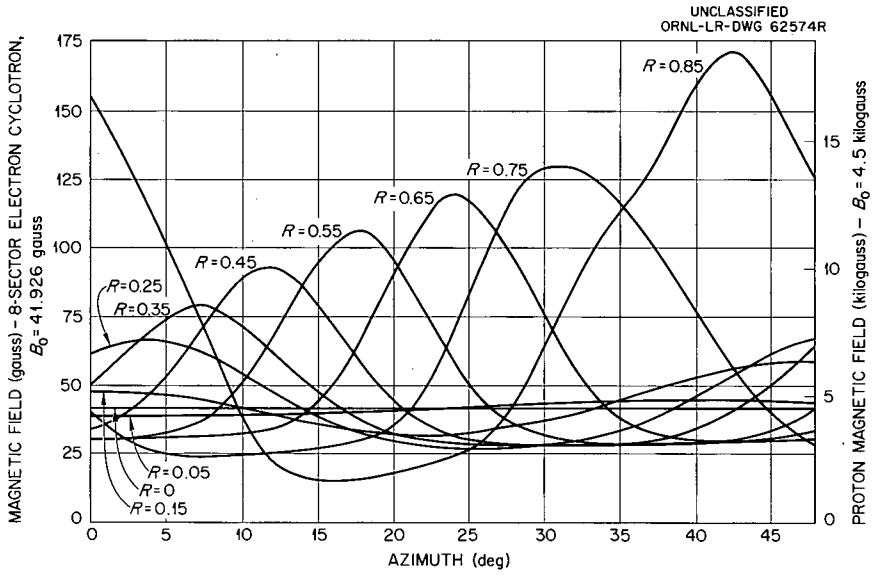

Fig. 6.2. Magnetic-Field Distribution Produced by the Coil System in the Electron Cyclotron.

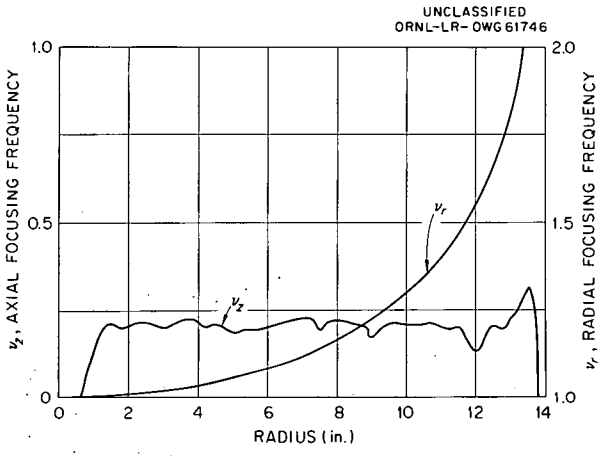

Fig. 6.3. Axial and Radial Focusing Frequencies, Plotted as a Function of Radius.

that considerable phase shift was occurring in the outer 1.5 in. of the machine. These early measurements were made without benefit of coils to cancel the horizontal component of the earth's magnetic field.

Observation of the beam profile on a phosphor-coated probe indicated distinct changes at several radii. A narrowing of the beam, both radially and axially, occurred at a radius of about 10.3 in., where $\nu_r = 1.33$. A further reduction in axial dimension of the beam occurred at 12.65 in. ($\nu_r = 1.7$); this had the appearance of a coupling resonance, but the nearest strong resonance $\nu_r + \nu_z = 2$ should be located at 12.9 in. A small change in intensity was observed at the calculated radius for $\nu_r = 2$ (R = 13.42 in.).

In the observations just described, the electron source was an incandescent filament mounted exactly at the center of the cyclotron, an arrangement known to lead to the generation of radial oscillations of large amplitude. Also, the horizontal component of the earth's field was approximately 0.050 gauss, as yet uncompensated.

In mid-October the Analogue was dismantled for for installation in its permanent site. At that time a single coil was installed to obtain approximate cancellation of the horizontal component of the earth's magnetic field. Also, an improved electron source was installed with the filament mounted 0.2 in. off center, which, although not optimum, reduced the amplitude of the radial oscillations substantially.

The first operation in the new location was obtained in late November. The performance is considerably improved; the beam perturbation at $\nu_r = 1.3$ is barely visible, and a much more intense beam is obtained at full radius. Several small perturbations in beam intensity, probably coupling resonances between the axial and radial motion, are observed in the region ν_r = 1.5 to 2.0. A time-exposure photograph of the phosphor-coated probe

being withdrawn at a constant rate (Fig. 6.4) illustrates these observations.

To determine which resonance was causing the beam perturbation at $\nu_r = 1.3$, a series of observations were made with the current in the sector coils at various values slightly above and below the standard value. For each setting, the average field-coil system was adjusted to maintain an isochronous average field, and computer calculations were made to obtain the new values of ν_r and ν_z as a function of radius for each sector-coil current setting. Observations of the new positions of the resonance correlate with the assumption that it is probably the difference coupling resonance $\nu_r - \nu_z = 1$. The data also suggested that the axial focusing frequency at the standard settings is slightly higher than calculated, a point which will be investigated further.

Energy Measurements

A series of electron energy determinations were made of various radii to determine the degree of correspondence to the calculated values. The energy determinations were made by analysis of the energy spectra of the bremsstrahlung emitted from the probe. The spectra were obtained with a 3 × 3 in. sodium iodide crystal and a 256-channel pulse-height analyzer. The results (Fig. 6.5) show good agreement with the calculated energies. These measurements and also the appearance of the spectra near the end point suggest that beyond the resonance the spectrum is possibly composed of two parts: electrons which are lost by radial blowup and a component which is accelerated through the resonance.

New threshold measurements, with the horizontal-field cancellation coil excited, give much lower values than those obtained previously. The minimum dee voltage for acceleration to a radius of 13.4 in. (445 kev, $\nu_r = 2$) is 60 v rms, indicating a maximum energy gain per turn of 170 ev. This indicates that a minimum of 2600 turns has been achieved. At a radius of 13.75 in. (530 kev) the threshold dee voltage is 65 v rms, indicating at least 2800 turns. The threshold is practically independent of radius; it decreases to 50 v rms at a radius of 7.5 in., where the energy is 67 kev.

Future Work

Much additional experimental and computer work is necessary before the first beam-extraction experiments are done. First, the operating characteristics must be further understood, the resonances

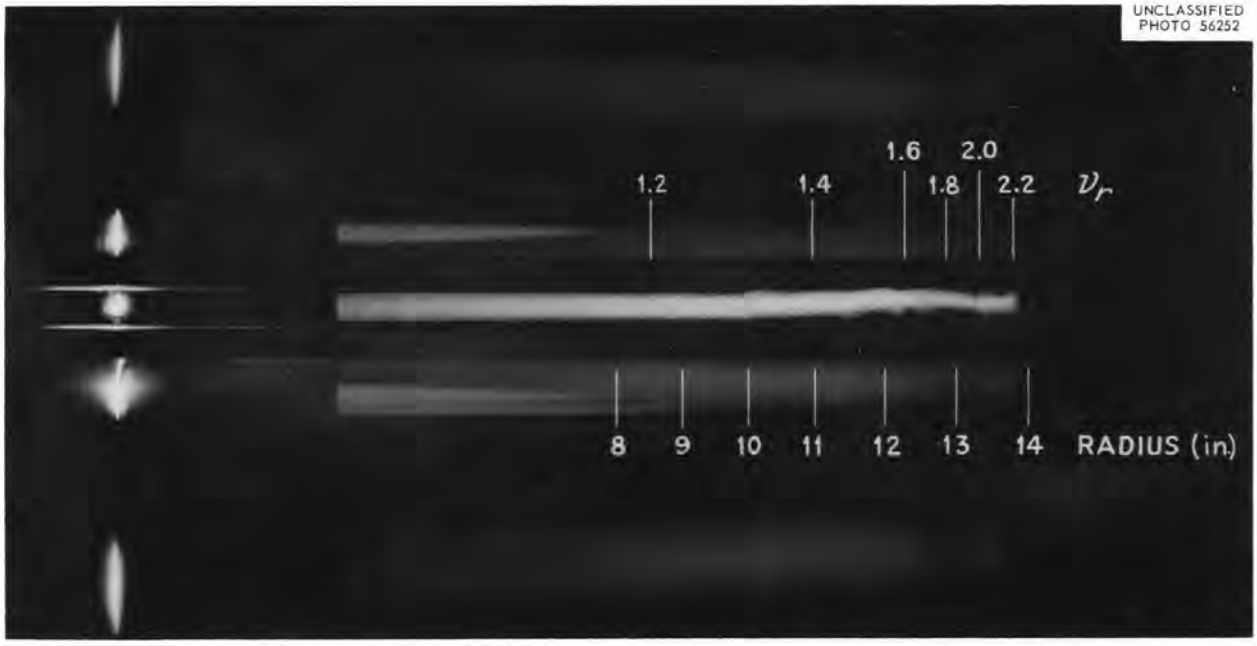

Fig. 6.4. Photographic Time Exposure of Electron Beam on Fluorescent Probe Withdrawn Radially. Electron source at left.

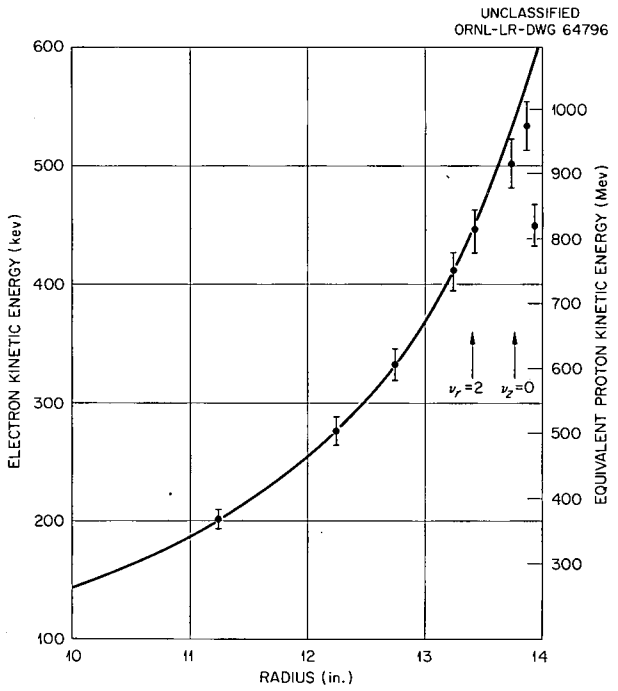

Fig. 6.5. Energies Attained in Cyclotron Analogue II. Calculated curve and experimental points.

must be identified, and the degree of correspondence of the axial focusing frequencies at various radii with calculated values must be determined. Better injection at the center must also be developed to provide a beam with very low radial amplitude. Finally, much additional computer calculation must be done to determine the optimum amplitude, phase, and shape for the cos 2θ extraction bump. If difficulty in maintaining axial stability of the beam during extraction is encountered, the changes in shape of the average field and flutter in the extraction region will have to be determined.

THE Mc^2 ISOCHRONOUS CYCLOTRON

A significant program of the last few years has been the investigation of a high-intensity isochronous cyclotron in the meson-producing energy range. Upon successful operation of the Electron Analogue II in the summer of 1961, a review of the various concepts for a full-scale proton cyclotron was started. Several phases of this review are separately described below. Basic to other considerations is the question of the experimental high energy physics which would be possible with such a machine. The studies outlined below indicate a wide variety of important experiments which could be undertaken. The preliminary design for a suitable research facility for such a program is described. For a successful proton machine, the complex magnetic field of Analogue II must be reproduced on a very large scale and at 100 to 200 times the field level. The production of such a field requires the use of ferromagnetic techniques, including precision measuring and positioning equipment and automatic data recording devices similar to but on a larger scale than those used in ORIC. Novel acceleration schemes in which the use of rf cavities may make possible significant reductions in magnet gap have been examined in increasing detail. The shielding required for any truly high intensity accelerator is very extensive, and the residual radiation levels reached will be higher than is encountered in any accelerators now in operation. Initial programs of study to understand and to reduce these problems to manageable proportions have been described in a separate report.[4] The concepts of the arrangement of the machine components including the vacuum system are also reviewed below.

Research Program for Mc^2 Cyclotron

It is obviously premature at this point to lay out a detailed research program for an accelerator whose completion is far in the future. The state of physics changes so rapidly that experiments which seem very exciting now may have been done by then, or may prove trivial; entirely new and unexpected fields are likely to open up. Necessarily, plans must be made far in advance; the experimental program outlined below is one which could be performed with intense proton and secondary beams, within the framework of the present state of the art.

Mu Mesons Physics. – Perhaps the most striking advantage of the cyclotron will be with respect to the intensity of the muon beam. The variety of experiments which can be done with mu mesons is very large; seven fields of study are described below:

[4] R. W. Boom, K. S. Toth, and A. Zucker, *Residual Radiation of the LRL 188-Inch Cyclotron*, ORNL-3235 (Nov. 27, 1961).

1. Of the three legs of Puppi's weak interaction triangle, muon capture by nuclei is the least well understood at present. Two avenues of progress are discernible. On the one hand, capture in pure hydrogen (which has only recently been detected[5]), deuterium, H-D mixtures, and He^3 promises to reveal the details of the weak capture interaction. As in the history of nuclear beta decay, refinements may be expected to continue to accumulate over the years with increasingly painstaking investigation. High intensity will greatly facilitate the more difficult polarization and angular correlation experiments. On the other hand, once the basic interaction is well pinned down, muon capture in complex nuclei can complement nuclear beta decay in providing information about nuclear structure through nuclear matrix elements, pair correlation functions, etc. The combined theoretical treatment of the nuclear structure effects and the strong interaction renormalization effects on the capture process should continue to propose challenging experiments for years to come.

2. Searches for rare, or theoretically forbidden, decays bearings on second-order weak interactions, radiative corrections, or intermediate bosons may still be important in several years. The high intensity will be particularly useful in these experiments.

3. Increasingly precise values of the basic constants characterizing the muon will be needed as time goes on. The mass and anomalous magnetic moment are important for quantum electrodynamics. The parameters for mu decay (e.g., the lifetime, asymmetry coefficients, and Michel's shape parameter) have fundamental significance for the theory of weak interactions. These parameters also affect the precision with which other quantities can be obtained. A national laboratory is well suited to carrying out a program of such careful measurements.

4. Muonium ($\mu^+ - e^-$, the analogue of positronium) has recently been observed after several years of effort. Its hyperfine structure, Lamb shift, decay modes, rate of formation, dependence on environment, etc. are of interest. Pionium, with a lifetime of the order of one hundredth the lifetime of muonium, should be sought.

5. Molecular phenomena such as rates of formation and dissociation of mu-mesic molecules, hyperfine state conversions, and fusion catalysis are of interest in their own right, for their bearing on nuclear mu-meson capture, and for possible technological applications. Many knotty problems may be expected to yield only to patient systematic study.

6. With regard to atomic phenomena, one can study the capture of μ^- into atomic orbits, the bound decay rate, depolarization, the mesonic x rays and Auger electrons, and radiationless transitions of several kinds. These processes have already given rise to several famous anomalies and discrepancies which are only now becoming understood. Even if much of the current interest may have waned in several years, mesic atoms will provide an increasingly useful tool for atomic physics.

7. Finally, mu mesons may be scattered from nucleons or nuclei to obtain form factors for charge and magnetic moment distributions. Although the intensity will be too low to seriously compete with electron scattering, such experiments could provide a useful check. Inelastic scattering might add something to the information obtained from inelastic scattering of electrons.

Nuclear Physics. – The beams from the Mc^2 cyclotron should be very useful for the study of nuclei and their structure, as well as the basic forces which act in them. High-energy protons even now provide interesting information about low-lying states in light nuclei, either by $(p,2p)$ or (p,d) reactions. Muon elastic scattering can be used for nuclear structure studies in a way similar to the present work with electron scattering. The whole field of π-nucleus interaction has been barely touched because of low intensities and lack of energy homogeneity of π beams. Finally, it may be possible to use results of μ-capture to measure nuclear moments and transition matrix elements.

The advantage of high-energy protons lies in the fact that the impulse approximation becomes valid, and the impact of a sufficiently fast particle on a nucleus can be interpreted as a sequence of a few collisions with free nucleons. Thus, one can investigate the nucleon-bound states by knocking out single nucleons $(p,2p)$ and (p,pn) or by picking up neutrons (p,d). Clusters can be investigated by knockout processes (p,pd), (p,pa).

[5] E. Bleser *et al.*, *Bull. Am. Phys. Soc.* 6(2), 519 (1961); R. H. Hildebrand, *Phys. Rev. Letters* 8, 34 (1962).

Equipment with very high resolution must be used, both to produce a narrow energy spread in the incident beam and to measure the energy of reaction products precisely.

In some cases, nuclear chemistry techniques can be used to advantage for experiments in this field, where the identification of the residual nucleus identifies the reaction taking place. For example, Te^{123} obtained from $I^{127} + \pi^-$ can result only from the reaction $I^{127}(\pi^-,4u)Te^{123}$. Although π-nucleus interactions do not seem very promising at this writing, new developments in theory or new experimental results may make this into a very important program.

Special Projects. – The Mc^2 cyclotron is designed primarily for the study of elementary interactions and nuclear physics. The various beams may prove very useful for the study of macroscopic phenomena such as the following:

1. The effect of high-energy particles on living material. The interest here lies in the investigation of the RBE of high-velocity particles, the radiation effects of protons as well as of stopped π^- mesons. Early and late somatic effects of proton and meson irradiation can be studied. Finally, the practical possibility of using a stopping π^- beam to destroy deep-seated cancer can be explored.

2. Related to the biological work is the study of shielding for space travel. Since the radiation belts around the earth contain protons with energies up to 700 Mev, and since some solar emissions have high intensities of protons around 1 Bev, studies of the secondary radiation produced by bombarding a shield with protons from the cyclotron could prove very valuable.

3. From time to time there has been considerable interest in developing an economical electronuclear process for large-scale production of neutrons. Such a process would consume depleted uranium, and hence would be useful for the production of Pu^{239} by neutron capture in U^{238}. The efficiency of this system, with a high-energy primary proton source can be investigated with the Mc^2 cyclotron.

Experiment Areas

The main feature of the shielded experiment area to be used with the Mc^2 cyclotron is a long corridor. Secondary particles will be produced in this corridor and deflected into large, 80 × 100 ft shielded rooms. The first scattering for production of polarized protons will also take place in this corridor. The corridor is made purposely long, so that even high-energy pions will decay, and one can obtain intense, pure, muon beams in the experiment rooms. In general, then the bulk of the radiation will be confined to the corridor, and the background in the experimental rooms will be kept to a minimum.

Three experiment rooms are provided, so that while experiments are in progress in one, the other rooms are accessible for setting up new apparatus. For reference purposes, the floor plan, Fig. 6.6, shows these rooms as, proton, pion, and muon areas; naturally, this does not preclude a pion experiment being done in the proton room, or a neutron experiment in the muon room. The proton room is well shielded and can take essentially the whole deflected beam; the other rooms are designed to contain beams of the order of 10^{11} particles/sec.

Bending magnets are provided in the corridor to steer the beam, to analyze it, and to deflect it into each experiment room. In each, a bending magnet will be used to switch the beam to any experiment. Quadrupoles will necessarily be provided, especially to contain the muons on their long flight path; they are not shown in the drawing.

A 6-ft-high horizontal slot centered about the beam height will run essentially the full length of the wall separating the experiment rooms from the corridor. This will allow changes in beam piping and the addition of heavier shielding if it is needed in this critical area.

Each experiment area is accessible through a 6-ft-wide maze for personnel and for moderately large equipment. Apparatus which will not go through the maze, such as a magnet or a large bubble-chamber assembly, will be brought in through openings usually sealed by removable plugs. Forty-ton bridge cranes are provided in each experiment room, and 50-ton cranes in the corridor.

Magnetic Field Study

If it were practical to build the full-scale machine without iron, the field of Analogue II could be scaled up directly. The introduction of iron into the system makes this impossible, however, for simple pole shapes. The pole tips being investigated in the first model have rectangular

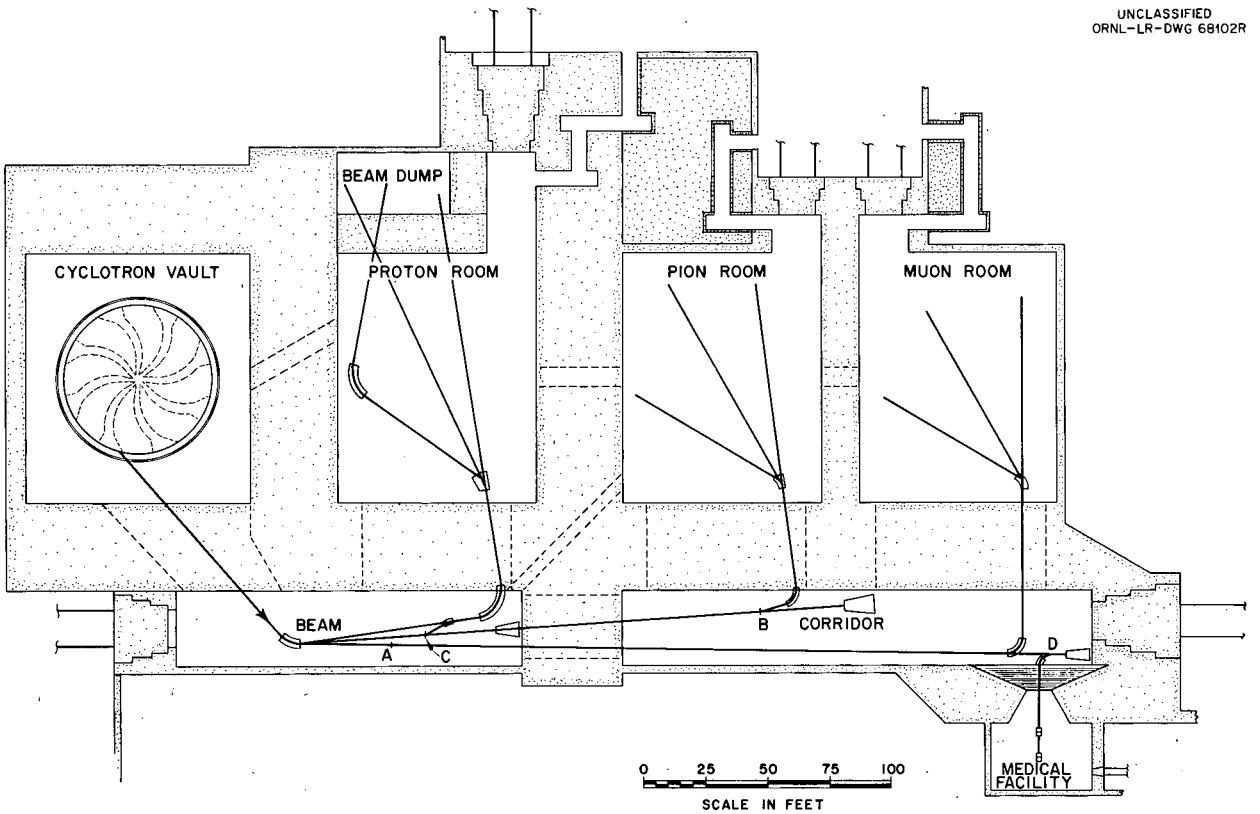

Fig. 6.6. Plan View of Cyclotron Vault and Experimental Area. Thin-walled sections of shielding are backed with earth.

edges and flat faces. The peak field in the gap is set at 18,000 to 19,000 gauss. This in turn sets the radius of the machine when the average field and flutter are specified. Three of the eight sectors have been modeled on a 0.15 scale (see Fig. 6.7). Field measurements will be made on the model with the same techniques and some of the same equipment used on the ORIC ¼-scale model. The first model will be sufficiently accurate to determine the general parameters of the magnet. Detailed orbit calculations will require more accurate models.

Radio-Frequency Cavities

The rf accelerating voltage can be applied without occupying expensive magnet gap space if cavity resonators are used. Two of the cavities which are being considered are shown in Fig. 6.8. These cavities would be curved to fit in the spiral slots in the magnet pole tips; there would be two cavities in the machine. The cavities would operate at twice the cyclotron frequency and would provide four accelerations per turn. Hence, for an energy gain of 1 Mev per turn, the maximum cavity voltage would be 250 kv. For this magnitude of voltage, an approximate calculation reveals a power loss of about 200 kw in the coaxial cavity and a comparable loss in the TE cavity. Therefore, the total rf power required for the machine would be about 600 kw including beam power. It may be possible to reduce the height of the cavity at the expense of increased rf power. Models of these are being constructed to check power calculations and the voltage variation along the accelerating gap.

There are, of course, other possible cavities for use in the machine. One possibility is the use of only one "racetrack" cavity operated at 500 kv maximum voltage and at three times the cyclotron frequency. Another possibility is the 45° coaxial cavity operating at four times the cyclotron frequency. These possibilities will also be investigated.

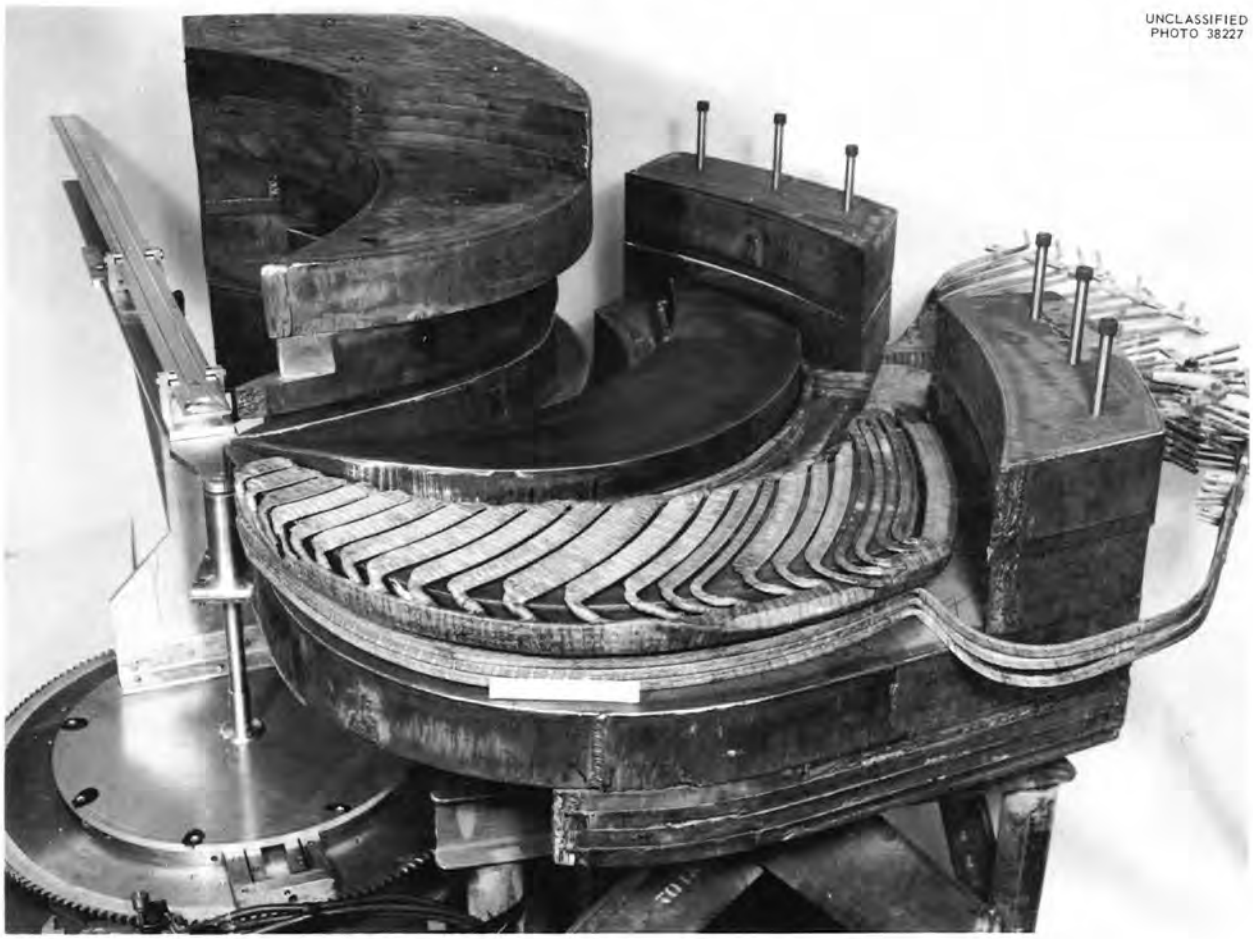

Fig. 6.7. Three-Sector Model of Eight-Sector Magnet with Steel Pole Pieces, 0.15 Scale.

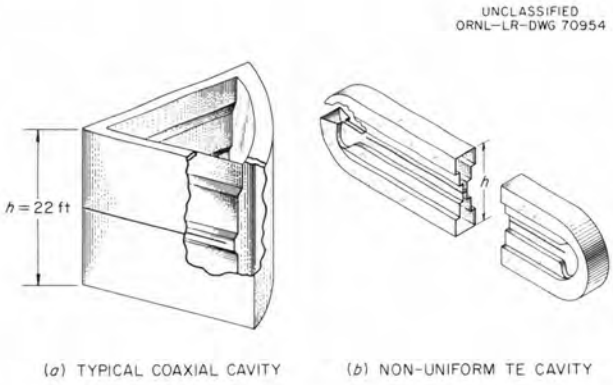

Fig. 6.8. Two Types of Cavities Being Investigated.

Magnet

The magnet will be composed of eight spiraled sectors as shown in Fig. 6.9. Spiraling the sectors reduces the flutter requirement and results in a smaller machine for the desired energy. To achieve sufficient flutter to produce the desired focusing, the magnetic gap must be small. A gap of 8 in. between iron, or 4 in. clear, has been chosen for initial model studies. If magnetic field precision of one or two gauss is required the pole-face gap tolerance will be in the order of 0.001 in.

A system of accelerating with cavities perpendicular to the median plane is under study. One

system is shown in Fig. 6.9 and 6.10. Since the cavities go through the center of the machine, the sectors cannot be structurally connected at the center. A clear space of 16 in. between sectors, except at the center, is provided for the cavities.

Because of the stringent magnet gap tolerance, no distortion of the sectors due to vacuum loading can be tolerated. For this reason, the vacuum chamber will completely enclose the magnet. All heavy magnet components will be assembled through the top of the vacuum tank, which will have a removable head.

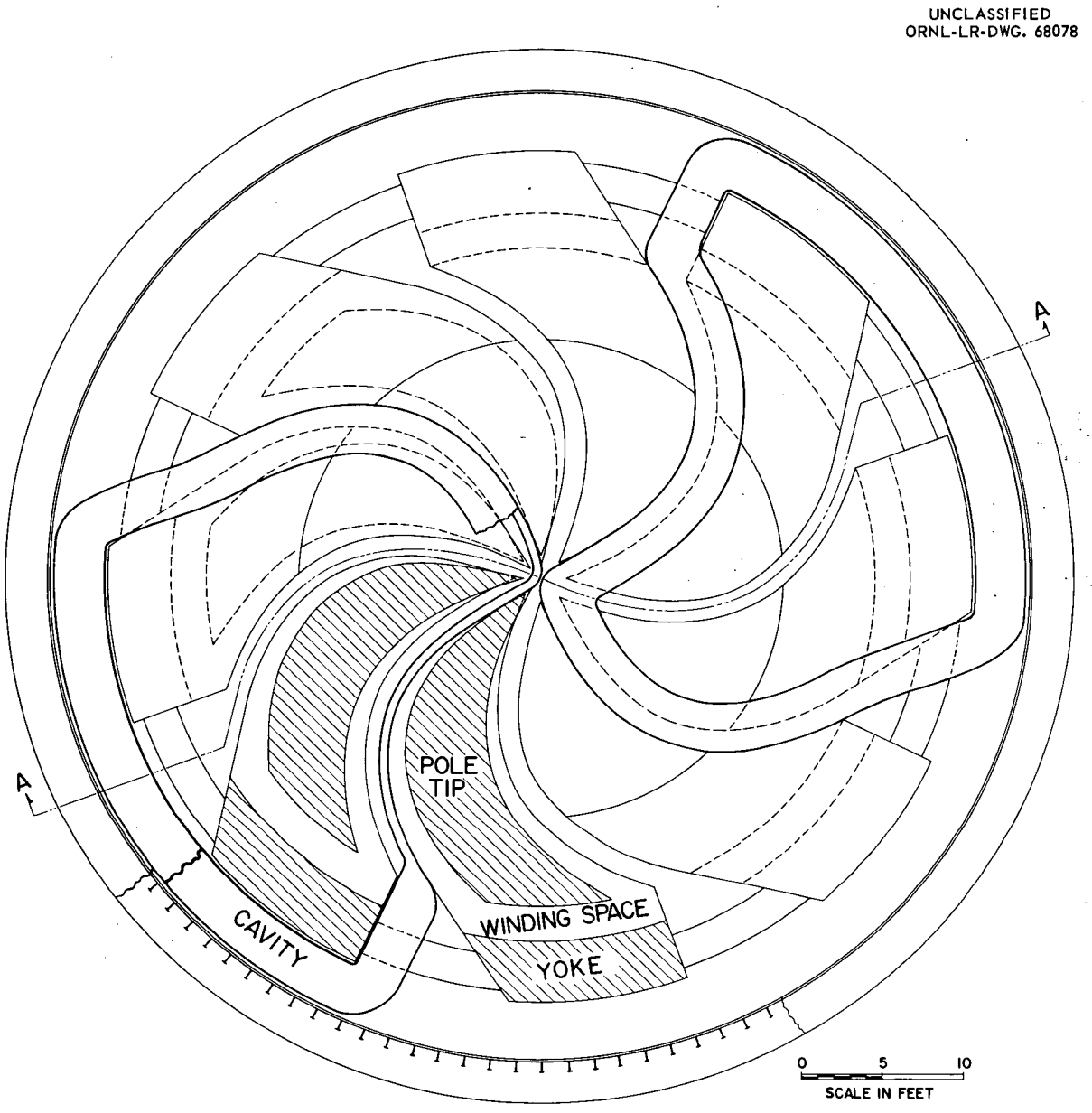

Fig. 6.9. Plan View and Section of Mc^2 Cyclotron.

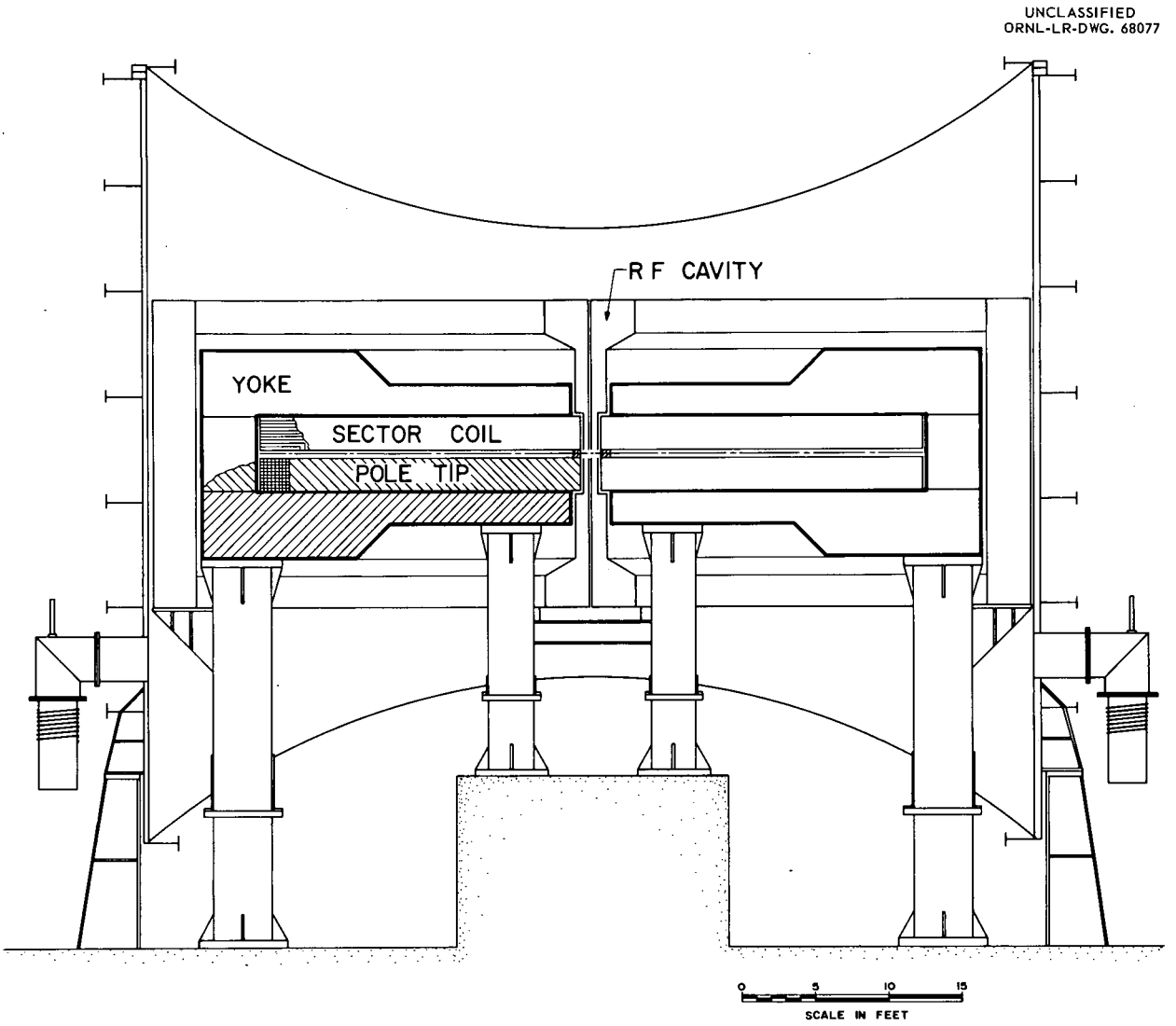

Fig. 6.10. Vertical Section of Mc^2 Cyclotron.

Vacuum System

At the present time, it appears that a tank 60 ft in diameter and 50 ft high will be required to fit around the magnet and cavities. This tank will have a volume of 112,800 ft^3 empty and 92,800 ft^3 with the cyclotron in place. The total estimated surface area would be about 45,300 ft^2. Depending on construction materials used, the outgassing rate would be about 2 torr-liters/sec after ten hours of pumping.

By using seven 780 CFM mechanical pumps and three 12,000 CFM Roots-blowers, this tank could be roughed down to $1\frac{1}{2}$ to 2 hr. Ten more hours of pumping would reduce the pressure to 5×10^{-6} torr.

For the diffusion pumps, this would require a total pumping speed of 600,000 liters/sec, which could be provided by thirty-two 32-in.-diam oil diffusion pumps with baffles.

Other pumping systems and methods will be studied.

Cyclotron Building

A preliminary layout is shown in Fig. 6.6. The cyclotron will be assembled in the vault with an overhead crane of about 125-tons capacity. The

vault will be closed with 100-ton roof shield blocks. A tunnel is provided for personnel and the utility entrance. Space in the high-bay building will be used for the preassembly and fabrication shop.

The office and laboratory building will contain the cyclotron control center as well as the counting room and light utilities. For convenience and ready access, two other small buildings are placed close to the areas they serve.

Entry to the experimental areas will be through tunnels for both personnel and utilities. For large equipment, a 20 × 20 ft opening is provided in one wall of each room. This opening will be closed with blocks, or possibly a plug-type door. Each room will have an overhead crane for handling experimental equipment.

Shielding will have to be very heavy; it will be composed of concrete, compacted rock, and earth in the most economic combinations.

7. Magnet Studies

The availability of new alloys with unusual superconducting properties suggests new possibilities in the design and development of devices utilizing high magnetic fields. For high-field studies, a 2-in.-ID solenoid was designed and constructed for steady operation at magnetic fields in excess of 100 kilogauss. A specimen of niobium–25% zirconium wire, 0.010 in. in diameter, tested in this high-field solenoid retains its superconducting properties at fields up to 70 kilogauss. At liquid-helium temperatures a 5000-turn model magnet wound from 0.5 lb of this wire produces a magnetic field of 32 kilogauss in a $\frac{1}{2}$-in.-diam core. The feasibility of using superconducting magnets with bubble chambers is being investigated.

HIGH-FIELD SOLENOID

R. S. Lord E. D. Hudson

To provide for studies of phenomena such as superconductivity and ionization processes in high magnetic fields, a solenoid was designed and constructed for continuous operation at 100 kilogauss. This iron-shell solenoid (Fig. 7.1) has a 2-in.-diam bore, 10 in. long.

The solenoid consists of 350 turns of $\frac{1}{4} \times \frac{1}{4}$ in. copper conductor with a $\frac{1}{8} \times \frac{1}{8}$ in. water passage. It was designed with sufficient water cooling to provide for a maximum dissipation of 3250 kw. The water flows through 112 parallel circuits, each about 60 in. long. Eight 60-in. conductor strands

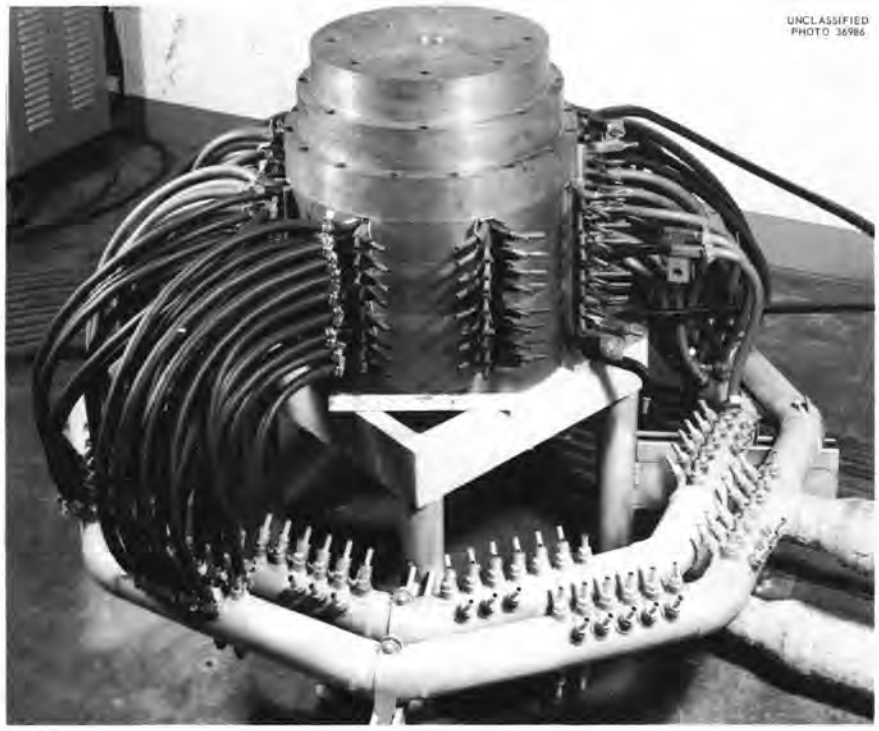

Fig. 7.1. The High-Field Solenoid. Access to the 2-in.-diam bore is at the top.

are wound to form a two-layer pancake; the current flows inward $1\frac{9}{16}$ turns in one layer and back outward $1\frac{9}{16}$ turns in the other layer. All eight strands in a pancake are connected in series, and all pancakes are connected in series. Each pancake contains 25 turns. The number of pancakes that can be assembled in the iron shell (Fig. 7.2) depends on the amount of insulation used between layers. The magnetization curves (Fig. 7.3) were obtained for a 350-turn assembly of 14 pancakes.

As shown by the magnetization curve, the iron shell increases the field about 12 kilogauss above the 88.3 kilogauss calculated for an iron-free solenoid. Insertion of iron plugs in the solenoid reduces the length of the usable magnetic volume to $\frac{5}{8}$ in. but increases the field at the center to 117 kilogauss. The total contribution of the iron to the magnet is then 28.7 kilogauss, and the power that would be required to obtain 117 kilogauss in the solenoid is reduced from 5700 to 3200 kw. When the central field is 100 kilogauss, the iron shell has not become sufficiently saturated to alter the slope of the magnetization curve at the center of the magnet; the slope is 13.5% greater than that for the nonferrous magnet.

A calculation neglecting the 2-in.-diam bore through the shell gives a central field of 104.6 kilogauss instead of the 100 kilogauss measured. The iron serves to produce a much larger volume of uniform field at the lower fields. It also makes a very good containment vessel for any flying objects that might be released in the event of a coil failure.

The magnet was designed with a liberal amount of iron in the shell so that portions of the shell could be removed in order to arrive at an optimum shell experimentally. These tests have not been made because of the demand for experiment time on the magnet.

Fig. 7.2. The High-Field Solenoid, Partially Assembled. The central positioning post and the straps on the coils are removed before final assembly.

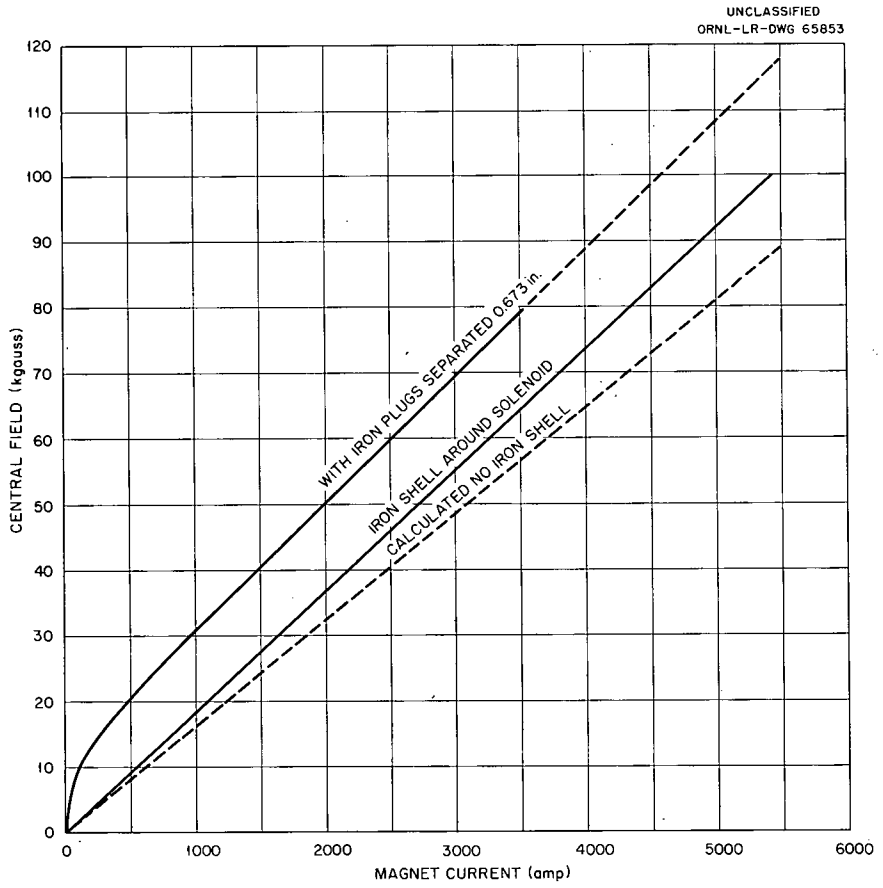

Fig. 7.3. Mognetization Curves for High-Field Solenoid.

CRYOGENIC ELECTROMAGNETS

R. W. Boom
C. J. Bergeron[1]
L. D. Roberts[2]
T. H. Boyer[3]

Basic studies of cryogenic electromagnets include (1) studies of superconducting properties of materials, (2) model-magnet investigations, and (3) magnet design studies.

Superconducting Materials

Two superconducting materials, NbSn and NbZr, were obtained in suitable forms, and their superconducting properties are being evaluated. Specifically, they are tested at liquid-helium temperatures to determine the critical current and critical field conditions at which the material ceases to be superconducting and exhibits normal resistance. Initially, tests were made in the pulsed-field magnet facility at Vanderbilt University in collaboration with C. E. Roos. As soon as the high-field solenoid was available, an experimental program was undertaken at ORNL. This solenoid has the advantage of continuous operation at magnetic fields in excess of 100 kilogauss.

Wires formed from niobium tubes packed with powdered Nb_3Sn, drawn, and then sintered (Bell Laboratory method) remained superconducting in magnetic fields up to 130 kilogauss. Samples of 0.015-in. wire $\frac{3}{4}$ in. long were tested by pulsed-current pulsed-field techniques at 4.2°K. Critical currents and magnetic fields at which the samples changed from superconducting to normal are shown in Fig. 7.4.

[1] Louisiana State University at New Orleans; collaborated in the superconducting-materials evaluation.

[2] ORNL Physics Division; collaborated in the model-magnet work.

[3] Assisted with the magnet design.

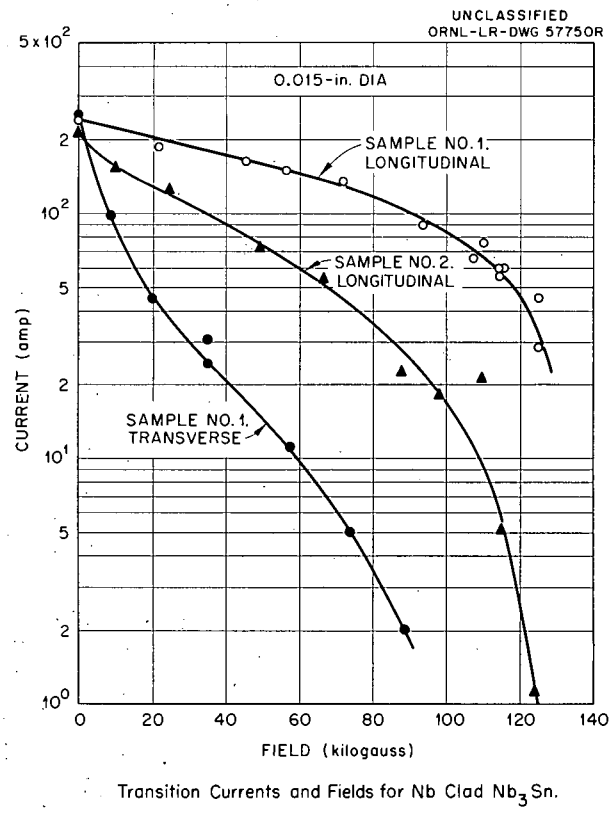

Fig. 7.4. Transition Currents and Fields for Niobium-Clad Nb_3Sn, 0.015-in. Wire at 4.2 K. J. O. Betterton, Jr., R. W. Boom, G. D. Kneip, Jr., R. E. Worsham, and C. E. Roos, "Superconductivity of Nb_3Sn in a Pulsed Magnetic Field," *Phys. Rev. Letters* **6**, 532 (1961).

Wires formed by depositing Nb_3Sn on platinum (RCA method) were tested by a pulsed-current technique in the constant field of the high-field solenoid. Samples of 0.007-in. wire ¾ in. long continued to carry as much as 10 amp at fields up to 96 kilogauss (Fig. 7.5).

A mechanical joint was developed to solve a major problem in testing short samples. Copper-to-superconductor joints are now made by inserting the superconductor into a hole drilled axially into the copper lead and then press-fitting (20,000 psi) the copper around the superconductor. Since the copper contracts more than the superconductor at low temperatures, an excellent joint is obtained.

Samples of drawn Nb–25% Zr and Nb–33% Zr wire were tested in both pulsed and constant magnetic fields. Higher current thresholds are obtained in constant-field tests. Improvements are being made in pulsing methods. A pulsed external field is expected to show fundamental properties involving transition times; 2-μsec transitions have been observed.

Results from constant-current constant-field tests of small solenoids of Nb–25% Zr wire are shown in Fig. 7.6. The dashed curve represents the transition threshold for 100 ft of 0.01-in.-diam wire,

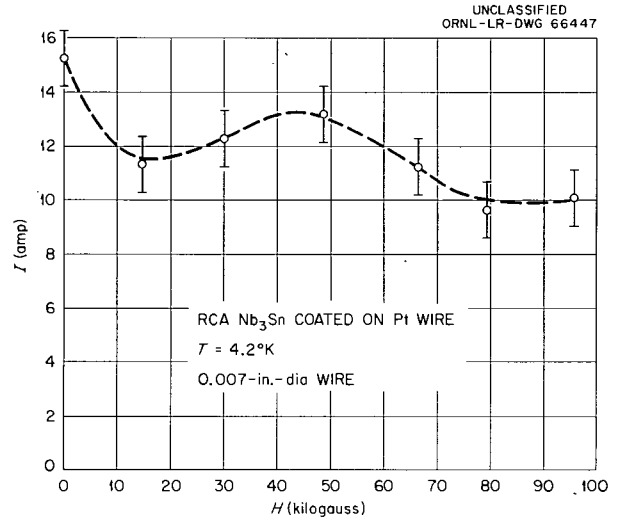

Fig. 7.5. Transition Currents and Fields for Nb_3Sn Deposited on Platinum (0.007-in. Wire) at 4.2 K.

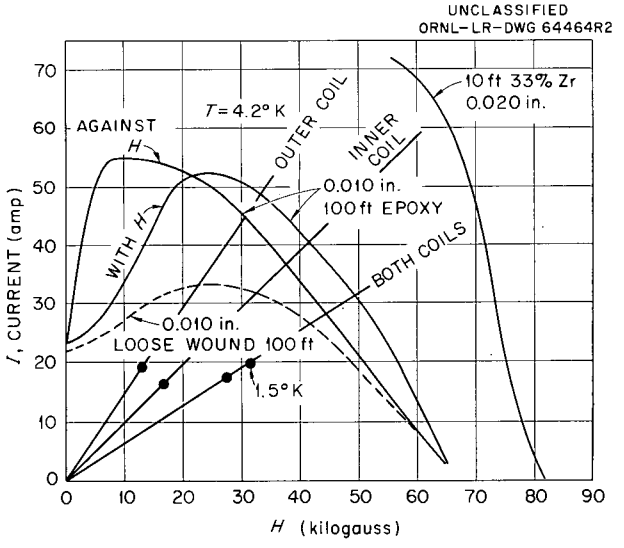

Fig. 7.6. Transition Currents and Fields for Nb–25% Zr in Constant Fields.

tightly wound into a solenoid 1 in. long. Measurements were made with the self-generated field both aiding and opposing the applied field, but the overlapping scatter did not justify more than a single curve. With the windings of a similar 100-ft coil anchored in an epoxy resin, the critical currents were significantly increased, as shown by the solid curves; above 20 kilogauss, higher critical current values were achieved with the self-generated field aiding the applied field.

In a preliminary investigation of the effect of space factor, 50 ft of the same NbZr wire was wound with a copper wire of equal size to provide spacing. The solenoid was cast in epoxy resin before it was tested in the high-field solenoid. Its response was similar to that of the 100-ft coil described above, except that at low applied fields its critical current continued upward to about 70 amp.

Model Superconducting Magnets

The model-magnet program has just begun. The first superconducting magnet (Fig. 7.7) was wound from $\frac{1}{2}$ lb of Nb–25% Zr. There are actually two coils, an inner 3000-turn coil and an outer 2000-turn coil wound from 800 and 1000 ft of 0.010-in. wire. The coil was built with 0.010-in. spacers between every four layers in order to provide space for the liquid helium. The self-quenching maximum fields at the conductor are shown as solid points in Fig. 7.6. At temperatures of 4.2 and 1.5°K, the critical current is 17 and 19 amp, and the field generated is 29 and 32 kilogauss.

When the coil went "normal," a 10-Mc oscillation accompanied by sparking was occasionally observed. Without sparking, a 10-msec transition was observed. With one section of the coil used as a pickup when the other section went normal, it was shown that the field decay resembles a cosine function with a 10-msec half-period.

Fig. 7.7. Model Cryogenic Magnet. With current from an automobile battery a field of 32,000 gauss is obtained in the 0.5-in.-ID core cavity.

Each time the coil was driven to the normal state, the field collapsed in milliseconds, high voltages were generated in the 0.4-henry coil, and currents were driven through the newly resistive material. This violent treatment was repeated more than 500 times before the coil failed.

In continuation of the epoxy tests mentioned above, Nb–25% Zr solenoids are being cast in epoxy resin. Larger test magnets are being designed to operate at higher fields.

Magnet Design

Parameters useful in magnet design were developed within the Fabry[4] notation. The formula is as follows:

$$H_0 = \frac{G\sqrt{\nu}\, Ia}{A} = \text{central field, gauss}$$

$$L = \frac{a^3 \nu}{A} = \text{conductor length, cm},$$

where

$$G = \frac{\sqrt{2\pi}}{5}\sqrt{\frac{\beta}{\alpha^2 - 1}}\,\log_e \frac{\alpha + \sqrt{\alpha^2 + \beta^2}}{1 + \sqrt{1 + \beta^2}}$$

= Fabry factor
(α = ratio of inner to outer diameters, β = ratio of length to inner diameters),

$\nu = 2\pi(\alpha^2 - 1)\beta$ = volume factor,

I = current per turn, amp,

a = inner radius, cm,

A = area per turn, cm^2/turn.

With this formula and several complementary graphs, such as Fig. 7.8, it becomes easy to compute the magnetic field at the center of a solenoid. Optimum use of wire dictates the choice of α, β, which in general lies at somewhat larger β than the optimum $G_{max} - \nu_{min}$ curve shown in the graph. That is, at present it appears that a longer, thinner coil produces more central field per pound of wire than a shorter coil. The shorter coil would produce the most field per unit of power for a resistive conductor. The difference is due to the additional field uniformity for longer coils, resulting in a decreased field (and high current ability) at the windings. Further, it should be noted that for coils of large diameter a good space factor is not very important (wire length is almost independent of space factor) and, in fact, may be undesirable from a stress standpoint.

In the simplest approximation[5] a solenoid is considered to be a pressure vessel with sides of thickness t and internal pressure $P = B^2R/1.735$, where P is in psi, B is in kilogauss, and R is radius in inches. Here the hoop stress S (in.-lb/in.^{2}) = $B^2R/1.735t$. For large coils the stresses are reduced by making t large (low space factor).

In addition to the standard calculations indicated above, a computer program was developed for plotting fields throughout the body of a coil. An example of the field in the test-model magnet described above is shown in Fig. 7.9. It is suggested that in order to save wire, different currents could be used in different sectors of the coil. Conversely, if a given safety factor is desired, one should know at each point in a magnet how close the current is to the transition value. From the results mentioned earlier for 100-ft lengths, it appears that high and low field points in a coil may quench out first. Models in which the current densities at various points can be varied are being constructed to test this speculation.

BUBBLE-CHAMBER STUDY

R. W. Boom

The Electronuclear Division participated during the year with the ORINS–ORNL Study Committee in an examination of the possibility of constructing a high-energy experimental device for collaborative research. The year-end report[6] of the Study Committee includes the following conclusion and recommendations:

1. A 100-kilogauss, 30- to 40-in.-diam hydrogen bubble chamber would be well suited to the needs of high-energy physicists in the area; efforts toward this end should be continued.

---

[4] Ch. Fabry, *L'Eclairage Electrique* 17(43), 133–41 (1898); *J. Phys.* 9, 129–34 (1910).

[5] See, for example, P. Hernandez *et al.*, *Brookhaven International Conference for High Energy Accelerators, August 1961* (in press).

[6] *A High Magnetic Field Bubble Chamber*, report of the ORINS-ORNL Study Committee, ORINS-40 (November 1951).

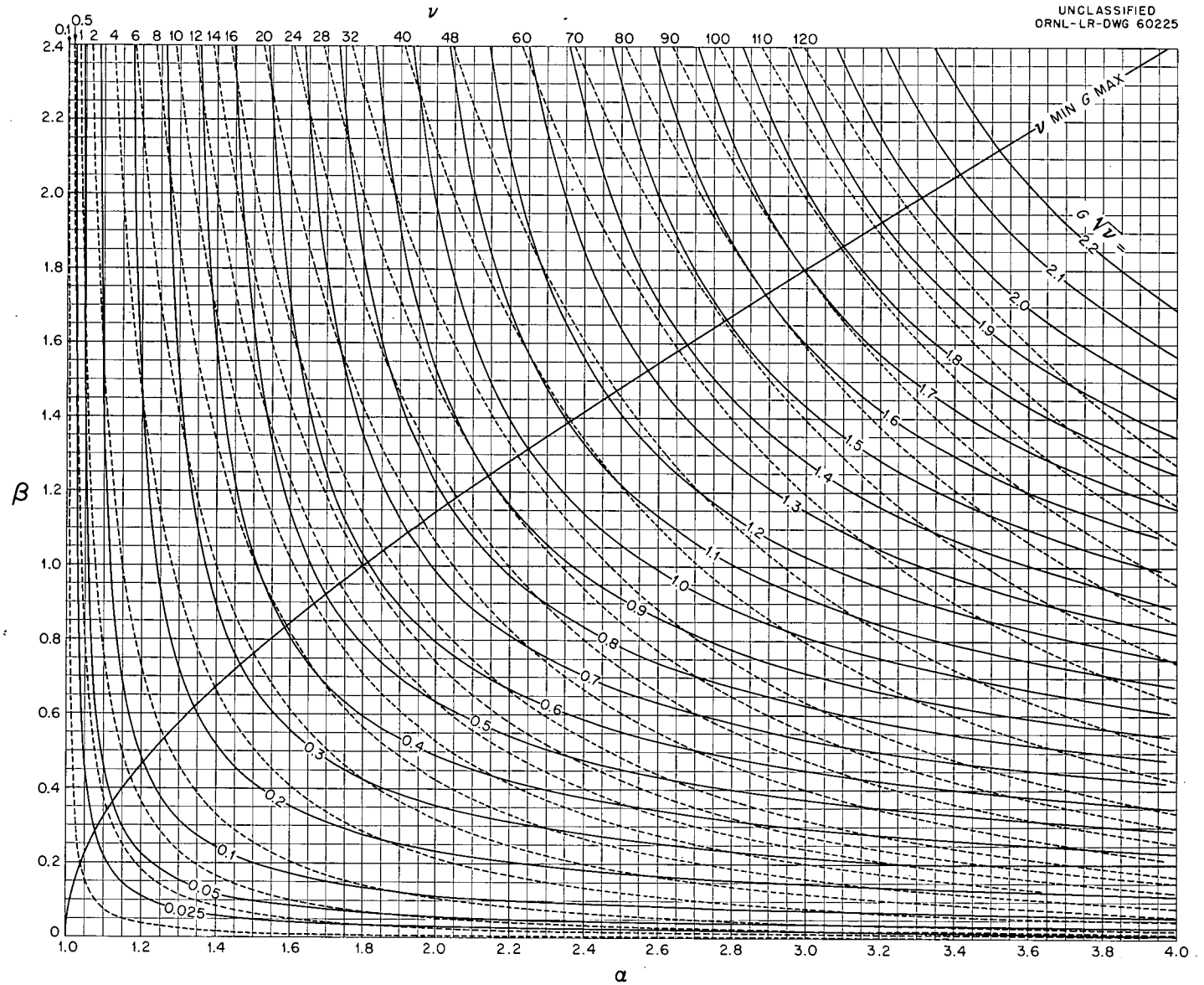

Fig. 7.8. $G\sqrt{\nu}$ *vs* α **and** β **for Square-Ended Constant-Current Solenoids.**

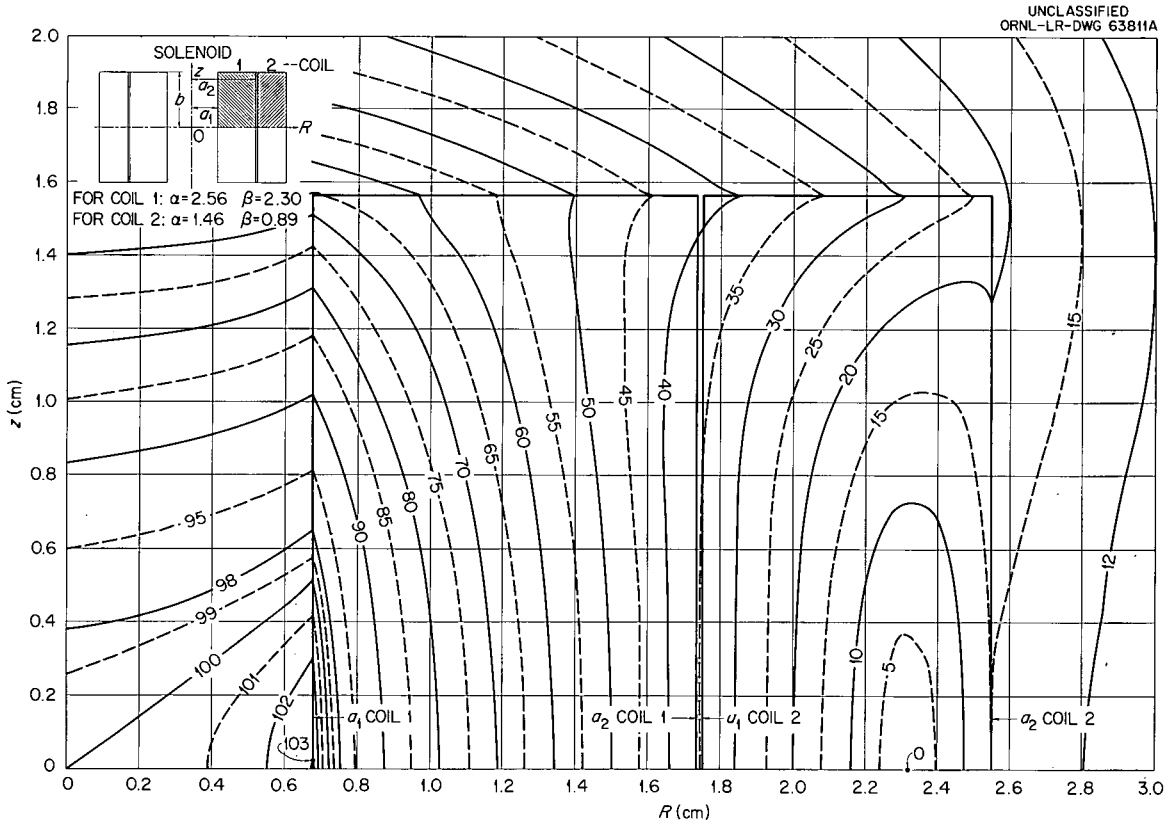

Fig. 7.9. Total Field, $\sqrt{H_R^2 + H_Z^2}$, for the Model Magnet Shown in Fig. 7.7. Lines of constant total field are shown.

2. As a first step, ORNL, in cooperation with the University of Chicago and Argonne National Laboratory, should design and construct a 15-in. superconducting high-field solenoid to accommodate an existing 10-in. bubble chamber.

3. These devices requiring high-field magnets should be implemented by the superconductivity program at ORNL.

A formal proposal for item 2 will be made as soon as possible. Design and operation of small superconducting magnets should give a firm foundation for such a proposal. The major question is the choice of a superconducting material. Secondary problems involve a careful evaluation of the physics programs, the costs, and the optimum field vs project delay. Detailed magnet design problems, while substantial, should not be insurmountable.

8. The Oak Ridge Isochronous Cyclotron

R. J. Jones
R. S. Livingston
R. H. Bassel
R. S. Bender
T. E. Bridge[2]
E. D. Hudson
R. S. Lord
M. B. Marshall
S. W. Mosko
P. D. Postma
E. G. Richardson, Jr.
A. Riikola
J. A. Russell[1]
W. R. Smith
W. H. White[1]
R. E. Worsham
N. F. Ziegler
A. Zucker

The Oak Ridge Isochronous Cyclotron (ORIC) is a variable-energy, three-sector, azimuthally-varying-field, 76-in. cyclotron designed to accelerate various particles, with e/m ratios from 1 to 0.125, to energies up to 145 Mev. The machine is designed to accommodate the power requirements for large ion currents, up to 75 kw or 1 ma of protons at 75 Mev.

Since the ORIC building (Bldg. 6000) was accepted from the construction contractor in mid-January, 1961, rapid progress has been made in the fabrication, assembly, testing, and installation of the various systems of the cyclotron. The complex magnet structure is now installed and an extensive program of detailed and precise field measurements is completed. Also, installation of the single-dee radio-frequency system is nearly completed.

A temporary rf system without the final-stage power amplifier is being readied for early test operation of the cyclotron. These early tests will be undertaken at reduced energy to verify orbit and magnetic field calculations, to prove the performance of the various component systems, and to provide the beam data needed for completion of the beam deflector system.

The magnet, radio-frequency, and control systems are described below in more detail. In addition, the ion source assembly has been completed and tested for the operation sequence required for remote control; it is ready for testing in the cyclotron. The system for water-cooling the many cyclotron parts is completed; the purification and cooling cycles and the safety interlocks have been test operated. The pole tips and other steel surfaces exposed to high vacuum were nickel plated, to reduce outgassing, before the vacuum system was assembled. This system is completed, leak checked, and tested; the pumping speed is 15,000 liters/sec at a base pressure of 2×10^{-6} torr.

THE ORIC MAGNETIC FIELD

The magnet yoke and main coils which had been assembled and tested in the Y-12 area were disassembled, moved to the new cyclotron building, Bldg. 6000, and reassembled outside the building. The magnet was then moved on rollers into its final position inside the cyclotron vault, Fig. 8.1. After the pole tips were carefully aligned, the harmonic coils, valley coils, and circular trimming coils were installed and their contributions to the magnet field were measured at nine levels of main field excitation. The data from the field measurements are processed on the IBM 7090 in such a way that it is possible to predict coil current settings required for an isochronous field for any specified particle or energy.

Magnet Installation

Any asymmetries in the magnet structure give rise to unwanted harmonics in the magnetic field. To

[1]Instrumentation and Controls Division.
[2]Catalytic Construction Company.

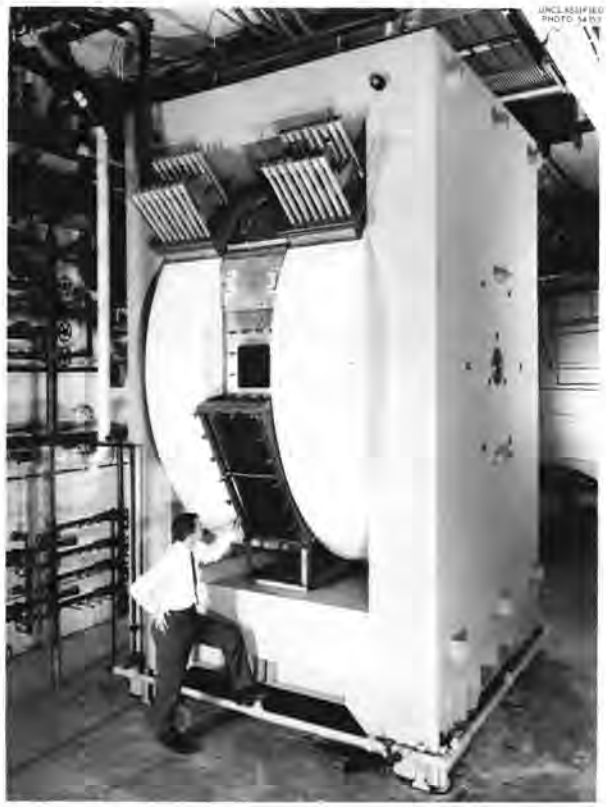

Fig. 8.1. The ORIC Magnet Being Installed in the Cyclotron Vault.

avoid this, careful alignment of all the components was necessary. The pole tips were aligned and dowelled onto the pole-base disks prior to installation in the magnet, Fig. 8.2. The straight edges of the pole tips were placed 120° apart to within ±0.0003 in., and the radius was set with a tolerance of ±0.001 in. The symmetry of the other surfaces parallel to the axis is inherent, due to the method of fabrication in which all pole tips were machined on the same jig.

The center holes in the pole bases determine the relative position of the axis of the tips on one side of the gap with respect to the axis of those on the other side. These holes were aligned opposite each other to within 0.0015 in. by shimming one vertical yoke member. The pole-tip assemblies were then installed, and the azimuth of two opposing pole tips was set the same, by use of a precision level and a sine bar; the estimated error is 0.0004 in. at the 38-in. radius.

The gap between the pole tips was measured with the magnet off and the magnet on. With no field, the gap varied over the surface of the poles from 7.5473 to 7.5539 in. With the magnet energized, the gap was from 7.5085 to 7.5162 in.

The magnet power supplies for the cyclotron were installed and used during the magnetic field measurements. The motor generator supplies for the main and valley coils are regulating to the required accuracy, 0.01%, and hold this regulation for long periods of time. The rectifier supplies for the AVF coils are regulated by a combination of transistors and saturable reactor control elements. The regulation for these supplies is also within the required 0.01%.

AVF Coils

To achieve versatility, the ORIC Magnet contains a number of pole-tip coils, Fig. 8.3. Three pairs of valley coils increase the flutter at large radii for high-energy protons. Ten pairs of circular trimming coils shape the radial gradient so that a wide range of particles and energies can be held in isochronism. Three pairs of harmonic coils, Fig. 8.4, in each valley are capable of cancelling unwanted harmonics due to any asymmetries of construction, or can be used to introduce harmonics if needed for beam extraction.

Some of the design criteria for the harmonic, circular trimming, and valley coils are as follows: (1) They must have a long life in a radiation field. (2) They must be sealed in a vacuum tight container. (3) They must have a high degree of dimensional accuracy in both construction and positioning so that they will not introduce unwanted disturbances in the magnetic field.

The insulation materials chosen for the coils were asbestos, glass, and silicone resins, Fig. 8.5. These materials all rate high in their resistance to radiation damage and in their ability to withstand the high temperatures encountered during the process of welding the stainless steel containers around the coils. All coils were impregnated with R-65 silicone resin to fill the voids and prevent motion of the coil inside the container. Prior to impregnation, the space between the coils and the containers was filled with 0.015-in. glass beads to prevent fracture of the resin during curing. This was necessary for only the harmonic and valley coils, where the voids were comparatively large. The dimensional accuracy was assured by the careful use of jigs for positioning the coils in the cans and for drilling the attachment holes in the containers, Fig. 8.6.

Fig. 8.2. Set of Pole Tips and Shims Mounted on Pole Base.

The containers for the circular trimming coils were the most difficult to seal. Heliarc welds were made around bolt holes only $\frac{1}{8}$ in. from the silicone impregnated asbestos paper insulation. Special cooling plugs, or heat sinks, were attached to the coil in the area to be welded. These prevented damage to the insulation.

A circular trimming coil assembly containing 10 coils is 76 in. in diameter and $\frac{1}{2}$ in. thick. The conductor is $\frac{1}{4}$ in.-square copper with a $\frac{1}{8}$-in. square hole. It is wound on a grooved stainless steel plate which forms one side of the container, Fig. 8.7. The wall thickness is 0.078 in. To withstand the pressure differential, the cover is spot welded to the ribs between the coils at 3-in. intervals. The total power required for one assembly of ten coils is 150 kw.

Field Measuring Program

The magnetic field was measured in considerable detail to: (1) discover any imperfections in the construction of the magnet that would introduce harmonics into the field, and (2) to gain sufficient information on the effect of the AVF coils so that proper current settings can be predicted for each coil for any desired particle and energy.

Because of saturation effects in the iron, the field effects produced by the pole-tip coils are different at different levels of main field excitation. Since the effects of the circular trimming coils are most critical, they were measured at nine levels of main field excitation. A total of 165 field measurement runs were made for the field mapping program. This required measuring and

UNCLASSIFIED
ORNL-LR-DWG 58399R2

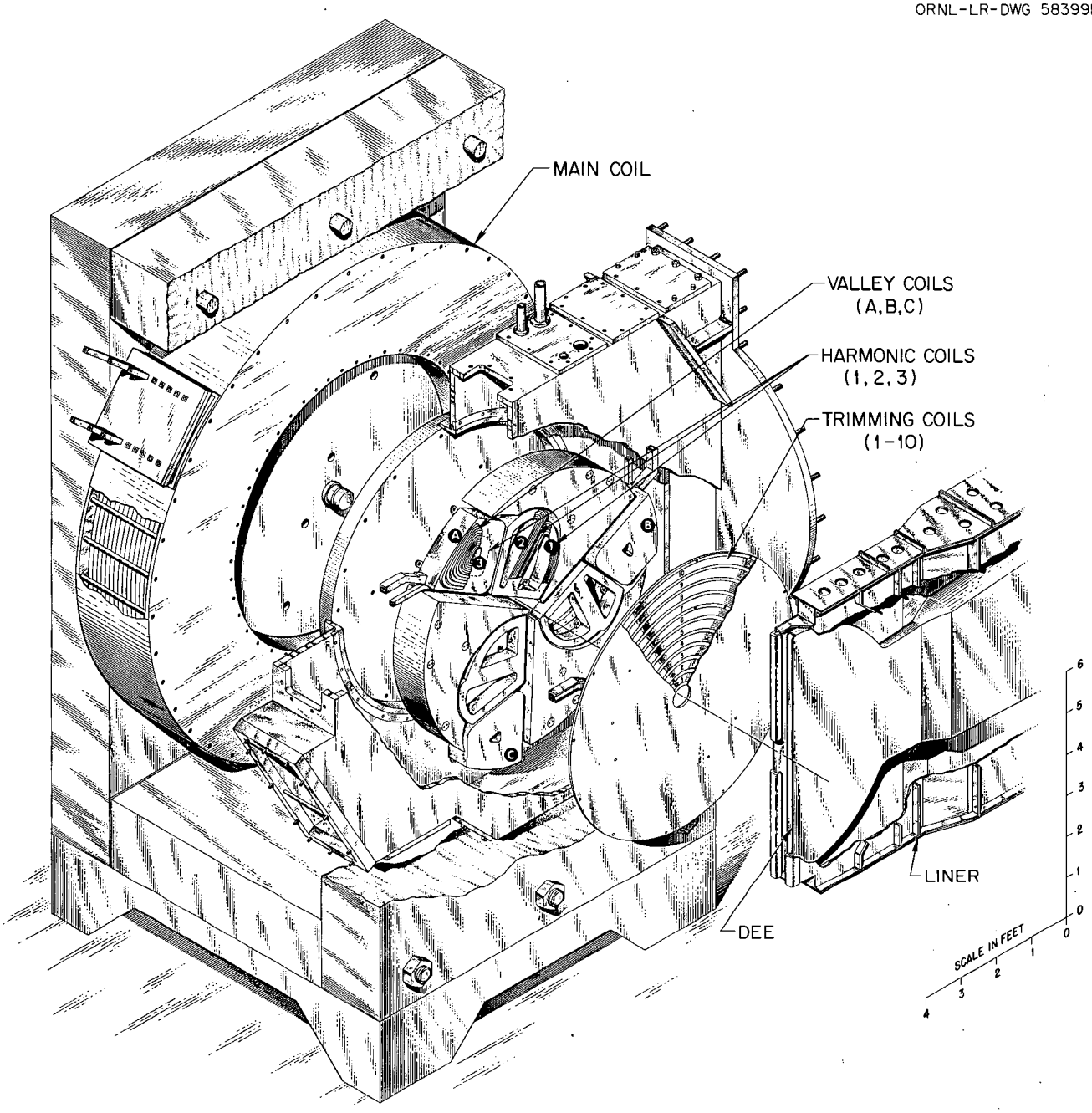

Fig. 8.3. Exploded View of ORIC Magnet Showing Details of One Pole.

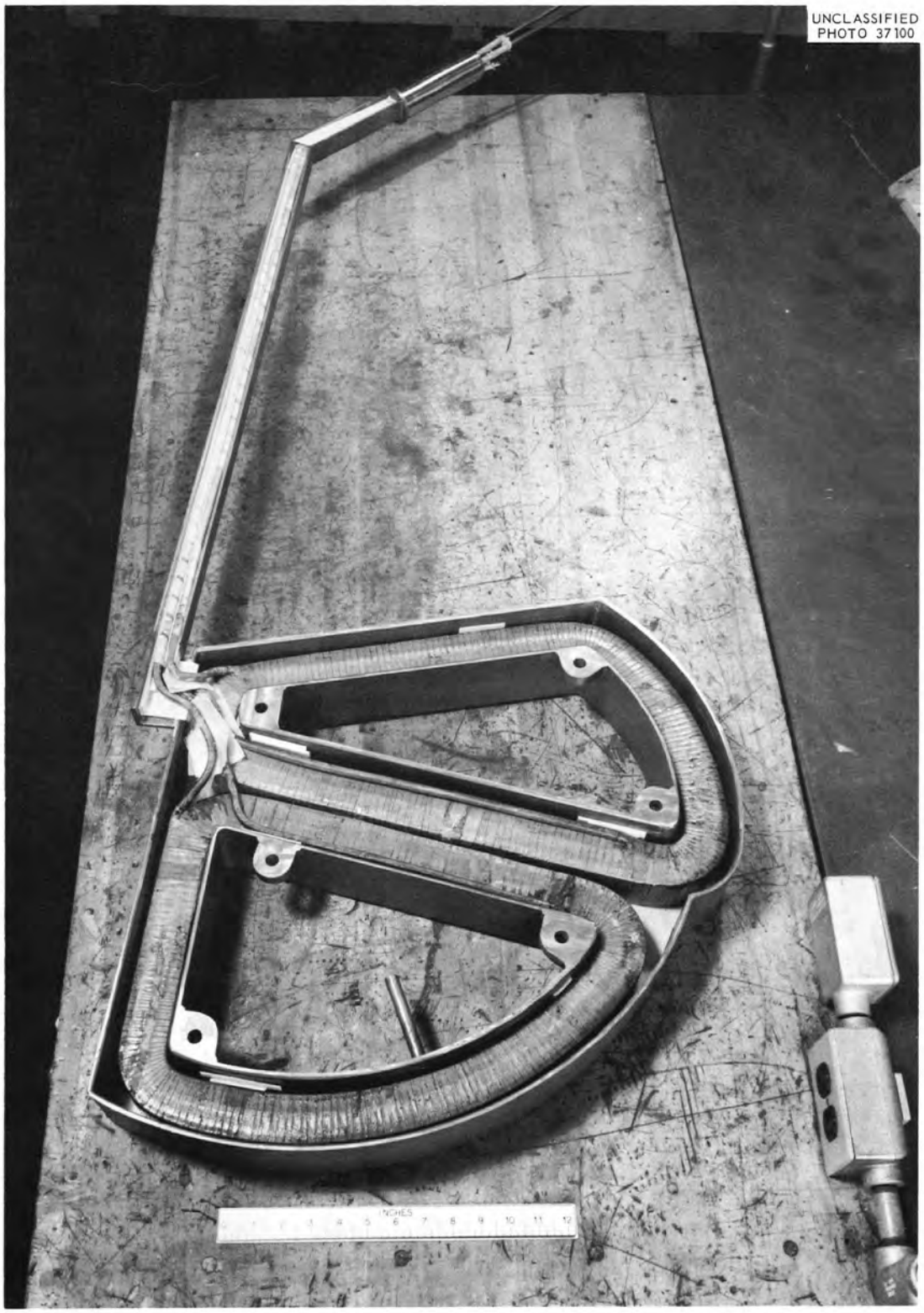

Fig. 8.4. Two of the Harmonic Coils Are Sealed in the Same Container; the Third Is Contained Within the Valley Coil.

Fig. 8.5. Valley Coil and Insulation; a Smaller Harmonic Coil Is Placed Concentrically in the Same Container.

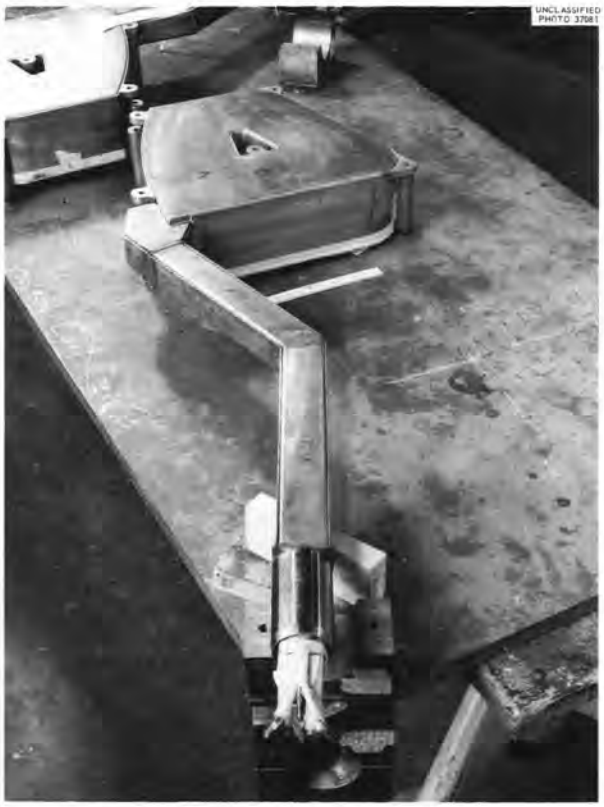

Fig. 8.6. Valley Coil in Welding Jig; All AVF Coils Are Sealed in Vacuum Tight Jackets.

recording 500,000 five-digit numbers for use in the computing programs for calculating the coil current settings.

Preliminary inspection of the data indicates that there are no serious asymmetries in either the iron pole tips or the valley coils. The maximum first harmonic is 19 gauss at a radius of 33 in.; this is well within the range that can be cancelled by the harmonic coils. Based on these field measurements the magnetic-field contour map for 75-Mev protons, Fig. 8.8, was calculated for a main coil excitation of 3220 amp and valley coil excitation of 1820 amps.

Data Processing and Orbit Studies

In January, 1961, the IBM 704 was replaced with the IBM 7090. The demand for computing time was so great that the use of a monitor system, where several different problems are run in sequence, was required. Although the total machine time for one production run was then half an hour, it took one week to process a single set of field measurements; twelve separate programs were involved and there was no way to transfer from one program to the next. The stable orbit computation was written in symbolic algebraic language for the IBM 704 with absolute memory location, and it was impractical to incorporate the twelve programs written in different languages into one continuous monitor run. The stable orbit code was revised in Fortran language and the connecting links established so that the production program now runs smoothly.

After the Hall probe voltages are converted to magnetic fields, each point is checked for error and smoothness by a radial and azimuthal six-point Lagrangian interpolation. Except when too many errors occur in adjacent radial or azimuthal points, the program operates reliably to an accuracy of 6 gauss. The accuracy is, of course, relative since

Fig. 8.7. Winding the Trim Coils, Ten Pairs of Concentric Coils Are Used to Control the Radial Gradient of the Magnetic Field.

systematic errors in the calibration of the Hall probe would remain. The isochronous average field is calculated to an accuracy of better than 3 gauss.

The trimming coil currents are found for minimizing both the phase slip and the effects of small deviations in the average magnetic field which could produce defocusing in limited regions, or excessive values of axial focusing in the deflection area. The field produced by these currents is added to the measured field, and the stable orbit properties calculated. The Fourier components of the field, radial derivatives of the flutter and average field, and various quantities used in the approximate formulas for AVF cyclotrons are evaluated. If only one sector of the field is used, this computation takes 8 min. If the entire magnet is measured, 7200 field points, the calculation takes 22 min.

The various measurements of the magnetic field are processed with no delay, once the paper-tape data are converted to punched cards. A very extensive number handling program is required to determine the fields produced by the 21 different coil currents. Since the fields vary due to severe saturation of the iron, an extremely extensive interpolation program is required. This program has been outlined and will be ready for use in January.

In the hope of saving time, a strong first-harmonic bump with a large radial gradient was tried for deflection. While this appears satisfactory for nitrogen, the slower increase of energy per turn and the stronger magnetic field needed for 75-Mev protons required a careful study of the interaction

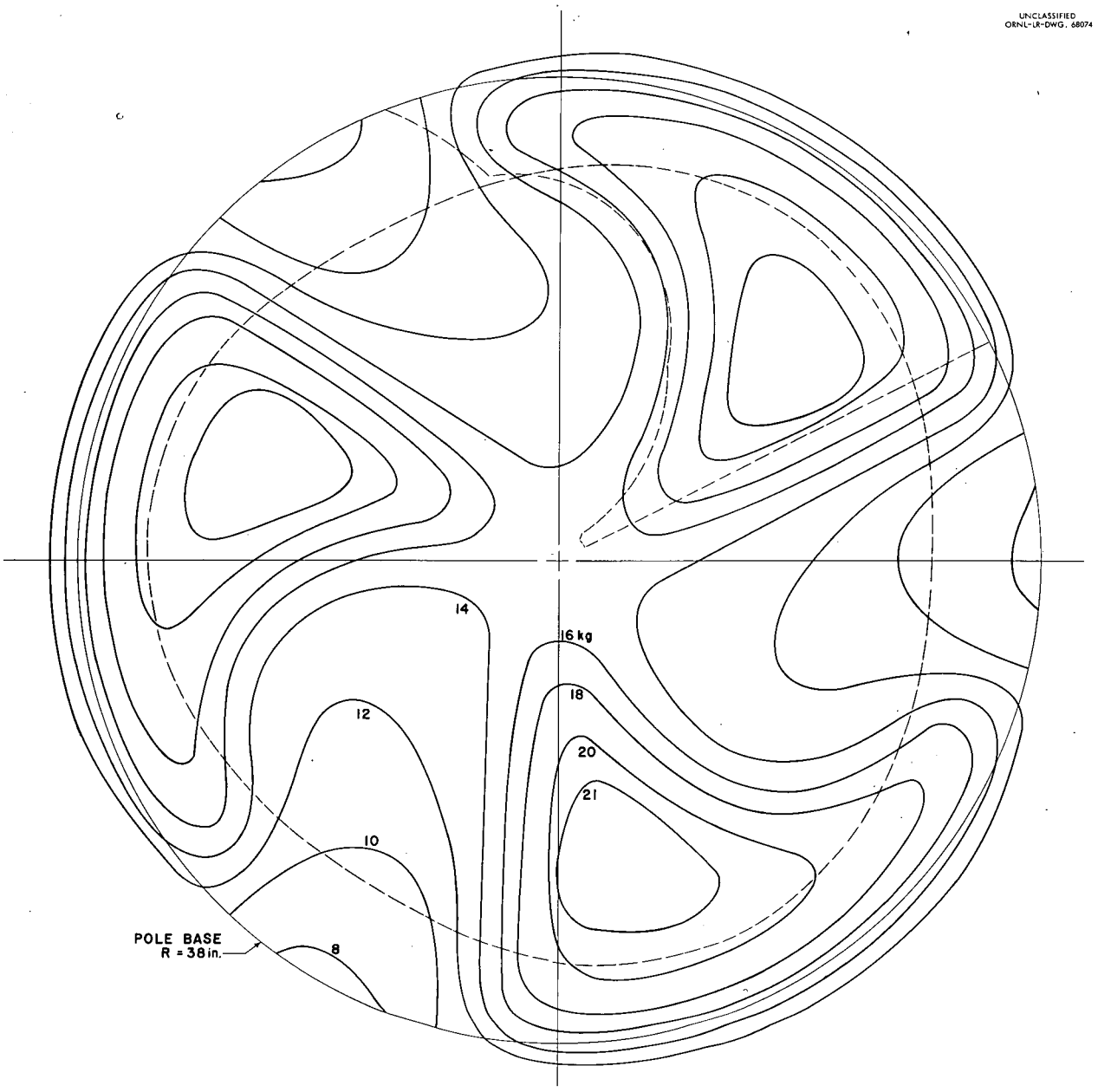

Fig. 8.8. Field Contour Map for 75-Mev Protons.

of the first and second harmonic with the $^3/_3$ resonance. It is clear that the angular position of the bump, as well as radial, is severely restricted; also, the start of the septum has a very limited angular orientation with respect to the hills and valleys of the magnetic field. Main emphasis now is on completing this problem.

THE ORIC RESONATOR AND RADIO-FREQUENCY SYSTEM

The major subassemblies of the single-dee resonant system are fabricated and are being assembled ready for installation. A full-scale model of the system was used in measuring the characteristics

of the resonator and in determining the specifications for the rf components required to drive it. Models of these components have been tested and the overall design has been established.

The Resonator

The dee, liner, dee stem, trimming capacitors, and other parts of the resonator were fabricated and are now mounted as subassemblies ready for installation. When completely assembled on the handling dolly, the resonator structure will weigh about 20 tons. The major subassemblies have been vacuum tested; the assembled resonator should be ready for preliminary testing under vacuum in January.

The Dee and Liner. – Conservation of magnet gap space dictates that these structures be as thin as possible and still remain stable; further, ample water cooling is required. Various designs and fabrication techniques were examined. A process with a copper plate with milled water passages covered with copper sheet was investigated and abandoned because of excessive weight. In the process finally selected, copper tubing was flattened while under constant hydraulic pressure and then brazed to copper sheet, Figs. 8.9 and 8.10.

The tubing was attached to the sheet by means of a fillet braze interrupted at 1.5-in. intervals and staggered to alternate sides of the tube. The fillets were made with a Heliarc torch, and BT braze metal was used as filler. This technique was developed to minimize warpage, to retain most of the original hardness of the metal, to eliminate trapped volumes which might become "virtual" leaks, and to still provide for adequate heat transfer.

Trimming Capacitors. – These capacitors were fabricated by the same tube-on-sheet techniques used on the dee and liner. The chief problem encountered was a method of mounting the capacitors in the vacuum chamber which will provide for remote-control positioning. A mechanical system involving

Fig. 8.9. The Outer Surface of the Liner, Like the Inner Surface of the Dee, Is Traced with Flattened Copper Tubes for Water Cooling.

Fig. 8.10. A Special Jig Was Used in Mounting the Dee to the Transition Piece.

linkages and screws operating through vacuum seals was examined but abandoned in favor of a hydraulic system. An external motor-driven transmitter bellows is connected through copper tubing to an internal receiver bellows which is linked to the capacitor. This constant-volume closed system provides a direct positive control which is found to operate very dependably.

The Shorting Plane. – This most complex part of the resonant system consists of a ring of 48 pneumatically driven, water-cooled shoes; it provides a movable short between the dee stem and and the dee-stem house, Fig. 8.11. The design for the shoes was developed during a long series of tests. Units of the final design survived cycling tests estimated to be comparable to at least 10 years of operation. The whole assembly has been tested mechanically, and for vacuum tightness of the hundreds of joints involved.

Dee Stem and Housing. – Since they were received from the fabricator, these major components of the resonator have been assembled and carefully aligned. The two copper-clad steel tubes, 50-in. OD and 75-in. ID, respectively, are cylindrical to within $\frac{1}{16}$ in. The dee stem is cantilevered in the housing and aligned coaxially within $\frac{1}{32}$ in. The shorting plane and its support rails and driving mechanism were mounted, Fig. 8.11, and tested for mechanical performance. The dee and the dee transition piece with their many water lines are now being installed and aligned.

The Oscillator and RF Drive

The designs for the oscillator and the several amplifier stages, which drive the resonator, have been developed from tests on a full-scale model of

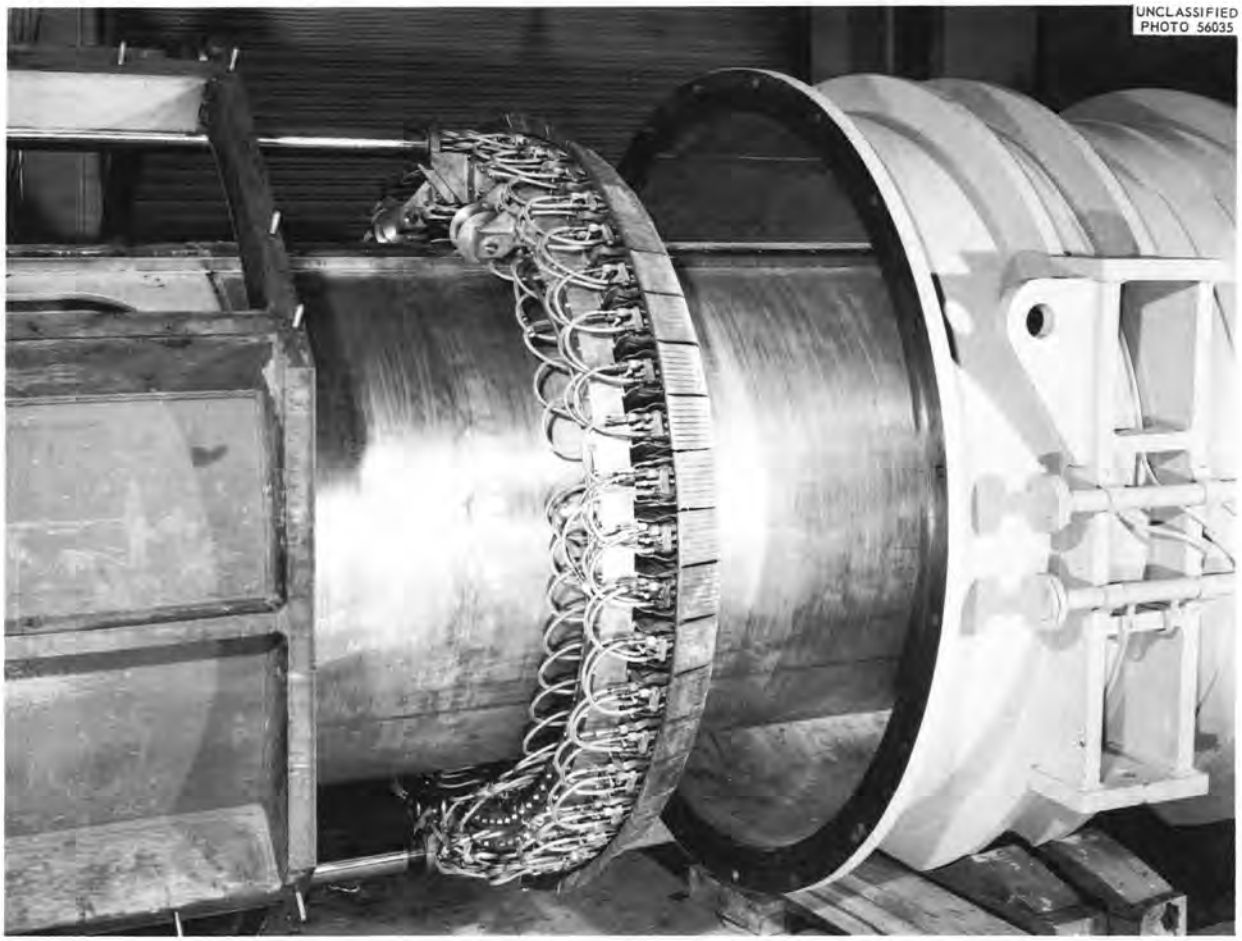

Fig. 8.11. The Moveable Shorting Plane Between the Dee Stem and the Housing Consists of a Ring of 48 Pneumatically Operated Shoes.

the resonator and from tests of breadboard test circuits. The system is outlined in Fig. 8.12. While the components of the final stage of the power amplifier are being fabricated, a temporary rf drive system is being prepared to permit test operation of the cyclotron in a more tractable low-power range.

The Oscillator. – The oscillator circuitry has been tested and operated during the past year. However, greater reliability is being achieved by redesign of the circuit to use transistors. The oscillators and oscillator-control circuits were rebuilt and tested on breadboard. The frequency-dividing and multiplying circuits are being tested.

Intermediate Amplifier. – The 7558, 7212, and 7094 intermediate amplifier stages were constructed for testing and have been in operation for about four months. Physical circuit modifications were necessary to stabilize operation. The basic circuit remains as described last year.

Driver-Power Amplifier. – The 4CX5000A driver tube circuitry and the π-network for coupling between the 4CX5000A plate and the 6949 grid were constructed for testing. Elimination of parasitic oscillations and measurements of the circuit losses and tuning parameters is in progress.

Resonator-Power Amplifier Coupling. – The intermediate amplifiers and the 4CX5000A amplifier were connected through a half-size model of the coupling network to the full-scale rf model. Measurements have been made with the system operating up to 10 kv. No automatic tuning was built in; however, all of the tuning detectors were installed. Measurements were beset by many parasitic oscillations, although over the tuning range which was checked, from 9 to 16 Mc, no serious discrepancy was found between computed and measured results. The coupling network is being redesigned to operate at lower impedance levels and to eliminate the inductive plate steel. This change requires

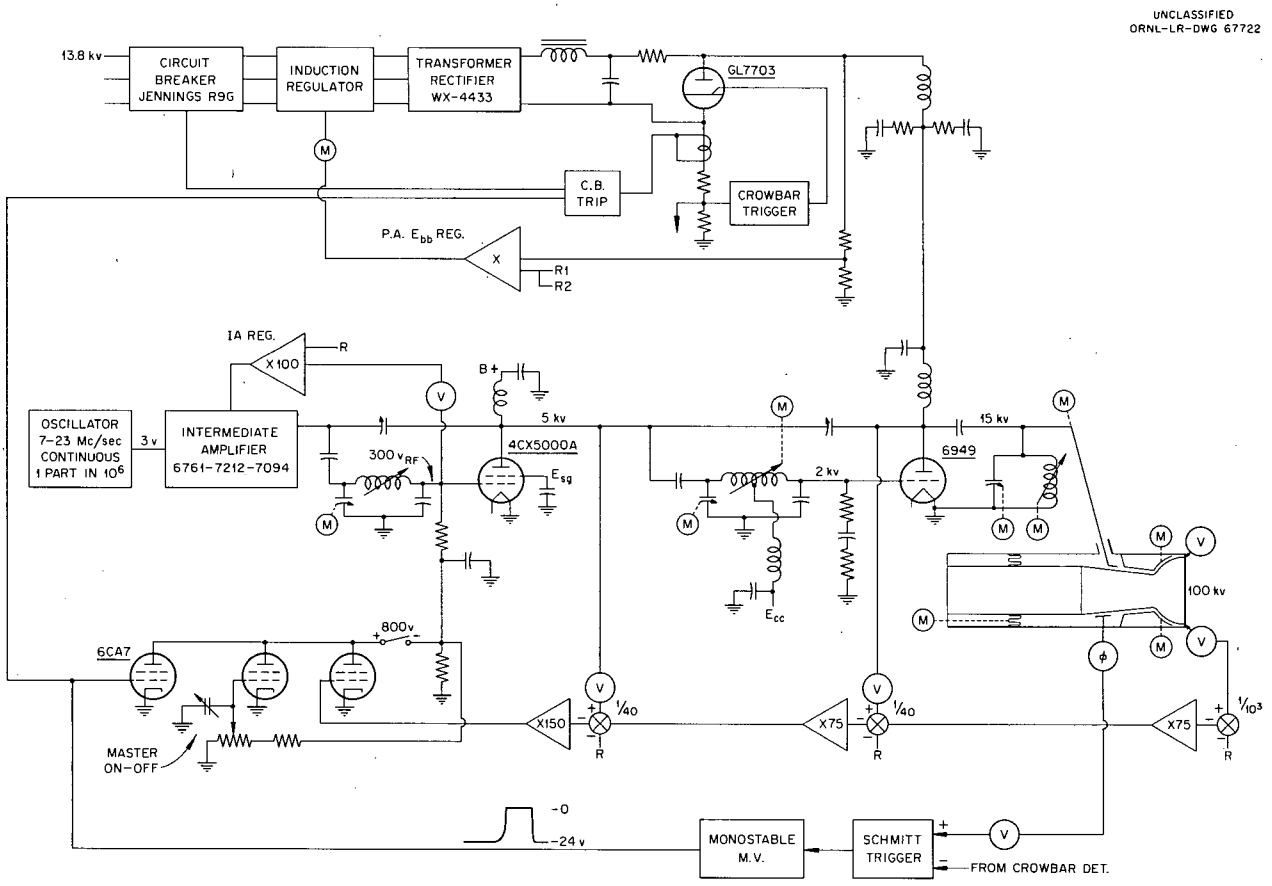

Fig. 8.12. Block Diagram of RF Amplifiers, Control, and Regulator Circuits.

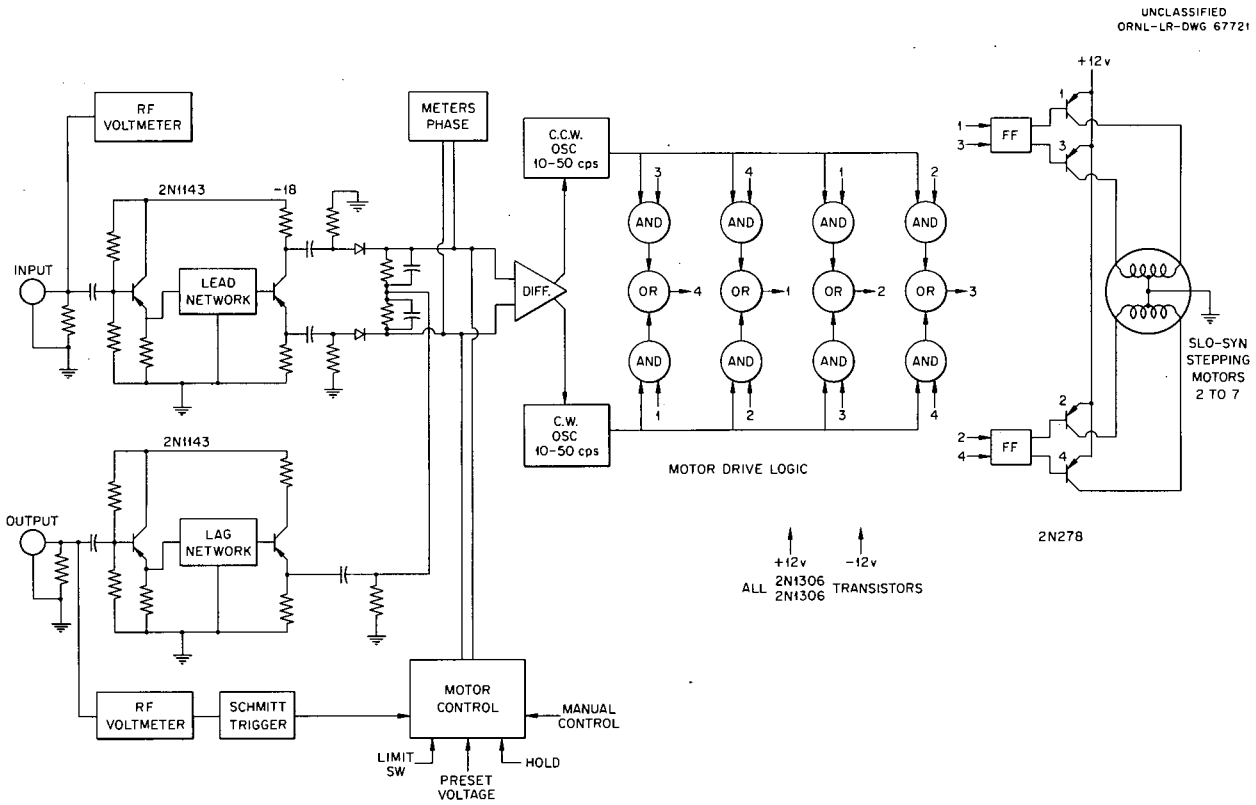

Fig. 8.13. Automatic Tuning Servomechanism for the RF System.

the plate-to-node transmission line to have a variable characteristic impedance.

Overload Protection. – The crowbar triggering circuitry and the circuitry for operating the breaker in the input to PA power supply were constructed and checked individually. The crowbar mounting was designed and is being fabricated.

A line termination for the high voltage cable between the power amplifier and its power supply was designed, breadboarded, and is being fabricated. This unit should help to eliminate high-voltage transients after sparking.

Voltage Regulation. – Two of the four amplifiers in the chain of the regulators were constructed and tested.

Tuning Servo. – The general scheme mentioned last year for automatic tuning is unchanged; however, the details have been completely changed, see Fig. 8.13. It was found possible to use transistors with high-frequency cutoff as phase splitters over the 7.5 to 22.5 Mc range and, then, to use a Foster-Luley discriminator for phase detection. Capacitive dividers and stabilized cathode followers at the rf voltage pickup points are to feed the rf signals to the phase detectors and rf voltmeters located about 100 ft outside the vault. The output of the phase detector controls a servo motor on the tuned element. For tuning, the servo system hunts at maximum motor speed between limits, depending on frequency, until a rf signal is detected. The signal causes the servo to switch from hunting to the phase-detector output. The speed of the motor is, then, a function of the error, approaching a minimum at small errors. To eliminate backlash caused by gears, slow speed dc stepping motors are being used for the servo drives; the stepping motors do not miss steps. Transistor motor-driving amplifiers (in addition to the phase detectors, voltmeters, and logic circuits) have been constructed and tested for one tuning servo.

ORIC CONTROL SYSTEM

The cyclotron control system is designed around a single-operator control center. The controls which immediately affect the performance of the

cyclotron and the indicators and controls which may require immediate attention for the protection of personnel and equipment are within reach of the operator at the control console. Displays and controls for routine operations such as beam-pipe gate valves, vacuum controls, rf and power supply controls, and water valve controls are also located conveniently in the central control room. These controls, along with the various protective interlocks and signals and the patch panels for connecting the several target areas with the experimental data collecting center, are in place; the interconnecting wiring is about 80% completed. Portions of the control system which have been checked out are in use, the remaining controls will be completed as the cyclotron components are installed.

Cyclotron Control System

The control system is designed for the convenience of a small operating crew. As many manual operations as possible have been converted for remote operation, with their controls located in the control room. Those controls which will be used for setting up an experiment and which will then need little or no adjustment during operation are on the vertical panel shown in Fig. 8.14. Those controls requiring adjustment during operation of the cyclotron are located on the desk-type control console. The central portion contains the controls most frequently adjusted, while less critical controls are toward the sides. In general, all controls which relate to a single component (such as ion source filament, arc, and gas controls) are located together and in vertical columns. Meters are on the upper portion of the console immediately above their respective controls.

Adjustments and indicators for the power supplies for the magnet and the rf system are located on the control panel or console. These controls were designed as an integral part of the individual systems and coordinated with the central control system.

The console control panel and three relay cabinets were received with all instruments installed; approximately 80% of the interconnection wiring has been completed. During testing some modifications were required, such as the introduction of diodes to eliminate voltage transients and to assure unambiguous operation of the signal circuits. The parts of the system complete and in use include vacuum controls, magnet power supply controls, and cooling water low-flow alarms. Most of the circuitry for equipment not yet installed has been run to junction boxes in the experiment areas to facilitate completion at installation.

The ion source and probe assembly is designed to permit remote control of insertion and removal from the cyclotron without affecting the cyclotron vacuum. Automatic sequential operation is obtained by the addition of a few motors and relays. To insert the assembly into the cyclotron, or remove it, the operator simply turns a selection switch on the control panel. The action sequence proceeds automatically, beginning each step as the previous one is completed. A complete cycle takes about 2 min, and the operator can stop the action at any time.

The ion source and internal probe positioning controls are installed and checked out. Remote control adjustments of the vertical, horizontal, and angular position of the ion source are provided. Similarly, control of the horizontal and angular positions of the beam probe are available.

Personnel Radiation Protection

Providing for flexibility in the operation of the cyclotron and at the same time assuring adequate radiation safety has received careful study. Safe access to experiment areas not in use at a given time is provided by a combination of plugs for shield-wall penetration plugs, shield doors, and their interlock switches. A selector switch on the console provides proper interlocking for nine predetermined target locations. The operator is able to direct the beam into one experiment area while experiments are being set up in other areas. The operator also maintains control of access to shielded rooms by key interlocks. The accidental removal of beam-port plugs or the opening of shield doors which violate safety criteria automatically shuts off the rf power to the cyclotron.

Building intercom and Southern Bell telephone facilities are installed in experiment areas to provide adequate communications from inside the shielded area.

Radiation measuring instruments will be located outside the experiment rooms to minimize the

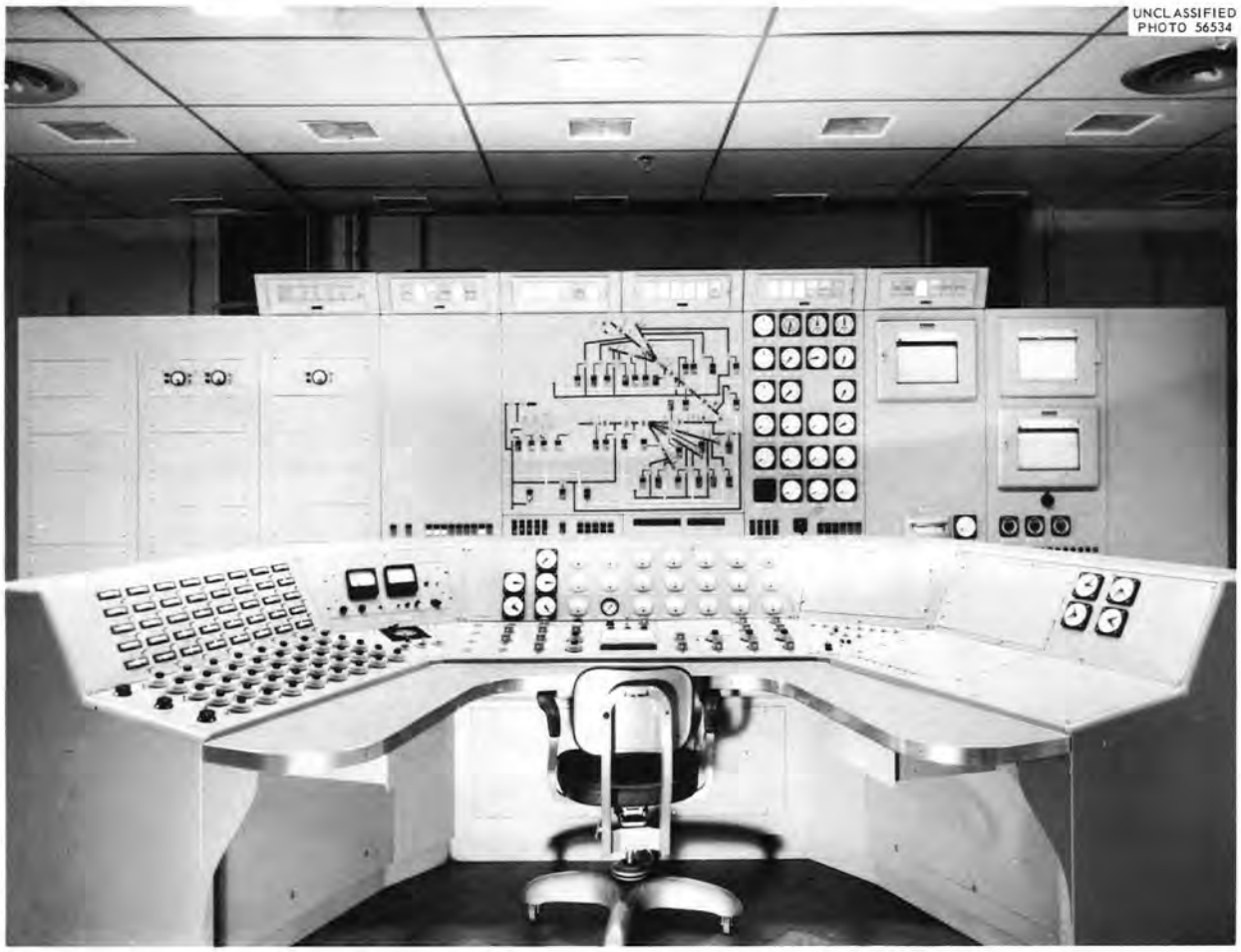

Fig. 8.14. Control Center for ORIC. The vacuum system graphic display and other monitoring signals and controls are placed on the vertical panels. Controls requiring the immediate attention of the operator are conveniently arranged on the console.

possibility of inadvertently carrying radioactive material out of the shielded area. A detailed description of the radiation safety system is being prepared for review.

Equipment Protection

Failure of a number of cooling water circuits, air pressure circuits, or abnormal temperatures could cause damage to the cyclotron. Interlock circuits are installed and tested to remove all power from components that would be damaged in these cases.

Patch Panels for Experimenters

One problem usually encountered in experiment areas is the installation and disposition of the large number of wires and cables required to accumulate experimental data. Usually experimenters are required to install these cables. In ORIC, patch panels are provided in each experiment area and in each data acquisition area; they are connected to identical patch panels on a central patch board in the counting room adjacent to the main control room. These panels provide reliable interconnections between experiment and data accumulating equipment by means of coaxial cables, twisted-pair shielded cables, and electrical control circuit wires, all properly installed through shielding penetrations originally provided. They should provide well for flexibility, dependability, and convenience of experimental work, and should markedly reduce the clutter usually encountered.

Papers Presented at Scientific and Technical Meetings

American Physical Society, New York, February 1–4, 1961

J. B. Ball, C. D. Goodman, and C. B. Fulmer, "Single Particle Neutron Bound States near $N = 28$ Studied with (p,d) Reactions, Part I."

R. H. Bassel, R. M. Drisko, and G. R. Satchler, "Numerical Study of Distortion Effects in Deuteron Stripping Reaction."

R. M. Drisko, R. H. Bassel, and G. R. Satchler, "Distortion Effects in the Scattering of High Energy Nucleons."

C. D. Goodman, J. B. Ball, and C. B. Fulmer, "Single Particle Neutron Bound States near $N = 28$ Studied with (p,d) Reactions, Part II."

C. E. Hunting, "Protons from N^{14} Bombardment of F^{19}."

G. R. Satchler, R. H. Bassel, and R. M. Drisko, "Gamma-Rays Following Direct Inelastic Scattering from Nuclei."

Southeastern Section of American Physical Society, Louisville, Kentucky, March 30–April 1, 1961

R. W. Boom, K. S. Toth, and A. Zucker, "Radiation Survey at the Berkeley 184-Inch Cyclotron."

American Physical Society, Washington, D.C., April 24–27, 1961

C. B. Fulmer, C. D. Goodman, and J. B. Ball, "Deuteron Spectra from the $Ni^{64}(p,d)Ni^{63}$ Reaction."

M. L. Halbert, "Alpha Particles from N^{14} Bombardment of O^{16}."

G. D. Kneip, Jr., R. E. Worsham, R. W. Boom, J. O. Betterton, Jr., and C. E. Roos, "Hysteresis Effects in the Nb_3Sn Superconducting Transition."

E. Newman, "Proton Transfer Reaction $B^{10}(N^{14},O^{15})Be^9$."

C. E. Roos, J. O. Betterton, Jr., R. W. Boom, G. D. Kneip, Jr., and R. E. Worsham, "Critical Currents in Nb_3Sn Superconductors."

K. S. Toth, "The Neutron Transfer Reaction $B^{10}(N^{14},N^{13})B^{11}$."

A. Zucker, "Elastic Scattering of N^{14} by Mg^{24}."

International Atomic Energy Agency, Conference on Nuclear Electronics, Belgrade, Yugoslavia, May 15–20, 1961

M. L. Halbert, "Surface-Barrier Counters for Nuclear Reaction Studies."

American Physical Society, Mexico City, Mexico, June 22–24, 1961

C. E. Roos, J. O. Betterton, Jr., G. D. Kneip, Jr., R. W. Boom, and R. E. Worsham, "High-Field Studies of Nb_3Sn Superconductivity."

XVIII International Congress of Pure and Applied Chemistry (Nuclear Chemistry Section), Montreal Quebec, August 6–12, 1961

M. L. Halbert, C. E. Hunting, E. Newman, K. S. Toth, and A. Zucker, "Transfer and Evaporation Reactions with 27-Mev N^{14} Ions."

Western Convention of Institute of Radio Engineers (WESCON), San Francisco, California, August 22–25, 1961

R. W. Boom and R. S. Livingston, "Superconducting Solenoids."

Rutherford Jubilee International Conference, Manchester, England, September 4–8, 1961

J. B. Ball and C. D. Goodman, "Evidence for Nuclear Distortion in the Iron Region."

C. D. Goodman, J. B. Ball, and C. B. Fulmer, "Pickup Reaction Studies of Neutron Bound States: Fe^{54} and Co^{59}."

C. D. Goodman, J. B. Ball, and C. B. Fulmer, "Pickup Reaction Evidence for Deformation of Fe^{56}, Fe^{57}, and Fe^{58}."

E. C. Halbert, R. M. Drisko, G. R. Satchler, and N. Austern, "Finite-Range Distorted-Waves Calculation of Direct Reactions."

M. L. Halbert and C. E. Hunting, "Angular Momentum Effects in Nuclear Evaporation."

E. Newman, K. S. Toth, M. L. Halbert, and A. Zucker, "Single-Nucleon Transfer Reactions Induced by 28-Mev N^{14} Ions."

Joint Nuclear Instrumentation Symposium, Raleigh, North Carolina, September 6–8, 1961

B. C. Behr, W. E. Lingar, and W. H. White, Jr., "High Current Regulated Supply Combining Transistors and Magnetic Amplifiers for ORIC."

International Conference on High Energy Accelerators, Brookhaven National Laboratory, Upton, Long Island, New York, September 6–12, 1961

J. A. Martin, J. E. Mann, and R. S. Livingston, "First Operation of the Electron Cyclotron Analogue at ORNL."

Symposium of Nuclear Instruments, Harwell, England, September 11–12, 1961

C. D. Goodman, G. D. O'Kelley, and D. A. Bromley, "A 20,000-Channel Pulse-Height Analyzer with Two-Coordinate Address."

C. D. Goodman and J. B. Ball, "A System for Detecting and Processing Energy Spectra for Several Types of Charged Particles Simultaneously."

American Institute of Electrical Engineers, Detroit, Michigan, October 19, 1961

J. A. Martin, "Development of High-Intensity Pion-Producing Accelerators."

Conference on Instrumentation and Technology Pertaining to Medium Energy Nuclear Physics, ORINS-ORNL, Oak Ridge, Tennessee, November 13–14, 1961

M. L. Halbert, "Surface-Barrier Counters for Nuclear Reaction Studies" (invited paper).

R. J. Jones, "Developments in Isochronous Cyclotrons" (invited paper).

American Physical Society, Los Angeles, California, December 27–29, 1961

R. S. Livingston, "Analogue of an Isochronous Cyclotron with Energy Mc^2."

K. S. Toth and E. Newman, "Transfer Reactions Resulting from 28-Mev N^{14} Particles on Cl^{35}."

Publications

Ball, J. B., and C. D. Goodman, "Evidence for Nuclear Distortion in the Iron Region," pp 527–28 in Proceedings of the *Rutherford Jubilee International Conference, Manchester, 1961*, ed. by J. B. Birks, Heywood and Co., Ltd., London, 1961.

Betterton, J. O., Jr., R. W. Boom, G. D. Kneip, Jr., R. E. Worsham, and C. E. Roos, "Superconductivity of Nb_3Sn in a Pulsed Magnetic Field," *Phys. Rev. Letters* **6**, 532 (May 15, 1961).

Boom, R. W., K. S. Toth, and A. Zucker, *Residual Radiation of the LRL 184-Inch Cyclotron*, ORNL-3158 (June 8, 1961).

Gleason, G. I., and J. L. Need, *The Production of* Ge^{68}, ORNL CF-61-5-55 (May 16, 1961).

Goodman, C. D., *Getting Multichannel Analyzer Data in and out of the IBM-7090 for Processing*, ORNL-3235 (Nov. 27, 1961).

Goodman, C. D., J. B. Ball, and C. B. Fulmer, "Pickup Reaction Studies of Neutron Bound States: Fe^{54} and Co^{59}," pp 523–24 in the Proceedings of the *Rutherford Jubilee International Conference, Manchester, 1961*, ed. by J. B. Birks, Heywood and Co., Ltd., London, 1961.

Goodman, C. D., J. B. Ball, and C. B. Fulmer, "Pickup Reaction Evidence for Deformation of Fe^{56}, Fe^{57}, and Fe^{58}," pp 525–26 in the Proceedings of the *Rutherford Jubilee International Conference, Manchester, 1961*, ed. by J. B. Birks, Heywood and Co., Ltd., London, 1961.

Halbert, E. C., R. M. Drisko, G. R. Satchler, and N. Austern, "Finite-Range Distorted-Waves Calculation of Direct Reactions," pp 555–56 in the Proceedings of the *Rutherford Jubilee International Conference, Manchester, 1961*, ed. by J. B. Birks, Heywood and Co., Ltd., London, 1961.

Halbert, M. L., and C. E. Hunting, "Angular Momentum Effects in Nuclear Evaporation," pp 773–74 in the Proceedings of the *Rutherford Jubilee International Conference, Manchester, 1961*, ed. by J. B. Birks, Heywood and Co., Ltd., London, 1961.

Halbert, M. L., and A. Zucker, "Inelastic Scattering of N^{14} by C^{12}," *Phys. Rev.* **121**, 236–42 (1961).

Harmatz, B., T. H. Handley, and J. W. Mihelich, "Nuclear Levels in a Number of Even-Even Rare Earths ($150 \leq A \leq 184$)," *Phys. Rev.* **123**, 1758–86 (1961).

Harper, P. V., K. Lathrop, and J. L. Need, *Thick-Target Yield and Excitation Function*, ORNL CF-61-5-67 (May 1961).

Hunting, C. E., "Proton Spectra from Nitrogen Bombardment of Fluorine," *Phys. Rev.* **123**, 606–15 (1961).

Kochanny, G. L., Jr., and A. Timnick, "Ferrate (VI) Formation by Hydrogen Peroxide in Presence of EDTA," *J. Am. Chem. Soc.* **83**, 2777 (1961).

Newman, E., K. S. Toth, M. L. Halbert, and A. Zucker, "Single-Nucleon Transfer Reactions Induced by 28-Mev N^{14} Ions," pp 547–48 in Proceedings of the *Rutherford Jubilee International Conference, Manchester, 1961*, ed. by J. B. Birks, Heywood and Co., Ltd., London, 1961.

Toth, K. S., and O. B. Nielsen, "Dy^{155} and Dy^{157} Decay Schemes," *Nuclear Phys.* **22**, 57 (1961).

Toth, K. S., "Neutron Transfer to Excited States in N^{15} in the Reaction $N^{14}(N^{14},N^{13})N^{15}$," *Phys. Rev.* **121**, 1190–92 (1961).

Toth, K. S., "Angular Distribution and Ranges of N^{13} Particles from N^{14} on N^{14}," *Phys. Rev.* **123**, 582–88 (1961).

Advisory Committee

The Annual Information Meeting of the Electronuclear Division was held jointly with the Physics Division on April 10–13, 1961. The Advisory Committee members reviewing these research programs were:

Prof. H. Feshbach	Massachusetts Institute of Technology Cambridge, Mass.
Prof. W. A. Fowler	California Institute of Technology Pasadena, Calif.
Dr. M. Goldhaber	Brookhaven National Laboratory Upton, Long Island, N.Y.
Prof. M. S. Livingston	Cambridge Electron Accelerator Cambridge, Mass.
Prof. J. R. Richardson	University of California Los Angeles, Calif.
Dean J. H. Van Vleck	Harvard University Cambridge, Mass.
Prof. J. A. Wheeler	Princeton University Princeton, N.J.

Research Consultants

University scientists serving, under subcontract, as consultants to the Division include:

C. J. Bergeron	Louisiana State University, New Orleans
H. G. Blosser	University of Michigan, Ann Arbor
H. F. Bowsher	University of Tennessee, Knoxville
G. Breit	Yale University, New Haven, Conn.
D. A. Bromley	Yale University, New Haven, Conn.
B. L. Cohen	University of Pittsburgh, Pittsburgh, Pa.
R. M. Drisko	University of Pittsburgh, Pittsburgh, Pa.
Morton Gordon	Michigan State University, East Lansing
M. S. Livingston	Massachusetts Institute of Technology, Cambridge
J. W. Mihelich	University of Notre Dame, Notre Dame, Ind.
H. M. Moseley	Texas Christian University, Forth Worth
H. K. Ticho	University of California, Los Angeles
A. Timnick	Michigan State University, East Lansing
L. D. Wyly, Jr.	Georgia Institute of Technology, Atlanta

Miscellaneous Activities of the Electronuclear Division

The Division continues to engage in a variety of educational activities as part of its research function and as a responsibility to the scientific community. Included in these are the employment and training of undergraduate and graduate students, lectures at various universities, seminars, and related matters.

THESIS RESEARCH

During the past year two graduate students continued their thesis research in the Electronuclear Division. G. L. Kochanny, Jr., from Michigan State University did his research problem with the 86-inch cyclotron nuclear physics group. J. W. Wachter, on leave from Union Carbide Nuclear Company (Y-12 Plant) continued research with the heavy-particle physics group in connection with his studies at the University of Tennessee. Both men have essentially completed their research and expect to receive their degrees in 1962.

COOPERATIVE RESEARCH PROJECT

A cooperative program of the Electronuclear Division and Vanderbilt University in the measurement of properties of superconductors at high magnetic fields was maintained throughout 1961. Both the pulsed-magnet facility at Vanderbilt and the high-field solenoid at ORNL were used for these measurements.

RESEARCH PARTICIPANTS

Six faculty members from southern universities were at the Laboratory during the summer of 1961. They actively participated in the various research programs of the Division as follows: B. Linder, Florida State University, and F. E. Durham, Tulane University, participated in the heavy-particle physics program. H. F. Bowsher, University of Tennessee, and J. C. Stoltzfus, Virginia Polytechnic Institute, were with the 86-inch cyclotron nuclear physics group. T. I. Hicks, Howard College, assisted the isochronous cyclotron group. C. J. Bergeron, Louisiana State University at New Orleans, was active in the superconductivity studies.

VISITING SCIENTISTS

Two visiting scientists arrived in the latter half of 1961 on assignments with the isochronous cyclotron group; they are Bruno Duelli from Kernforschungszentrum, Zyklotron Laboratorium, Karlsruhe, Germany, and F. M. Russell from the National Institute for Research in Nuclear Science, Rutherford High Energy Laboratory, Harwell, England.

SUMMER EMPLOYEES

Three university students were employed for three months during the summer of 1961: T. H. Boyer, Yale University, worked with the high-energy electronuclear machines group. M. P. Fricke, Drexel Institute of Technology, and G. L. Settle, University of Tennessee, worked with the isochronous cyclotron group.

CO-OP STUDENTS

Four student trainees in cooperative work-study programs have been employed on a continuing basis in the Division. These students spend about half their time in residence at their universities and half working at the Laboratory. J. H. Hemman and, alternately, B. W. Jaeger, both from the University of Missouri School of Mines and Metallurgy, work with the isochronous cyclotron group. R. W. Rutkowski and, alternately, S. Cushner, both from Drexel Institute of Technology, work with the high-energy electronuclear machines group.

INVITATION LECTURES

Members of the Division gave a number of special invitation lectures at American universities and and at institutions abroad.

M. L. Halbert	Rice University, February 15, 1961 Mississippi State University, February 16, 1961 "Semiconductor Counters for Nuclear Physics"
C. D. Goodman	University of Kentucky, March 8, 1961 "Studies of Nuclear Structure with Direct Interaction Proton Reactions"
R. S. Livingston	Emory University, March 10, 1961 "Modern Cyclotron Design Trends"
J. J. Pinajian	Emory University, April 7, 1961 "Production of Radioisotopes on ORNL 86-Inch Cyclotron"
A. Zucker	Yugoslav Nuclear Energy Commission Institutes, June, 1961 Presented a series of lectures on heavy-ion nuclear physics and a few on cyclotron technology. Three of the seven lectures were in Serbo-Croatian.
C. D. Goodman	Centre d'Etudes Nucleaire, Saclay, France, September 15, 1961 Laboratoire de Physique Nucleaires, Orsay, France, September 19, 1961 "Nuclear Structure Studies with Protons at the 86-Inch Cyclotron"
M. L. Halbert	Institute for Nuclear Physics, Amsterdam, September 26, 1961 "Nuclear Reaction Mechanisms with Heavy Ions"
A. Zucker	Yale University, December 4, 1961 "Nuclear Reactions with 28-Mev Nitrogen Ions"

Division Research Seminars

The Division has sponsored regularly scheduled research seminars on timely topics of special interest to the various programs. The 1961 schedule of seminars, with C. B. Fulmer as chairman, included:

February 14	T. Foelsche, NASA, Langley Field, Virginia "Survey About Space Radiations with Emphasis on Their Implications to Space Flight"
February 21	V. P. Kenny, University of Kentucky, Lexington "Bubble Chambers"
March 14	R. B. Setlow, Biology Division, ORNL "Action of Radiation on Large Molecules"
March 28	F. C. Maienschein, Neutron Physics Division, ORNL "The Proposed ORNL Linear Accelerator"
April 14	J. R. Richardson, University of California, Los Angeles "Preliminary Operation of the UCLA 50-Mev Cyclotron"
May 9	W. D. Whitehead, University of Virginia, Charlottsville "Angular Distributions of Fast Photoneutrons"
June 6	Sergio Michiletti, University of Pittsburgh, Pittsburgh, Pa. "(n,d) Pickup Reaction on Elements Belonging to the $f_{7/2}$ Proton Shell"
June 30	M. A. Melkanoff, University of California, Los Angeles "Optical Model Analyses of Proton Scattering Against Carbon at 10–20 Mev"
July 18	Vernon Hughes, Yale University, New Haven, Conn. "A High Intensity, Proton Linear Accelerator"
July 25	B. L. Cohen, University of Pittsburgh, Pittsburgh, Pa. "Nuclear Structure Studies with Nuclear Reactions"
August 1	A. Zucker, Electronuclear Division, ORNL "A Journey to Yugoslavia"
October 17	R. J. Mackin, Thermonuclear Division, ORNL "Report on International Plasma Physics Meeting at Munich and Salzbury"
October 24	J. E. Hooper, University of Tennessee, Knoxville "Use of $K+$ Secondaries to Redetermine the Range–Energy Relation"
December 19	R. A. Dandl, Thermonuclear Division, ORNL "Electron-Cyclotron Plasma Heating Experiment"

ORNL-3257
UC-34 – Physics
TID-4500 (17th ed., Rev.)

INTERNAL DISTRIBUTION

1. Biology Library
2–4. Central Research Library
5. Reactor Division Library
6–55. Laboratory Records Department
56. Laboratory Records, ORNL R.C.
57–58. ORNL – Y-12 Technical Library, Document Reference Section
59. Laboratory Shift Supervisor
60. C. E. Larson
61. A. M. Weinberg
62. J. P. Murray (K-25)
63. R. G. Jordan (Y-12)
64. J. A. Swartout
65. E. H. Taylor
66. E. D. Shipley
67. S. C. Lind
68. M. L. Nelson
69. W. H. Jordan
70. F. L. Culler
71. A. H. Snell
72. A. Hollaender
73. M. T. Kelley
74. G. E. Boyd
75. K. Z. Morgan
76. T. A. Lincoln
77. A. S. Householder
78. C. S. Harrill
79. R. W. Johnson
80. J. A. Lane
81. R. S. Livingston
82. J. B. Ball
83. R. H. Bassel
84. R. S. Bender
85. L. N. Blumberg
86. R. W. Boom
87. G. L. Broyles
88. C. H. Burbage
89. H. L. Dickerson
90. B. Duelli
91. C. B. Fulmer
92. C. A. Gault
93. C. D. Goodman
94. E. E. Gross
95. M. L. Halbert
96. B. Harmatz
97. F. T. Howard
98. E. D. Hudson
99. R. J. Jones
100. R. S. Lord
101. F. E. McDaniel
102. J. E. Mann
103. M. B. Marshall
104. J. A. Martin
105. S. W. Mosko
106. E. Newman
107. E. L. Olson
108. G. A. Palmer
109. J. J. Pinajian
110. R. F. Pruitt
111. A. E. Pugh
112. E. G. Richardson, Jr.
113. A. W. Riikola
114. F. M. Russell
115. J. A. Russell
116. L. B. Schneider
117. W. R. Smith
118. K. S. Toth
119. C. L. Viar
120. W. H. White, Jr.
121. R. E. Worsham
122. N. F. Ziegler
123. A. Zucker
124. W. A. Fowler (consultant)
125. H. Feshback (consultant)
126. M. Goldhaber (consultant)
127. M. S. Livingston (consultant)
128. J. R. Richardson (consultant)
129. J. H. Van Vleck (consultant)
130. J. A. Wheeler (consultant)

EXTERNAL DISTRIBUTION

131. R. W. McNamee, Union Carbide Corporation, New York
132. Division of Research and Development, AEC, ORO
133–766. Given distribution as shown in TID-4500 (17th ed., Rev.) under Physics category (75 copies – OTS)

Progress reports have been issued by the Electronuclear Division for the periods ending on the dates listed below:

ORNL-1173	September 30, 1951, Part I
ORNL-1235	September 30, 1951, Part II
ORNL-1269	December 31, 1951, Part I
ORNL-1270	December 31, 1951, Part II
ORNL-1315	March 31, 1952, Part II
ORNL-1339	March 31, 1952, Part I
ORNL-1345	June 30, 1952, Part I
ORNL-1346	June 30, 1952, Part II
ORNL-1383	September 30, 1952
ORNL-1531	March 20, 1953
ORNL-1663	September 20, 1953
ORNL-1670	March 20, 1954
ORNL-1795	September 20, 1954
ORNL-1884	March 20, 1955
ORNL-2030	September 20, 1955
ORNL-2139	March 20, 1956
ORNL-2140	March 20, 1956
ORNL-2434	October 1, 1957
ORNL-2740	October 1, 1958
ORNL-3047	March 1, 1960
ORNL-3083	January 16, 1961